DEVELOPMENT OF MIXED-MATRIX MEMBRANES FOR CARBON DIOXIDE SEPARATION

BY

MUHAMMAD SARFRAZ

A Dissertation Presented to the

DEANSHIP OF GRADUATE STUDIES

KING FAHD UNIVERSITY OF PETROLEUM & MINERALS

DHAHRAN, SAUDI ARABIA

In Partial Fulfillment of the

Requirements for the Degree of

DOCTOR OF PHILOSOPHY

In

CHEMICAL ENGINEERING

OCTOBER 2015

KING FAHD UNIVERSITY OF PETROLEUM & MINERALS

DHAHRAN- 31261, SAUDI ARABIA

DEANSHIP OF GRADUATE STUDIES

This thesis, written by **MUHAMMAD SARFRAZ** under the direction of his thesis advisor and approved by his thesis committee, has been presented and accepted by the Dean of Graduate Studies, in partial fulfillment of the requirements for the degree of **DOCTOR OF PHILOSOPHY IN CHEMICAL ENGINEERING.**

Dr. Mohammed Ba-Shammakh
(Advisor)

Dr. Mohammed Ba-Shammakh
Department Chairman

Dr. Mohamed B. Amin
(Member)

Dr. Salam A. Zummo
Dean of Graduate Studies

Dr. Mamdouh A. Al-Harthi
(Member)

5/10/15
Date

Dr. Housam Binous
(Member)

Dr. M. Mozahar Hossain
(Member)

Dedicated to my beloved parents

Mr. and Mrs. Abdul Wahab

Dedicated to my siblings, wife and children

Dedicated to friends and well wishers

ACKNOWLEDGMENTS

I express my appreciation to Almighty Allah, the most Beneficent and the most Merciful, who blessed me physical and mental integrity to accomplish this task. I show great respect to Holy Prophet Muhammad (peace be upon him) who advised and order to learn knowledge in all circumstances. I am thankful to the Department of Chemical Engineering, King Fahd University Petroleum & Minerals, Saudi Arabia for granting me scholarship to pursue my PhD. I pay special thanks to KACST-TIC on Carbon Capture & Sequestration (CCS) for providing technical support and research facilities. I express my sincere thanks to my advisor Dr. Mohammed Ba-Shammakh for providing continued guidance and supervising my research all the way. Without his technical and moral support I would not have been able to complete this work. I am cordially thankful to my committee members Dr. Mohamed Bakar Amin, Dr. Mamdouh Ahmed Al-Harthi, Dr. Housam Binous and Dr. Mohammad Mozahar Hossain for their useful comments and suggestions. My sincere thanks are paid to Dr. Mohamed A. Habib, Director CoRE CCS for allowing me to work in the Centre Laboratories. I am also thankful to laboratory staff of the Department of Chemical Engineering for helping me characterization. Last but not least, I am thankful to my parents, siblings, wife, children and people in my country who sincerely urged for my educational accomplishment.

TABLE OF CONTENTS

LIST OF TABLES

LIST OF FIGURES

ABSTRACT

Full Name :MUHAMMAD SARFRAZ

Thesis Title :DEVELOPMENT OF MIXED-MATRIX MEMBRANES FOR CARBON DIOXIDE SEPARATION

Major Field :CHEMICAL ENGINEERING

Date of Degree :OCTOBER 2015

Global warming mainly caused by carbon dioxide (CO_2) emissions can be reduced by its capture and/or sequestration from post combustion flue gases via economically viable processes such as gas separation technology using polymer-based mixed-matrix membranes (MMMs). A series of MMMs were fabricated by incorporating various hydrothermally stable microprorous zeolitic imidazole frameworks (ZIFs: ZIF-300, ZIF-301, ZIF-302) nanocrystals, carbon nanotubes (CNTs) and/or their combinations into glassy polymers via solution-casting method. Different loadings of CNTs and/or ZIFs nanocrystals were incorporated into polysulfone (PSF) matrix to find the separation effectiveness of MMMs to remove CO_2 from dry and wet CO_2/N_2 gaseous mixtures. The flexible MMMs rendered homogeneous dispersion of nanofillers, improved polymer-filler interfacial adhesion, and hydrothermally stable structure as characterized by x-ray diffraction (XRD), scanning electron microscopy (SEM), and thermal gravimetric analysis (TGA). Gas sorption analyses along with dry and wet gas permeation tests helped to determine the optimized CO_2 permeability as well as CO_2/N_2 permselectivity of the MMMs. The permeation features of MMMs were slightly improved under humid conditions as compared to dry ones.

ملخص الرسالة

الاسم الكامل: محمد سرفراز

عنوان الرسالة: تطوير أغشية مصفوفة المختلطة لفصل ثاني أكسيد الكربون

التخصص: هندسة كيميائية

تاريخ الدرجة العلمية: أكتوبر 2015

ظاهرة الاحتباس الحراري الناجمة أساسا عن ثاني أكسيد الكربون (CO_2) الانبعاثات يمكن خفضها عن طريق الاستيلاء عليها و / أو عزل من غازات المداخن بعد احتراق عبر عمليات قابلة للحياة اقتصاديا مثل تكنولوجيا فصل الغاز باستخدام الأغشية مختلطة مصفوفة البوليمر المستندة (باستخدام الحاسب الآلي الشخصي). ملفقة سلسلة من باستخدام الحاسب الآلي الشخصي من خلال دمج مختلف الأطر إميدازول الزيوليت الصغيرة التي يسهل اختراقها (ZIFs: زيف-300، زيف-301، زيف-302) البلورات النانوية، أنابيب الكربون النانوية (CNTs) و / أو مجموعاتها في البوليمرات زجاجي عبر طريقة حل الصب . وقد أدرجت شحنات مختلفة من الأنابيب النانوية الكربونية و / أو ZIFs البلورات النانوية في بـ ولـ يـ سـ لـ فون (PSF) مصفوفة للعثور على فعالية فصل باستخدام الحاسب الآلي الشخصي لإزالة CO_2 من CO_2 - N_2 مخاليط غازية الجافة والرطبة. وباستخدام الحاسب الآلي الشخصي مرونة تقديم تشتت متجانسة من المالئة النانومترية، وتحسين البوليمر حشو التصاق بينية، وبنية مستقرة المياه الحارة كما تتميز حيود الأشعة السينية (XRD) والمسح الضوئي المجهر الإلكتروني (SEM)، والتحليل الوزني الحراري (TGA). يحلل الامتصاص الغاز جنبا إلى جنب مع ساعدت الاختبارات نفاذ الغاز الجاف والرطب لتحديد نفاذية ثاني أكسيد الكربون الأمثل وكذلك ثاني أكسيد الكربون إلى النيتروجين الانتقائية للباستخدام الحاسب الآلي الشخصي. الميزات تخلل باستخدام الحاسب الآلي الشخصي وتحسنت قليلا تحت الظروف الرطبة بالمقارنة مع تلك الجافة.

CHAPTER 1

INTRODUCTION

CO_2 emissions from burning of fossil fuels induce environmental warming concerns throughout the globe [1-3]. Economically viable processes to reduce CO_2 releases include its sequestration or capture from a mixture of CO_2-containing gases [4-5]. Effective method to capture CO_2 is its implementation at stationary point sources, like natural gas- and coal-fired power plants.

1.1 CO_2 Capture Techniques

In this regard, three major options to utilize novel materials include post combustion capture, pre-combustion capture and oxy-fuel combustion as depicted in Fig. 1.1. In post-combustion capture- an easily applicable method to existing power plants- CO_2 is captured from flue gas evolved from combustion of fossil fuel in air. This is mainly the separation of CO_2 from CO_2/N_2 gas mixture. Pre-combustion CO_2 capture can be implemented to separate CO_2 from a high-pressure H_2/CO_2 flue gas mixture produced as a result of coal gasification. In oxy-fuel combustion, an O_2/N_2 separation from air is performed.

Fig. 1.2 schematically illustrates the technologies and methods used to separate CO_2 from different gas mixtures. Solvent scrubbing using amines, Rectisol, Selexol, ammonia solutions, and fluorinated solvents to capture CO_2 can occur via either physical or

chemical absorption. Solvent recovery requires large quantities of energy to desorb the absorbed CO_2. Cryogenic distillation, separating CO_2 on the basis of condensation principle, can be adopted in oxygen production for oxyfuel combustion consumes where CO_2 concentration is high. This process also demands considerable energy inputs.

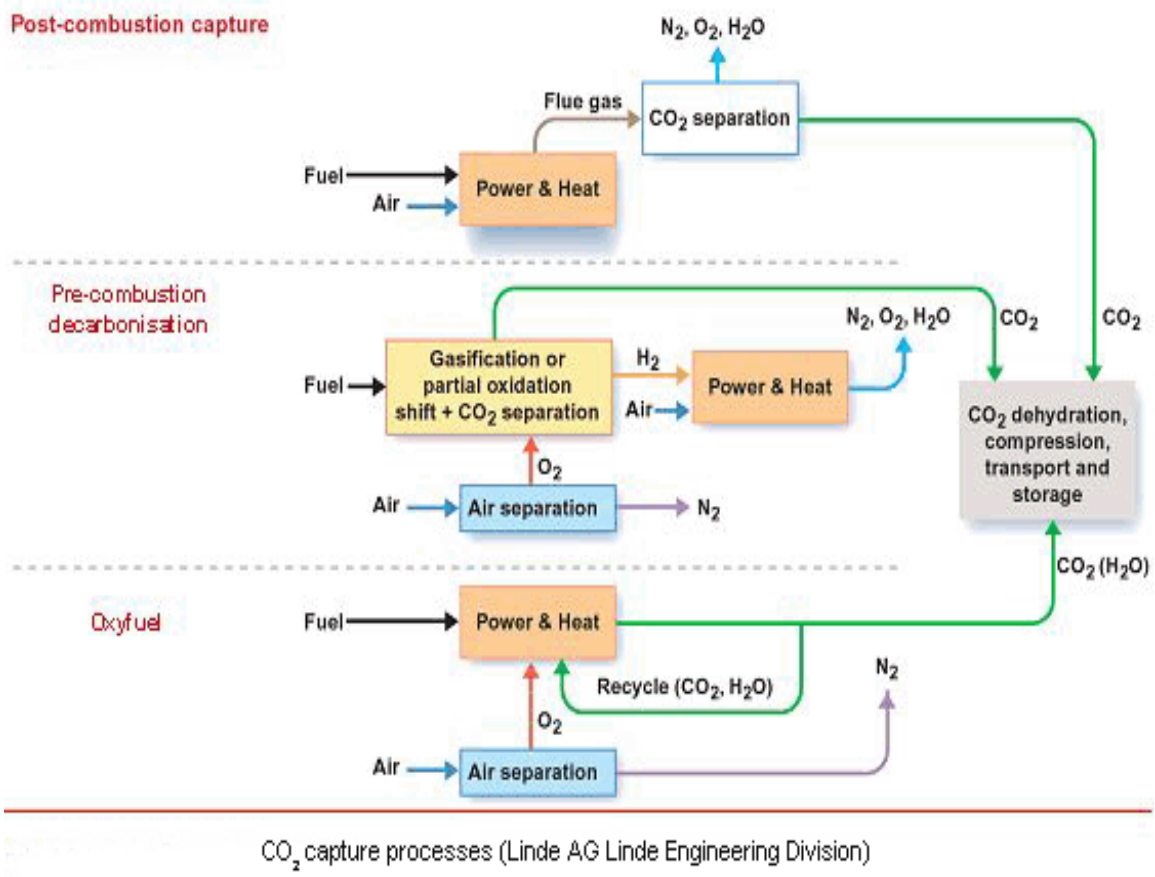

Fig. 1.1 Basic schemes showing the types of CO2 capture in different processes

Gas separation based on physical or chemical adsorption has been well established, in which choosing a potential solid adsorbent is an important parameter for a particular separation. The materials for gas adsorptive separation have been well established and a broad range of useful sorbents are accessible for CO2 separation. Conventional solid

adsorbents comprise activated alumina, silica gel, activated carbons, metal oxides, zeolites, ion-exchange resins, mesoporous silicates, and other surface-modified porous media. In addition, a few novel adsorbent materials like carbon fibres and their composites along with metal-organic frameworks have been established for gas separation.

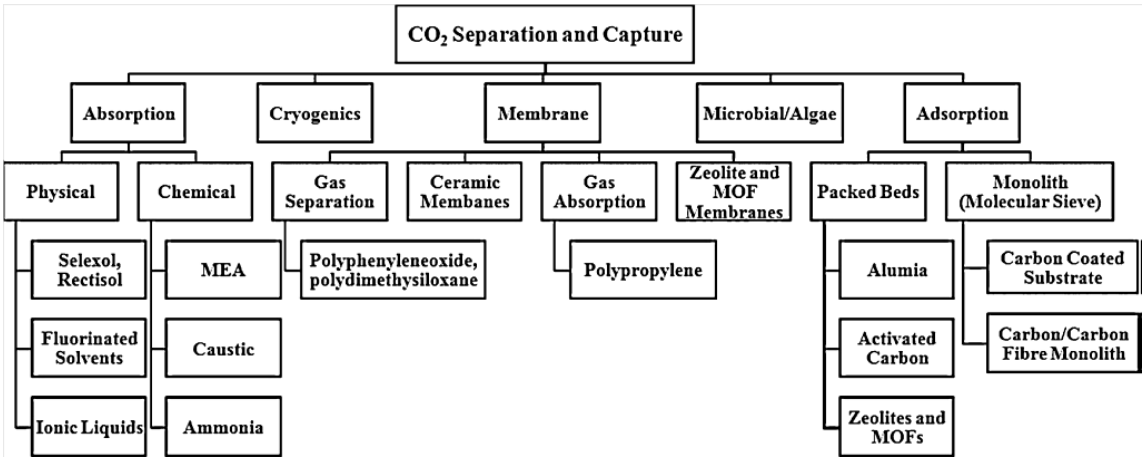

Fig. 1.2 Different technologies and materials for CO_2 separation and capture

Gas separation via membranes works on the basis of differences in chemical and/or physical interactions between gases and the membrane material, which can be altered to permit some components to pass preferentially through the membrane based on size difference (kinetic-based separation) and/or chemical affinity (separation based on thermodynamics principles). Membranes have vast prospective in post-combustion CO_2/N_2 separation and CO_2/H_2 separation in pre-combustion capture. Various membrane materials and processes are existing, a few of which have previously launched on an industrial scale, and potentially appropriate in CO_2 separation. The performance and related price of these membrane-based technologies in big scale CO_2 capture largely

relies on the membrane materials themselves. Organic polymeric membranes and inorganic ceramic membranes have been used in CO_2 separation from flue gas in post-combustion processes. However, attaining a high point of CO_2 separation by using single-stage polymeric or ceramic membranes is not easy, though it is viable in terms of expenditure. New materials are still needed to attain the preferred success in CO_2 separation by membranes.

Apart from afore mentioned chemical and physical techniques, biological methods have also been proposed for CO_2 separation. Algal bio-fixation of CO_2 in photo-bioreactors has recently gained immense interest in CO_2 capture. In addition, attempts using chemoautotrophic microorganisms which use inorganic chemicals instead of light energy for CO_2 removal have also been investigated.

1.2 Use of Metal Organic Frameworks in CO_2 Capture

A number of porous adsorbent materials can be used to capture CO_2 from post-combustion flue gases either in adsorbent columns or mixed-matrix membranes. Metal organic frameworks (MOFs), a new class of porous adsorbent materials, have recently caught attention due to their promising uses in large number of areas, such as molecular separations, gas storage, heterogeneous catalysis, and drug delivery. Application wise, finely tunable pore surface properties, extraordinary surface areas, and scalability of these materials to industrial level have made them a good choice for further study.

Isoreticular metal-organic frameworks (IRMOFs) exhibiting considerably varying pore sizes and functionalities have been intensely studied since their properties can be delicately adjusted by employing the suitable linker type. These include MOF-5, MIL-53,

UiO-66, and NOTT-100 structure types. The CO_2 capturing capability can be readily enhanced by introducing suitable polar groups (e.g., amines, alcohols, aldehydes etc.) via post-synthetic modification. Examples of functionalized MOFs include IRMOF-3, UiO-66-Br, DMOF-1-NH2, and MIL-101(Cr) etc. Alternatively the functionalized MOFs exhibiting highly selective exposed metal cation sites in their pores can be prepared without an post-synthetic modification. These type of porous materials include HKUST-1, M_2(dobdc), M-BTT, MIL-53, and MIL-88 etc.

To exploit these porous materials for practical applications, their chemical stability should be given significant attention since most MOFs cannot sustain prolonged contact with water even at room temperature leading to their decomposition into basic constituents i.e., metal salts and organic linkers. Water stability of IRMOF-series is low, HKUST-1 (Cu-BTC, $[Cu_3(BTC)_2]$) is intermediate but eventually decomposes. The MIL compounds, including MIL-101 and ZIF-8, and UiO-66 are of higher water stability.

To update the above literature search, we have looked at a number of additional articles which are very closely related to the research topic, namely CO_2 separation from a typical N_2/CO_2 exhaust mixture. From a material point of view, MOF-210 has the largest specific surface area reported to date (6240 m^2/g BET) followed by MOF-200 (4530 m^2/g BET), MOF-177 (4500 m^2/g BET), MOF-205 (4460 m^2/g BET), MOF-5 (2340 m^2/g BET), Mg-MOF-74 (1800 m^2/g BET), HKUST-1 (1570 m^2/g BET) and so forth. The large-pore MOFs have very high capacity for CO_2 at higher pressures but perform the worst at low pressure (e.g., MOF-210, MOF-200 etc); these MOFs find great potential for CO_2 storage. MOFs having coordinatively unsaturated metal sites (open-metal sites) demonstrate the best performance (e.g., Mg-MOF-74) under ambient conditions and are

strong candidates for CO_2 separation. Selectivity of Mg-MOF-74 for CO_2 is highest than any other MOF material. Unfortunately IRMOF series is highly unstable under humid conditions and their porous structure immediately collapses in presence of water vapor. The trinuclear chromium clusters found in many of the MIL series of frameworks (MIL-53, MIL-100, MIL-101, UiO-66) and ZIF are the most stable of the studied building units. The copper paddlewheel carboxylate clusters found in HKUST-1 exhibit intermediate stability. The selected MOFs for the proposed work include ZIF-300, ZIF-301, ZIF-302 etc owing to their good CO_2/N_2 separation efficiency and hydrothermal stabile characteristics.

1.3 Polymer-based Mixed-Matrix Membranes for CO_2 Separation

On account of its flexible design, ease of scale up, high efficiency, low energy requirement, simple function, low capital and operating costs and environmental friendliness, polymer-based mixed-matrix membrane gas separation technology- among other conventional processes- has gained momentous attention [6-13].

Mixed-matrix membranes (MMMs) filled with MOFs as additives (fillers) exhibit enhanced gas permeabilities and possibly also selectivities when compared to the pure MOF and/or pure polymer. Polyimides (Matrimid®) and polysulfones are popular polymer matrices for MOF fillers. MOF-polymer MMMs are investigated for the permeability of the single gases H_2, N_2, O_2, CH_4, CO_2 and of the gas mixtures O_2/N_2, H_2/CH_4, CO_2/CH_4, H_2/CO_2, CH_4/N_2 and CO_2/N_2. Permeability increases can be traced to the MOF porosity. Since the porosity of MOFs can be tuned very precisely, which is not possible with polymeric material, MMMs offer the opportunity of significantly increasing

the selectivity compared to the pure polymeric matrix. Additionally in most of the cases the permeability is increased for MMM membranes compared to the pure polymer. Addition of MOFs to polymers in MMMs easily yields performances similar to the best polymer membranes and gives higher selectivities than those reported to date for any pure MOF membrane for the same gas separation. MOF-polymer MMMs allow for easier synthesis and handability compared to pure MOF membranes.

Majority of glassy polymers have been studied to fabricate MMMs by adding inorganic fillers like nonporous silica [14-15], structured mesoporous silica [16-18], carbon molecular sieves [19], carbon nanotubes [20-21], zeolites [22], and microporous metal organic frameworks (MOFs) [23] in order to design efficient composite membranes showing better permselectivity characteristics as compared to unfilled polymer membranes. Advantages of adding microporous nanomaterials (such as ZIFs/MOFs and/or CNTs/graphenes etc.) into polymer matrix to form MMMs comprise the ability to combine the simplicity of casting and processability, enhanced mechanical and chemical performance of polymers conjoined with improved gas separation efficiency of nanocrystals possessing adjustable pore dimensions, modifiable surface functionality, and high surface areas [24].

Nanocrystals of microporous zeolitic imidazolate frameworks are interesting materials to fabricate efficient MMMs for gas separation on account of their high surface areas, tunable nano-sized pores, modifiable surface functionality, good wetting characteristics, improved thermal and chemical stability [25–27]. Hydrothermally stable ZIF-302 crystals [28] selectively capture CO_2 gas from $CO_2/N_2/H_2O$ wet gaseous mixture and their

inclusion into polymer matrices is expected to improve separation performance of MMMs under wet conditions.

Owing to their internal smooth walls, nano-sized configuration, large pore diameter, high aspect ratio, excellent mechanical and thermal properties [29–31], gas permeation through CNTs is exceptionally higher as compared to other microporous materials. The selectivity of as-synthesized CNTs for various gas molecules is comparatively low and tricky to recover by chemical modification/functionalization due to their inert nature [32–34]. Although CNTs-filled MMMs are significantly efficient as compared to MOF/ZIF-based MMMs, good adhesion and uniform dispersion of nanofillers in polymer matrices is the central challenge. A more refined strategy to engineer MMMs with enhanced permselectivity is the collegial incorporation of naonfillers possessing diversified morphology, nature, and dimensions into a polymer matrix [35].

Different types of zeolites (e.g. S1C), MOFs (e.g. HKUST-1), MILs (e.g. NH_2-MIL-53(Al)) and ZIFs (e.g. ZIF-8) were added into PSF to prepare MMMs to study the permeation of CO_2, N_2, CH_4, O_2, and H_2 gases [36]. The CO_2/N_2 selectivity did not ameliorate for S1C-ZIF-8/PSF MMMs. CO_2 permeation of HKUST-1/ZIF-8/PSF, S1C/PSF, HKUST-1/PSF, and ZIF-8/PSF MMMs were found to be 8.4, 9.4, 9.5 and 12.3 Barrers respectively with corresponding CO_2/N_2 permselectivities of 38, 23, 24, and 19. Collegial impact of adding mesoporous silica MCM-41 and amine-functionalized MIL-53(Al) nanofillers into polymer-based MMMs improved their gas separation efficiency [37]. Galve and group [38] fabricated hybrid membranes by introducing mesoporous silica MCM-41 spheres and layered microporous titanosilicate JDF-L1 sheets into glassy polyimide matrix; the uniform distribution of MCM-41 spheres in the polymer matrix

were facilitated by JDF-L1 sheets. Li et al. [39] investigated the combined inclusion of graphene oxide and CNTs into PSF to determine optimal loadings of the nanofillers.

The exclusive incorporation of CNTs and ZIFs into PSF matrix helped to improve gas separation efficiency of CO_2. The current work focuses on combined inclusion of CNTs and ZIF-302 nanocrystals into glassy PSF matrix for the first time to fabricate PSF/CNTs/ZIF-302 MMMs to efficiently separate CO_2 from CO_2/N_2 mixture. The main objective of this study is to determine the optimum loadings of both the nanofillers to attain high CO_2 permselectivity and to systematically investigate the solubility-diffusivity separation mechanism under dry and wet conditions.

1.4 Thesis Objectives

The current dissertation focuses on preparation and characterization of different types of membranes to capture CO_2 in the form of manuscripts deduced from the research work.

Chapter 1

Chapter 1 discusses different process techniques, porous materials and polymer-based mixed matrix membranes being used to capture CO_2. It also encompasses the dissertation objectives and brief outline.

Chapter 2

Chapter 2 discusses polymer-based mixed-matrix membranes (MMMs) prepared by filling glassy polysulfone (PSF) with zeolitic imidazole framework ZIF-300 nanocrystals using solution-casting method. Different loadings of ZIF-300 nanocrystals were incorporated in PSF matrix for the first time to find the separation effectiveness of

MMMs to remove carbon dioxide from dry and wet CO_2/N_2 gaseous mixture. Hydrothermally stable flexible MMMs demonstrating consistent distribution and fine adhesion of filler-matrix were characterized by XRD, SEM, and TGA. Gas sorption analysis along with dry and wet gas permeation tests exhibited that CO_2 permeability of MMM containing 40 wt % ZIF-300 was increased by three times as compared to bare PSF without affecting CO_2/N_2 permselectivity.

Chapter 3

In this chapter high performance MMMs for CO_2 separation prepared by collegial incorporation of carbon nanotubes (CNTs) and zeolitic imidazole frameworks (ZIF-300) nanocrystals into glassy polysulfone (PSF) matrix using solution-casting technique are described. Different loadings of the nanofillers were doped into PSF to optimize the CO_2 separation performance of MMMs. The flexible MMMs exhibiting homogeneous dispersion and good adhesion of nanofillers with polymer matrix were characterized by SEM, XRD, and TGA. Pure gas sorption studies coupled with dry and wet gas permeation tests demonstrated that both CO_2 permeability and CO_2/N_2 selectivity of MMMs were enhanced due to synergistic effect of nanofillers. The MMM doped with 6 wt % CNTs and 18 wt % ZIF-300 nanofillers exhibited an optimal separation performance rendering a CO_2 permeability of 34 Barrers with CO_2/N_2 selectivity of 72.

Chapter 4

Chapter 4 discusses the fabrication of water stable mixed-matrix membranes by incorporating microporous crystalline nanoparticles of ZIF-301 into PSF matrix using solution mixing technique. Different loading levels of ZIF-301 nanocrystals in PSF were

tried to determine the separation efficiency of MMMs to separate carbon dioxide from a mixture of dry and humid gases. Hydrothermally stable MMMs exhibiting homogeneous dispersion and good adhesion of ZIF-301 nanoparticles with polymer matrix were characterized by XRD, SEM, and TGA. Pure gas sorption studies coupled with dry and wet gas permeation tests demonstrated that CO_2 permeability of MMMs were enhanced by four times compared to pure PSF while retaining most of the CO_2/N_2 selectivity.

Chapter 5

Multiwalled CNTs and zeolitic imidazole frameworks (ZIF-301) were collegially incorporated into glassy polysulfone (PSF) to prepare mixed-matrix membranes (MMMs) to separate CO_2 from post combustion flue gases as described in chapter 5. Varying loadings of both nanofillers were incorporated into PSF using solution-casting technique to engineer CO_2 separation performance of MMMs. The flexible MMMs rendering consistent distribution and improved adhesion of nanofillers with polymer matrix were characterized by scanning electron microscopy (SEM), x-ray diffraction (XRD) and thermal gravimetric analysis (TGA). Gas sorption analysis along with dry and wet gas permeation experiments exhibited that both CO_2 permeability and CO_2/N_2 selectivity of MMMs were improved owing to collegial effect of nanofillers. The MMM filled with 18 wt % ZIF-301 nanofillers and 6 wt % CNTs showed an optimum separation performance by providing a CO_2 permeability of 19 Barrers with CO_2/N_2 selectivity of 48.

Chapter 6

Chapter 6 focuses on the synergistic effect of adding multiwalled CNTs and zeolitic imidazole frameworks (ZIF-302) into glassy polysulfone (PSF) to prepare mixed-matrix

membranes (MMMs) to separate CO_2 from post combustion flue gas stream. Varying loadings of both nanofillers were incorporated into PSF using solution-casting technique to optimize CO_2 separation performance of MMMs under dry and wet conditions. The flexible MMMs rendered homogeneous dispersion of fillers, improved polymer-filler adhesion, and thermally stable structure. Gas sorption analyses along with dry and wet gas permeation experiments demonstrated improved CO_2 permeability and CO_2/N_2 ideal selectivity of MMMs owing to collegial effect of nanofillers. The composite membrane containing 8 wt % CNTs and 12 wt % ZIF-302 nanofillers showed an optimum separation performance by providing a CO_2 permeability of 18 Barrers with CO_2/N_2 selectivity of 35. The permeation features of MMMs were slightly improved under humid conditions as compared to dry ones.

Chapter 7

Chapter 7 concludes the thesis by summarizing and proposing some recommendations to further extend the current research work.

References

[1] D. M. D'Alessandro, B. Smit, J. R. Long, Carbon Dioxide Capture: Prospects for New Materials, Angew. Chem. Int. Ed. 49 (2010) 6058-6082.

[2] M. Z. Jacobson, Review of Solutions to Global Warming, Air Pollution, and Energy Security, Energy Environ. Sci. 2 (2009) 148-173.

[3] N. MacDowell, N. Florin, A. Buchard, J. Hallett, A. Galindo, G. Jackson, C. S. Adjiman, C. K. Williams, N. Shah, P. Fennell, An Overview of CO_2 Capture Technologies, Energy Environ. Sci. 3 (2010) 1645-1669.

[4] H. Herzog, D. Golomb, Carbon capture and storage from fossil fuel use, Encyc. Energy 1 (2004) 277-287.

[5] A. Hussain, M.B. Hägg, A feasibility study of CO_2 capture from flue gas by a facilitated transport membrane, J. Membr. Sci. 359 (2010) 140-148.

[6] J. Zhao, Z. Wang, J.X. Wang, S.C. Wang, Influence of heat-treatment on CO_2 separation performance of novel fixed carrier composite membranes prepared by interfacial polymerization, J. Membr. Sci. 283 (2006) 346-356.

[7] P. Pandey, R.S. Chauhan, Membranes for gas separation, Prog. Polym. Sci. 26 (2001) 853-893.

[8] R. Mahajan, W.J. Koros, Factors controlling successful formation of mixed-matrix gas separation materials, Ind. Eng. Chem. Res. 39 (2000) 2692–2696.

[9] E.P. Fawas, G.C. Kapantaidakis, J.W. Nolan, A.C. Mitropoulos, N.K. Kanellopoulos, Preparation, characterization and gas permeation properties of carbon hollow fiber membranes based on Matrimid® 5218 precursor, J. Mater. Process. Technol. 186 (2007) 102–110.

[10] R.W. Baker, Future directions of membrane gas separation technology, J. Ind. Eng. Chem. Res. 41 (2002) 1393–1411.

[11] D.L. Gin, R.D. Noble, Designing the next generation of chemical separation membranes, Science 332 (2011) 674-676.

[12] Y. Xiao, T.-S. Chung, Grafting thermally labile molecules on cross-linkable polyimide to design membrane materials for natural gas purification and CO_2 capture. Energy Environ. Sci. 4 (2011) 201-208.

[13] C. Staudt-Bickel, W.J. Koros, Improvement of CO_2/CH_4 separation characteristics of polyimides by chemical crosslinking. J. Membr. Sci. 155 (1999) 145-154.

[14] T.C. Merkel, B.D. Freeman, R.J. Spontak, Z. He, I. Pinnau, P. Meakin, A. Hill, J. Ultrapermeable, reverse-selective nanocomposite membranes, Science 296 (2002) 519-522.

[15] J. Ahn, W.-J. Chung, I. Pinnau, M.D. Guiver, Polysulfone/silica nanoparticle mixed-matrix membranes for gas separation, J. Membr. Sci. 314 (2008) 123-133.

[16] B.D. Reid, A. Ruiz-Trevino, I.H. Musselman, K.J. Balkus, J.P. Ferraris, Gas permeability properties of polysulfone membranes containing the mesoporous molecular sieve MCM-41, Chem. Mater. 13 (2001) 2366-2373.

[17] S. Kim, E. Marand, J. Ida, V.V. Guliants, Polysulfone and mesoporous molecular sieve MCM-48 mixed matrix membranes for gas separation, Chem. Mater. 18 (2006) 1149-1155.

[18] S. Kim, E. Marand, High permeability nano-composite membranes based on mesoporous MCM-41 nanoparticles in a polysulfone matrix, Microp. Mesop. Mater. 114 (2008) 129-136.

[19] D.Q. Vu, W.J. Koros, S.J. Miller, Mixed matrix membranes using carbon molecular sieves. II. Modeling permeation behavior, J. Membr. Sci. 211 (2003) 335-348.

[20] H.L. Cong, J.M. Zhang, M. Radosz, Y.Q. Shen, Carbon nanotube composite membranes of brominated poly(2,6-diphenyl-1,4-phenylene oxide) for gas separation, J. Membr. Sci. 294 (2007) 178–185.

[21] S. Kim, L. Chen, J.K. Johnson, E. Marand, Polysulfone and functionalized carbon nanotube mixed matrix membranes for gas separation: Theory and experiment, J. Membr. Sci. 294 (2007) 147–158.

[22] P. Gorgojo, S. Uriel, C. Tellez, J. Coronas, Development of mixed matrix membranes based on zeolite Nu-6(2) for gas separation, J. Microporous Mesoporous Mater. 115 (2008) 85–92.

[23] Y. Liu, D. Peng, G. He, S. Wang, Y. Li, H. Wu, Z. Jiang, Enhanced CO_2 permeability of membranes by incorporating polyzwitterion@CNT composite particles into polyimide matrix, ACS Appl. Mater. Interfaces 6 (2014) 13051-13060.

[24] B. Harold, T. Jeazet, C. Staudt, C. Janiak, Metal–organic frameworks in mixed-matrix membranes for gas separation, Dalton Trans. 41 (2012) 14003–14027.

[25] T. Li, Y. Pan, K.V. Peinemann, Z. Lai, Carbon dioxide selective mixed matrix composite membrane containing ZIF-7 nano-fillers, J. Membr. Sci. 425–426 (2013) 235–242.

[26] Chen Zhang, Kuang Zhang, Liren Xu, Ying Labreche, Brian Kraftschik, W.J. Koros, Highly scalable ZIF-based mixed-matrix hollow fiber membranes for advanced hydrocarbon separations, AIChE J. 60 (2014) 2625–2635.

[27] Mohammad Askari, T.S. Chung, Natural gas purification and olefin/paraffin separation using thermal cross-link ableco-polyimide/ZIF-8 mixed matrix membranes, J. Membr. Sci. 444 (2013) 173–183.

[28] T.T.N. Nhung, H. Furukawa, F. Gandara, H.T. Nguyen, K.E. Cordova, O.M. Yaghi, Selective capture of carbon dioxide under humid conditions by hydrophobic chabazite-type zeolitic imidazolate frameworks, Angew. Chem. 126 (2014) 10821–10824.

[29] H. Chen, D.S. Sholl, Predictions of selectivity and flux for CH_4/H_2 separations using single walled carbon nanotubes as membranes, J. Membr. Sci. 269 (2006) 152–160.

[30] D.S. Sholl, J.K. Johnson, Making high-flux membranes with carbon nanotubes, Science 312 (2006) 1003–1004.

[31] A.I. Skoulidas, D.S. Sholl, J.K. Johnson, Adsorption and diffusion of carbon dioxide and nitrogen through single-walled carbon nanotube membranes, J. Chem. Phys. 124 (2006) 054708.

[32] S. Kim, J.R. Jinschek, H. Chen, D.S. Sholl, E. Marand, Scalable fabrication of carbon nanotube/polymer nanocomposite membranes for high flux gas transport, Nano Lett. 7 (2007) 2806–2811.

[33] T.W. Chamberlain, J.C. Meyer, J. Biskupek, J. Leschner, A. Santana, N.A. Besley, E. Bichoutskaia, U. Kaiser, A.N. Khlobystov, Reactions of the inner surface of carbon nanotubes and nanoprotrusion processes imaged at the atomic scale, Nat. Chem. 3 (2011) 732–737.

[34] A.F. Ismail, P.S. Goh, S.M. Sanip, M. Aziz, Transport and separation properties of carbon nanotube-mixed matrix membrane, Sep. Purif. Technol. 70 (2009) 12–26.

[35] L. Ge, L. Wang, V. Rudolph, Z. Zhu, Hierarchically structured metal-organic framework/vertically-aligned carbon nanotubes hybrids for CO_2 capture, RSC Adv. 3 (2013) 25360–25366.

[36] B. Zornoza, B. Seoane, J. M. Zamaro, C. Téllez and J. Coronas, Combination of MOFs and zeolites for mixed-matrix membranes, Chem-PhysChem, 12 (2011) 2781–2785.

[37] M. Valero, B. Zornoza, C. Téllez, J. Coronas, Mixed matrix membranes for gas separation by combination of silica MCM-41 and MOF NH2-MIL-53 (Al) in glassy polymers, Microporous Mesoporous Mater. 192 (2013) 23–28.

[38] A. Galve, D. Sieffert, C. Staudt, M. Ferrando, C. Güell, C. Téllez, J. Coronas, Combination of ordered mesoporous silica MCM-41 and layered titanosilicate JDF-L1 fillers for 6FDA-based copolyimide mixed matrix membranes, J. Membr. Sci. 431 (2013) 163-170.

[39] X. Li, L. Ma, H. Zhang, S. Wang, Z. Jiang, R. Guo, H. Wu, X.Z. Cao, J. Yang, B. Wang, Synergistic effect of combining carbon nanotubes and grapheme oxide in mixed matrix membranes for efficient CO_2 separation, J. Memb. Sc. 479 (2015) 1-10.

CHAPTER 2

WATER-STABLE ZIF-300/POLYSULFONE MIXED-MATRIX MEMBRANES FOR SELECTIVE CO_2 SEPARATION FROM HUMID POST COMBUSTION FLUE GASES

Abstract

Water stable mixed-matrix membranes (MMMs) were prepared by incorporating microporous crystalline nanoparticles of zeolitic imidazole framework (ZIF-300) into glassy polysulfone (PSF) matrix using solution mixing technique. Different loading levels of ZIF-300 nanocrystals in PSF were tried to determine the separation efficiency of MMMs to separate carbon dioxide from a mixture of dry and humid gases. Hydrothermally stable flexible MMMs exhibiting homogeneous dispersion and good adhesion of ZIF-300 nanoparticles with polymer matrix were characterized by x-ray diffraction (XRD), scanning electron microscopy (SEM), and thermal gravimetric analysis (TGA). Pure gas sorption studies coupled with dry and wet gas permeation tests demonstrated that CO_2 permeability of MMMs were enhanced by four times compared to that of pure PSF while retaining most of the CO_2/N_2 ideal selectivity.

2.1 Introduction

Global warming caused by carbon dioxide (CO_2) gas emissions from burning of fossil fuels has turned out to be a severe environmental issue throughout the globe [1-3]. CO_2 emissions can be reduced by its capture or sequestration via economically feasible methods [4-5]. As compared to other conventional processes, polymer-based mixed-matrix membrane (MMM) gas separation technology has received significant consideration on account of its low capital and operating costs, high efficiency, low energy requirement, simple function, flexible design, ease of scale up, and environmental kindliness [6-13].

The key parameters of a superior quality gas separation membrane include improved permselectivity and separation factor, good mechanical strength, improved chemical and thermal stability, and good operational stability [14-20]. Due to its inherent structural constraints (chain mobility and inter-chain spacing), a glassy polymer membrane being highly permeable is generally less selective [15, 21-23]; it requires considerable improvements for practical applications.

To formulate efficient hybrid membranes having improved permselectivity characteristics as compared to unfilled polymer membranes, a lot of glassy polymers have been tailored to develop MMMs by incorporating inorganic fillers like nonporous silica [24-25], structured mesoporous silica [26-28], carbon molecular sieves [29], carbon nanotubes [30-31], zeolites [32], and microporous metal organic frameworks (MOFs) [33]. Some key benefits of MMMs made by incorporating microporous MOF or ZIF crystals into polymer matrix include the ability to integrate the ease of fabrication and processability, improved mechanical and chemical stability of polymers coupled with exceptional gas

separation characteristics of microporous crystalline materials possessing tunable pore size, modifiable surface functionality, and high surface areas [34].

Polysulfone membrane, commonly used for CO_2 separation, has gained substantial research interest on account of its high permselectivity values [34]. Effective approaches to enhance CO_2 permeability of a polymer membrane include either its chemical modification or preparation of a hybrid membrane by incorporation of microporous particles into the polymer. Car et al. (2006) reported the development of HKUST-1/PSF MMMs by incorporating varying loadings of HKUST-1 into glassy polysulfone [35]. The CO_2 permeability of the MMMs gradually enhanced with increasing HKUST-1 contents up to 10 % by weight. The CO_2/N_2 selectivity improved with HKUST-1 loadings, reached a maximum value of 25 at 5 wt % loading, and then started decreasing with further addition of HKUST-1. Zornoza and coworkers (2009) developed MMMs by incorporating mesoporous silica spheres into polysulfone Udel® matrix up to a maximum loading of 32 % by weight; the optimum CO_2/N_2 selectivity was obtained at 8 wt % HKUST-1 loading [36]. Various combinations of MOFs (HKUST-1), ZIFs (ZIF-8) and zeolites (S1C) were incorporated into PSF to develop different MMMs for gas permeation of CO_2, N_2, CH_4, O_2, and H_2 [37]. The CO_2/N_2 separation efficiency did not improve for S1C-ZIF-8/PSF MMMs. The CO_2 permeabilities of S1C/PSF, HKUST-1/PSF, ZIF-8/PSF and HKUST-1/ZIF-8/PSF MMMs were found to be 9.4, 9.5, 12.3 and 8.4 Barrers respectively with corresponding CO_2/N_2 selectivities of 23, 24, 19 and 38. CO_2 permeability of MIL-101(Cr)/PSF membranes developed by Harold et al. (2013) increased linearly with MIL-101(Cr) loading while CO_2/N_2 ideal selectivity was slightly improved with MIL-101(Cr) contents [38].

ZIF-300, a hydrothermally stable microporous crystalline material [39], is highly capable to selectively capture CO_2 gas under real post combustion conditions. A typical flue gas contains 75% N_2, 15% CO_2, 6% H_2O and 4% trace gases by volume [40]. In the present study ZIF-300 nanocrystals have been incorporated into glassy polysulfone matrix for the first time to develop ZIF-300/PSF MMMs to efficiently enhance CO_2 separation performance. The main objective of this study is to check the effect of moisture contents on permselectivity values of ZIF-300/PSF MMMs with increasing ZIF-300 contents by performing the permeation tests under dry and wet conditions. The experimentally obtained gas permeation data were assessed using two- and three-phase permeation models.

2.2 Experimentation and Data Validation

2.2.1 Materials

Commercially available polysulfone, having density 1.25 g cm^{-3} and average molecular weight ~ 35000 by LS, was obtained from Sigma Aldrich. Zinc nitrate tetrahydrate and 2-methylimidazole were obtained from Merck Chemical Company. 5(6)-chlorobenzimidazole and solvent N,N-dimethylformamide (DMF) were obtained from Aldrich Chemical Company. Organic solvents such as anhydrous methanol (for ZIF-300 washing) and chloroform (for polymer dissolution) were obtained from Fisher Scientific. The polymer and chemicals were used as received without any additional treatment. Highly pure CO_2, N_2 and He gases were used for gas sorption and permeation experiments.

2.2.2 Synthesis of ZIF-300 nanocrystals

ZIF-300 nanocrystals were synthesized via cold synthesis procedure by slightly modifying the process conditions originally report by Nhung T. et al. [39]. 67.8 mg of $Zn(NO_3)_2 \cdot 6H_2O$ (the metal salt), 23.4 mg of 2-methylimidazole (primary organic linker), and 43.6 mg of 5(6)-chlorobenzimidazole (secondary organic linker) were dissolved in a mixture of 9.5 mL DMF and 0.5 mL distilled water by sonication in a 20-mL vial for 10 minutes. The resulting mixture was then moderately stirred on a hot plate at 50 °C for 70 hours to obtain light brown suspension. The suspended nanocrystals were separated from the mother liquor by centrifuge and daily washed with 7 mL of fresh DMF followed by solvent exchange with anhydrous methanol thrice a day at room temperature for 3 days. After decanting spent methanol, ZIF-300 nanocrystals were washed three times with chloroform, and lastly redispersed in fresh chloroform to incorporate them into polymer matrix to prepare MMMs of varying compositions.

2.2.3 Preparation of ZIF-300/PSF MMMs

To prepare bare PSF membrane and ZIF-300/PSF MMMs, PSF was degassed at 100 ^{o}C under vacuum for 5 h to remove any adsorbed gas or moisture. Bare polymer membrane was fabricated by dissolving 500 mg of PSF into 5 mL of chloroform followed by stirring at room temperature for 24 hours until a thick viscous solution was formed. The MMMs containing 10, 20, 30 and 40 weight % ZIF-300 nanocrystals were prepared by redispersing a weighed quantity of ZIF-300 nanocrystals in 5 mL of chloroform for 10 minutes, adding weighed quantity of PSF into the system, and stirring the whole mixture for 24 hours. All the membranes were knife casted on clean glass plates at a fixed gate

height using Flat Sheet Membrane Casting System (FSMCS). After slowly evaporating the solvent under ambient conditions overnight, the membranes were detached from the glass plates and placed in a VO 200 vacuum oven at 100 ^{o}C under a pressure of 10 mbar for 24 hours to ensure complete removal of the remaining solvent before subjecting it to gas permeation tests.

2.2.4 Material Characterization Methods

The ZIF-300 nanocrystals, bare polysulfone membrane and ZIF-300/PSF mixed-matrix membranes were characterized by x-ray diffraction, scanning electron microscopy, thermogravimetric analysis, and gas sorption measurement techniques. The fractional volume (Φ_D expressed in %) of ZIF-300 in MMMs can be defined as:

$$\Phi_D = \frac{(m_D/\rho_D)}{(m_D/\rho_D)+(m_C/\rho_C)} \times 100 \qquad (1)$$

where m and ρ represent mass and density of PSF (continuous phase denoted by subscript C) and ZIF-300 (dispersed phase denoted by subscript D) respectively. Normally the void volume of MMMs is negligible as supported by SEM images and gas sorption analysis. Hence the apparent volume fraction can safely be considered as the exact volume fraction of ZIF-300 in MMMs.

Powder x-ray diffraction patterns of ZIF-300 nanocrystals, bare PSF and ZIF-300/PSF MMMs were performed using a Bruker D8 X-ray diffractometer using Cu Kα radiation (λ = 1.5406 Å) run at 45 mA and 40 kV with an increment of 0.02^{o} in 2θ and a step scan size of 0.02^{o} s^{-1}. The membrane sample was loaded on silicon substrate placed in a

sample holder. The MMMs were characterized by XRD to check whether the polymeric matrix alters the crystalline pattern of ZIF-300 or not.

Scanning electron microscopy images of all the samples were taken to explore the morphology of ZIF-300 nanocrystals, bare PSF membrane and MMMs having different ZIF-300 loadings by Hitachi S-4300SE/N SEM instrument. Testing specimens were cryofractured in liquid nitrogen and their outer surfaces were covered with a thin gold film to avoid charging of electrons. The SEM machine was operated at an accelerating voltage of 20 kV.

Glass transition temperature (T_g) of ZIF-300 nanocrystals, bare PSF membrane and their MMMs were assessed by thermal gravimetric analysis by using a TGA/SDTA 851 (Mettler Toledo) system in air by heating from ambient temperature to 700 ^{o}C at a rate of 10 ^{o}C min^{-1}.

Nitrogen and carbon dioxide adsorption isotherms measured at different temperatures using a Quantachrome Autosorb iQ gas sorption analyzer helped in determining various characteristics (e.g., specific BET and Langmuir surface areas, total microporous volume, CO_2 and N_2 gas uptakes) of ZIF-300 microporous particles, PSF membrane and their composite membranes. The membrane samples were cut into small pieces and degassed at 100 ^{o}C under vacuum (<10^{-6} bar) for 5 hours. Physisorption data of CO_2 and N_2 gases were measured at 298 K under a gas pressure ranging from 10^{-6} -1 bar.

2.2.5 Gas Permeation Measurements

Pure gas (CO_2 and N_2) transport properties (i.e., permeability, ideal selectivity, and separation factor) of the membranes were estimated using single gas permeation cell

following the variable pressure (constant volume) method at room temperature [41-42]. After measuring its average thickness and effective cross sectional area, the membrane was affixed into the cell. While keeping the feed side valve closed, both the upstream (feed side) and downstream (permeate side) lines of the cell were evacuated. The valve between the permeate side line and the vacuum pump was then closed followed by opening the feed side valve to maintain a low feed pressure (e.g., 2 bars) for a specific time (i.e., 2 h) to record the permeation measurements after stabilization. In order to estimate error and identify imperfect membranes, at least three replicas were prepared and tested corresponding to each composition of the MMMs.

Gas permeability (P_i, *Barrer*) of the membrane was computed using eq. (2):

$$P_i = \frac{22414}{A} \times \frac{V}{RT} \times \frac{l}{\Delta P_i} \frac{dP_i}{dt} \qquad (2)$$

where *l, A, V, R, T,* ΔP and $\Delta P_i/dt$ are respectively membrane thickness (*cm*), membrane effective area (cm^2), downstream volume (cm^3), universal gas constant (6236.56 cm^3 *cmHg/mol/K*), absolute temperature (*K*), pressure difference across the membrane (*psi*), and permeation rate (*psi/s*) of component i.

Time-lag method, suggested by Paul and Kemp [43], was used to determine diffusion coefficient (D) by using *diffusivity vs. time-lag* (D-θ) relationship for MMMs:

$$D = \frac{l^2}{6\theta}\left[1 + \frac{6K}{y^3}\left\{\frac{y^2}{2} + y - (1+y)\ln(1+y)\right\}\left(\frac{V_d}{V_p}\right)\right] \qquad (3)$$

where V_d and V_p are respectively the volume fractions of filler and polymer phases; K and y are adsorption parameters determined from Langmuir adsorption isotherm.

The solubility coefficient (S) can be calculated from Eq. (4):

$$S = \frac{P}{D} \qquad (4)$$

The ideal selectivity (α_{ij}) for gases i and j can be determined using Eq. (5):

$$\alpha_{ij} = \frac{P_i}{P_j} = \left(\frac{D_i}{D_j}\right)\left(\frac{S_i}{S_j}\right) \qquad (5)$$

Here (D_i/Dj) and (S_i/S_j) represent diffusion- and solubility-based selectivity terms respectively.

2.2.6 Modeling in ZIF-300/PSF MMMs

Analogous to electrical/thermal conductivity models through composite materials, several hypothetical models [44-46] have been proposed to estimate gas permeation through ideal and non-ideal morphology of MMMs. A two-phase system comprising continuous polymer matrix and dispersed inorganic filler particles constitutes an ideal morphology without any distortion and defect at the polymer-filler interface. Occurrence of defects and imperfections at organic-inorganic interface leads to a three-phase non-ideal morphology which addresses the polymer-filler interface in addition to matrix and filler phases. The two-phase permeation models to predict gas permeability through MMMs can be presented by the following expressions.

Maxwell:
$$P_r = \frac{1 + 2\phi\left(\frac{\lambda_{dm} - 1}{\lambda_{dm} + 2}\right)}{1 - \phi\left(\frac{\lambda_{dm} - 1}{\lambda_{dm} + 2}\right)} \quad (6)$$

Bruggeman:
$$P_r^{\frac{1}{3}}\left(\frac{\lambda_{dm} - 1}{\lambda_{dm} - P_r}\right) = (1 - \Phi)^{-1} \quad (7)$$

Singh:
$$P_r = 1 + 3.74\left(\frac{\lambda_{dm} - 1}{\lambda_{dm} + 2}\right)\Phi^{2/3} \quad (8)$$

where

$$P_r = \frac{P_{eff}}{P_m} = \frac{Effective\ permeability\ of\ MMM}{Permeability\ of\ polymer\ matrix}$$

$$\lambda_{dm} = \frac{P_d}{P_m} = \frac{Permeability\ of\ dispersed\ phase}{Permeability\ of\ polymer\ matrix}$$

$$\Psi = 1 + \left(\frac{1 - \Phi_m}{\Phi_m^2}\right)\Phi$$

$\Phi_m = volume\ fraction\ of\ fillers\ at\ maximum\ packing = 0.64$

Φ = volume fraction of fillers

The three-phase modified Felske model can be expressed as follows.

Modified Felske:
$$P_r = \frac{1 + \frac{2\Phi(\beta - \gamma)}{(\beta + 2\gamma)}}{1 - \frac{\Phi\Psi(\beta - \gamma)}{(\beta + 2\gamma)}} \quad (9)$$

where

$$\beta = (2 + \delta^3)\lambda_{dm} - 2(1 - \delta^3)\lambda_{im}$$

$$\gamma = 1 + 2\delta^3 - (1 - \delta^3)\lambda_{di}$$

$$\lambda_{di} = \frac{P_d}{P_i} = \frac{Permeability\ of\ dispersed\ phase}{Permeability\ of\ interphase}$$

$$\lambda_{im} = \frac{P_i}{P_m} = \frac{Permeability\ of\ interphase}{Permeability\ of\ matrix\ phase}$$

$$\lambda_{dm} = \lambda_{di}\lambda_{im} = \frac{\beta}{\gamma}$$

$$\delta = ratio\ of\ the\ interphase\ radius\ to\ the\ particle\ radius$$

2.3 Results and discussion

The end results of different characterization techniques i.e., XRD, SEM, TGA, gas sorption and gas permeation are briefly described here.

2.3.1 Powder X-ray Diffraction

Powder x-ray diffraction is a good practice to confirm the existence of crystalline particles in amorphous matrices. XRD measurements ranging from 2^o to 50^o were

recorded to determine and confirm the existence of ZIF-300 crystalline structure in composite membranes. For microporous ZIF-300 nanocrystals, the peak intensities appearing at angles of 10.6^{o}, 13.1^{o} and 22.8^{o} correspond to its trigonal crystal structure [Fig. 2.1].

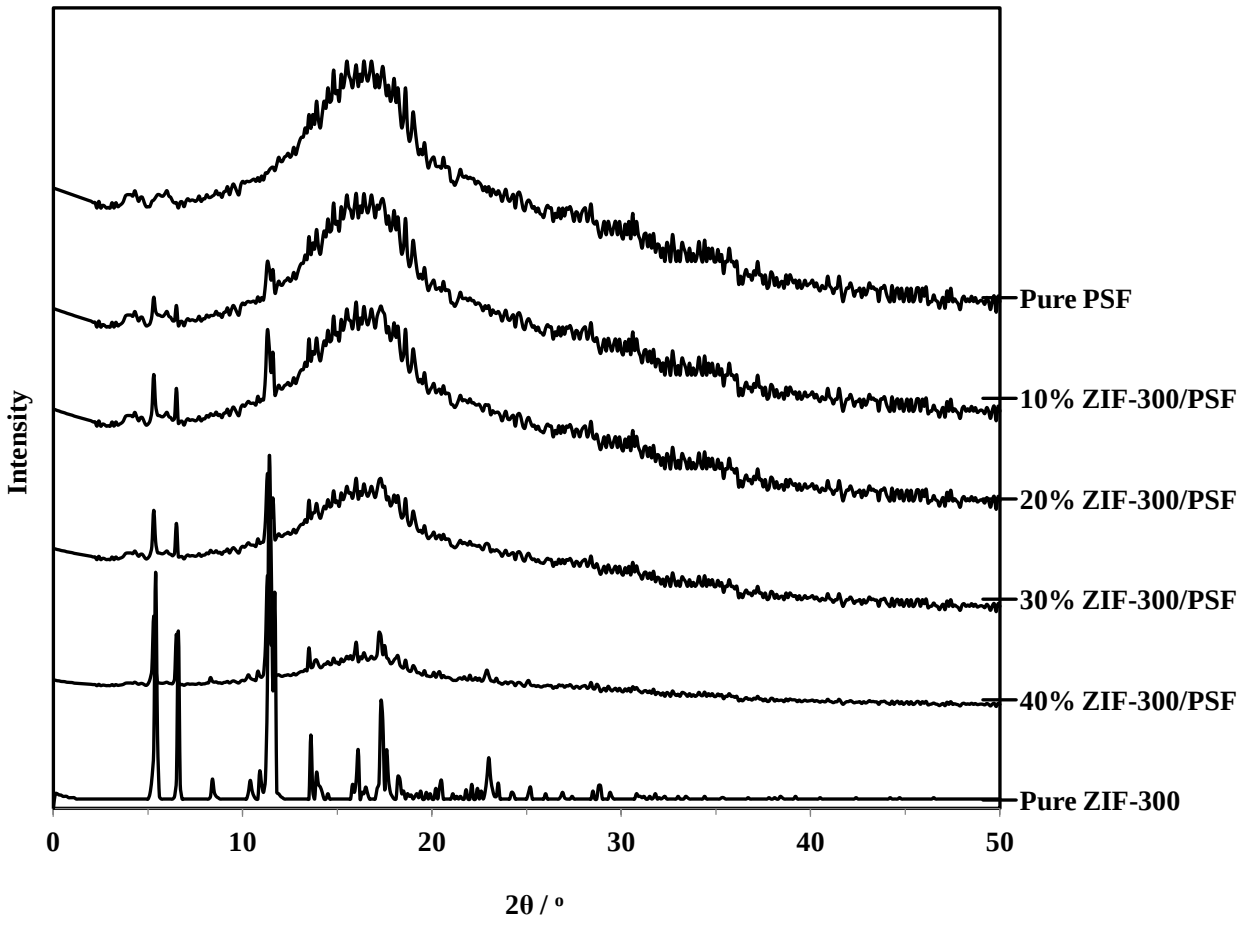

Fig. 2.1 XRD patterns of pure ZIF-300, pure PSF, and ZIF-300/PSF MMMs containing 10, 20, 30 and 40 % by weight of ZIF-300

The fine coincidence of XRD patterns of MMMs with those of pure ZIF-300 nanocrystals suggests the preservation of ZIF-300 crystal structure even after their incorporation into the polymer matrix. Furthermore the slight shift of broad peak position (2θ) of neat PSF from 17.3° (d-spacing = 5.1 Å) to ~ 17.1° (d-spacing = 5.15 Å) can be attributed to the filler-polymer interaction thus altering the polymer inter-chain distance. Also the addition of ZIF-300 contents in different MMMs successively heightens their corresponding peak intensities at the specified 2θ positions.

2.3.2 Morphology of ZIF-300/PSF MMMs

The morphology and structural characteristics of the MMMs strongly depend on the nature of organic polymer matrix and the incorporated inorganic filler. Generally the glassy polymers exhibit an inflexible structure, usually create interfacial voids between the two phases, and influence the free volume of MMMs. To explore the morphology, adhesion and dispersion of ZIF-300 particles within the polymer matrix, surface and cross sectional micrographs of the membranes were probed by SEM as depicted in Fig. 2.2. Continuous ZIF-300/PSF phases are obtained for all MMMS having different loadings of the filler. Owing to their fairly tiny particle size the dispersion of trigonal ZIF-300 nanocrystals is reasonably uniform and homogeneous (Fig. 2.2), sparse on 10 wt % ZIF-300 loading (Fig. 2.2 B), and a minute aggregation and slightly rough cross section in 40 wt % ZIF-300/PSF MMM (Fig. 2.2 E). In addition, the interfacial voids are absent in all the MMMs. The ZIF-300 nanocrystals demonstrated excellent interfacial adhesion and contact with PSF matrix as the cross sectional view of MMMs exhibits defect-free interconnected network morphology.

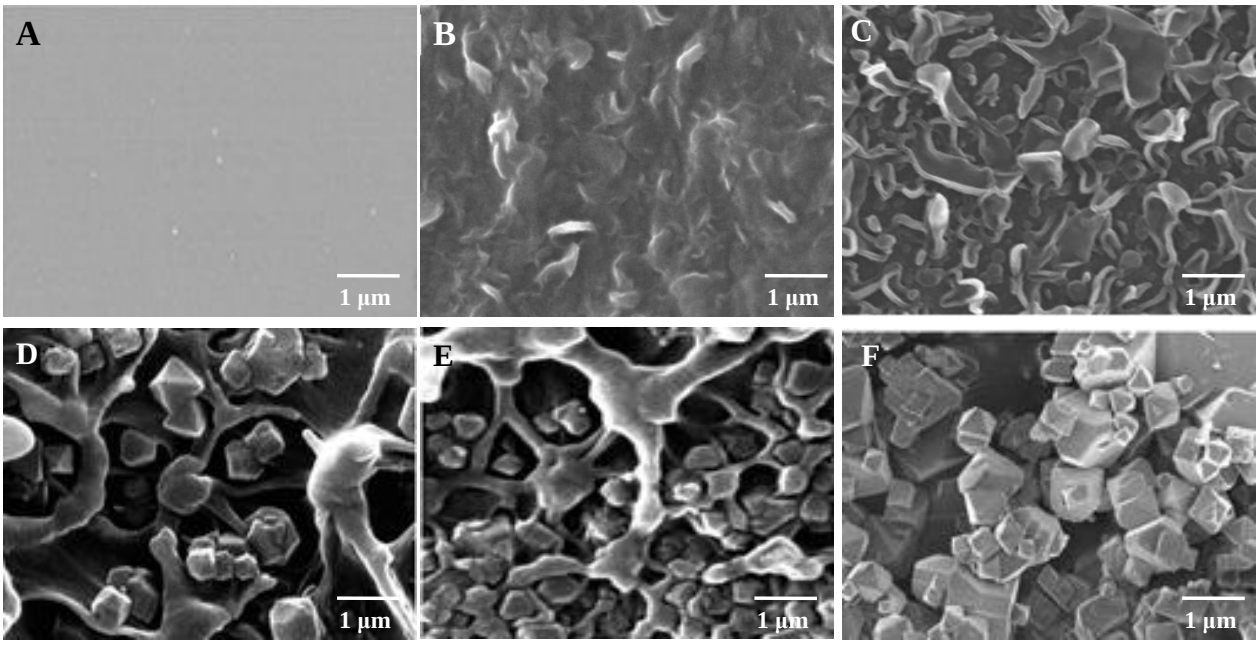

Fig. 2.2 Scanning electron micrographs of pure ZIF-300 [F], pure PSF [A], and ZIF-300/PSF MMMs containing 10 [B], 20 [C], 30 [D] and 40 [E] % by weight of ZIF-300

2.3.3 Thermal Gravimetric Analysis

In order to study their thermal stability, phase transitions, physical and chemical phenomena, TGA-DTG analyses of ZIF-300 nanocrystals, bare PSF membrane, and ZIF-300/PSF MMMs having different loadings were conducted from room temperature to a final temperature of 700 ^{o}C. The TGA curves of the prepared samples indicate a two step weight loss at around 100-200 ^{o}C (desolvation) and 510-640 ^{o}C (pyrolysis) as depicted in Fig. 2.3 (A). The weight loss corresponding to first peak can be attributed to the liberation of volatile solvent molecules (water, DMF, CCl_4 etc.) trapped within the pores of ZIF-300 and PSF. The weight loss related to second peak can be attributed to the decomposition of organic ligands (2-methylimidazole and 5(6)-bromobenzimidazole) of the imidazole framework and complete degradation of PSF constituting entities (benzene,

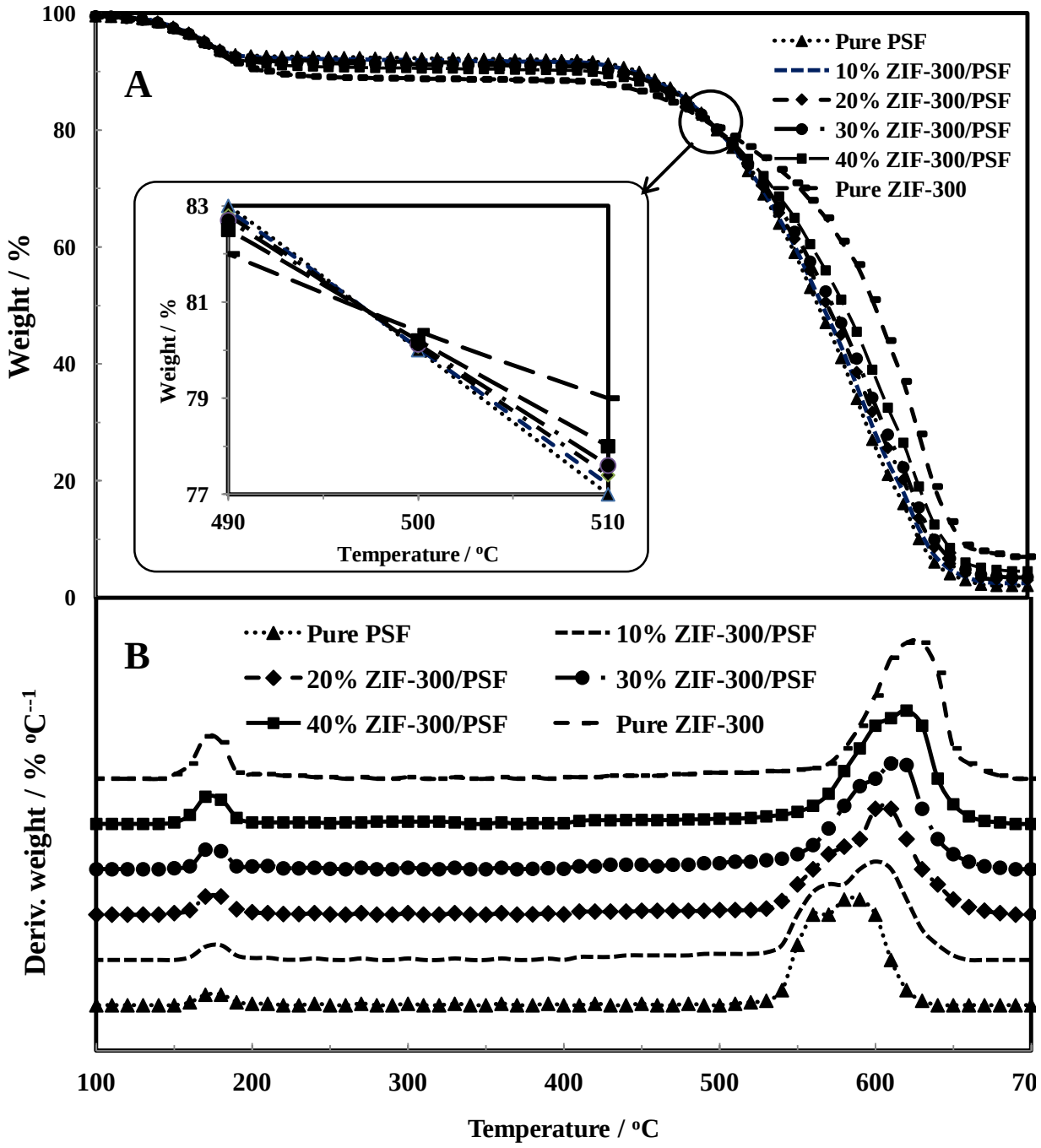

Fig. 2.3 TGA-DTG curves: TGA (A) and DTG (B) of pure ZIF-300, pure PSF, and ZIF-300/PSF MMMs containing 10, 20, 30 and 40 % by weight of ZIF-300

SO_2, phenol, toluene, styrene, xylene etc.). The residual weight at the end of analyses helped to verify the nominal mass contents of the filled ZIF-300 nanocrystals in corresponding MMMs.

The temperatures at which testing specimen loses its 5 and 10 percent weight, denoted by $T_{d5\%}$ and $T_{d10\%}$ respectively, in TGA analysis determine the thermal stability of a material [47]. Table 2.1 summarizes some important thermal parameters of the synthesized materials. Both parameters being decreasing function of ZIF-300 contents, values of $T_{d5\%}$ and $T_{d10\%}$ occur between 165-175 °C and 210-450 °C respectively. The DTG curves illustrated in Fig. 2.3 (B) also give information on pyrolysis rates; the residual masses of all the materials are enlisted in Table 2.1.

Table 2.1 Characteristic temperatures of membrane materials acquired from TGA-DTG data

Sample Designation	**$T_{d5\%}$** (^oC)	**$T_{d10\%}$** (^oC)	**Residual mass** (%)	**1st DTG peak** (^oC)	**2nd DTG peak** (^oC)
Pure PSF	175	450	1.9	176	583
10% ZIF/PSF	173	444	2.5	173	597
20% ZIF/PSF	171	441	3.1	171	604
30% ZIF/PSF	170	436	3.6	169	609
40% ZIF/PSF	168	420	4.5	167	617
Pure ZIF	165	212	7.2	165	626

As indicated by weight loss curves the thermal stability of MMMs, determined in terms of 2nd DTG peaks, improved with increasing ZIF-300 contents. Since the maximum temperature experienced in different gas separation and combustion processes falls in the range of 30 to 500 °C, these MMMs can safely be used in gas separation applications [48]. Also the advancement in glass transition temperature (T_g) and rigidity of MMMs with increased ZIF loadings can be associated with the constrained motion of polymer chains owing to mutual interactions occurring among polymer chains and ZIF-300 microporosity.

2.3.4 Gas Sorption Analysis

Low pressure CO_2 and N_2 adsorption isotherms with increasing pressure up to 1 bar were measured at 298 K for ZIF-300 nanocrystals, bare PSF membrane, and ZIF-300/PSF MMMs containing varying contents of ZIF-300 nanocrystals (see Fig. 2.4). Main macroscopic properties (density, ZIF fractional volume) and microporous characteristics such as Brunauer-Emmett-Teller (S_{BET}) and Langmuir (S_{Lang}) surface areas, total micropore volume, CO_2 and N_2 uptakes, and CO_2/N_2 adsorption selectivity, of the specimen are enhanced with ZIF-300 loading as summarized in Table 2.2. These findings directly validate excellent adhesion, homogeneous dispersion and flawless interfaces between ZIF-300 nanoparticles and PSF matrix leading to good quality membranes.

CO_2 uptake for all the samples appreciably increased with pressure due to the chemical affinity of chabazite-topologic ZIF-300 frameworks for quadro-polar CO_2 molecules. The CO_2 loading rate successively declined with increasing adsorption pressure: CO_2 adsorption rate with pressure was fastest in the very low pressure region ~ 0-0.1 bar, went

on decreasing in the pressure range of ~ 0.1-0.5 bar, and further reduced in the pressure range of ~ 0.5-1 bar. Pure ZIF-300 had the highest CO2 loading ca. 27 cm^3/g (≈1.3 mmol/g) at 25 ^oC which can be increased by lowering the temperature. The N_2 adsorption isotherms for all the materials almost followed a proportional correlation with pressure up to 1 bar. In addition all the samples showed preferably high adsorption affinity for CO_2 as compared to N_2, especially at low CO_2 partial pressure. The CO_2/N_2 sorption selectivities of the MMMs gradually increased with PSF contents. These facts suggest potential applications for the separation of CO_2/N_2 mixture from post combustion flue gases.

Table 2.2 Microporous properties of ZIF-300, PSF, and ZIF-300/PSF MMMs

Sample Designation	**Density** ($g\ cm^{-3}$)	**Φ_d** (%)	**S_{BET}** (m^2g^{-1})	**S_{Lang}** (m^2g^{-1})	**V_{micro}** (m^3g^{-1})	**CO_2 uptake** ($cm^3\ g^{-1}$)	**N_2 uptake** ($cm^3\ g^{-1}$)	**CO_2/N_2 selectivity**
Pure PSF	1.25	0	10	19.7	0.019	4.3	0.23	18
10% ZIF/PSF	1.27	8.68	50	60	0.071	6.4	0.28	23
20% ZIF/PSF	1.28	17.48	90	110	0.123	8.6	0.33	26
30% ZIF/PSF	1.30	26.40	130	160	0.175	10.8	0.38	28
40% ZIF/PSF	1.31	35.46	170	200	0.228	12.8	0.41	32
Pure ZIF	1.45	100	400	470	0.538	26.4	1.18	22

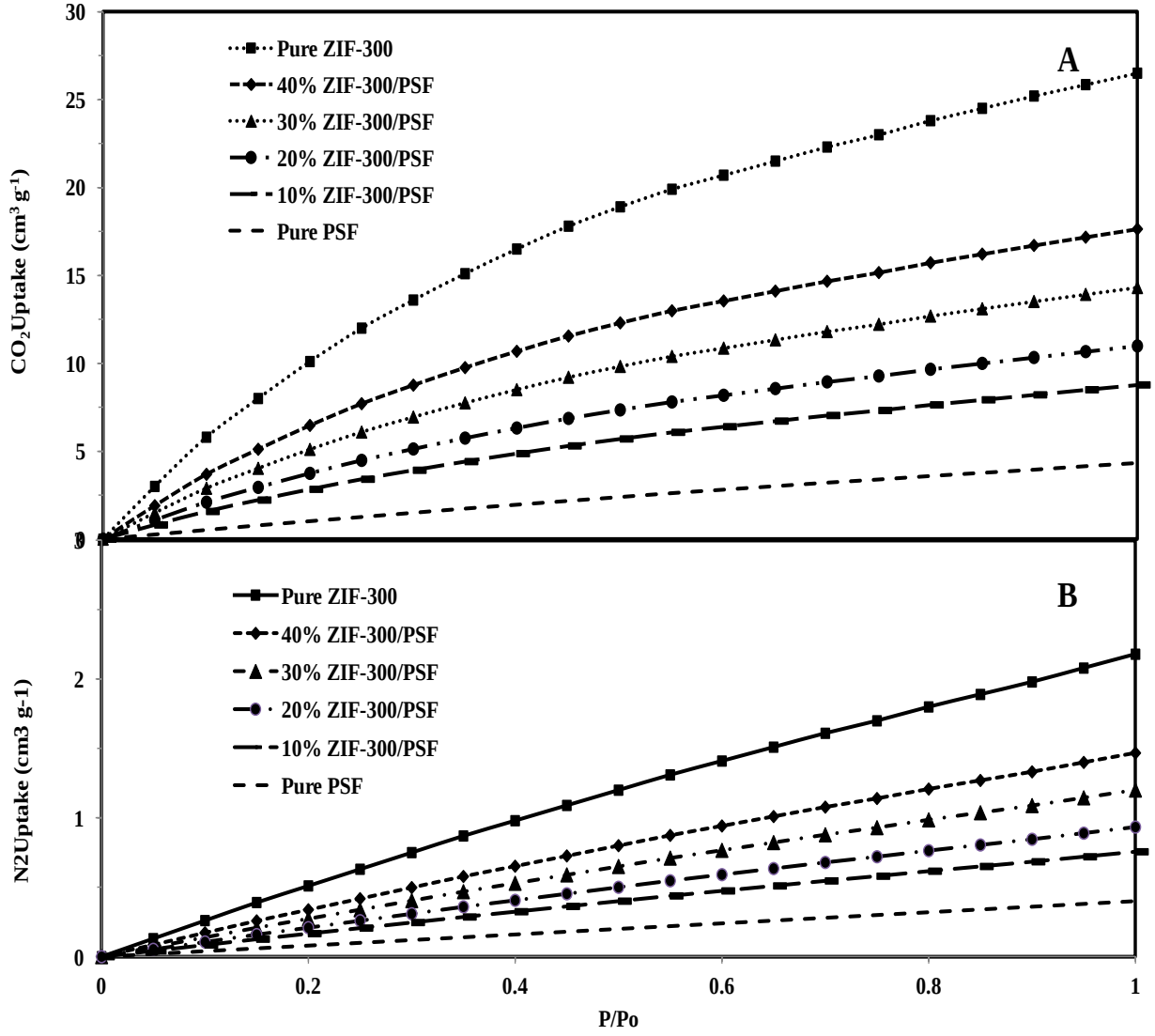

Fig. 2.4 CO_2 and N_2 adsorption isotherms for pure ZIF-300, pure PSF, and ZIF-300/PSF MMMs containing 10, 20, 30 and 40 % by weight of ZIF-300 at 298 ^{o}C

2.3.5 Gas Permeation Properties of MMMs

2.3.5.1 Dry and Wet gas permeation. Single gas (CO_2 and N_2) dry and wet permeation experiments for ZIF-300/PSF MMMs containing different ZIF-300 loadings were performed at 25 °C under an upstream pressure of 2 bar. Owing its strong affinity for

ZIF-300 microporous crystals, CO_2 permeability values of the MMMs were substantially enhanced with increasing ZIF-300 contents as represented in Fig. 2.5. The CO_2/N_2 ideal selectivity values stay almost unaffected by the incorporation of ZIF-300 nanocrystals into PSF. The permeation experiments accomplished using humid gases did not significantly affect the transport properties of CO_2 and N_2 on account of strong ZIF-300/PSF interfacial adhesion and homogeneous filler dispersion.

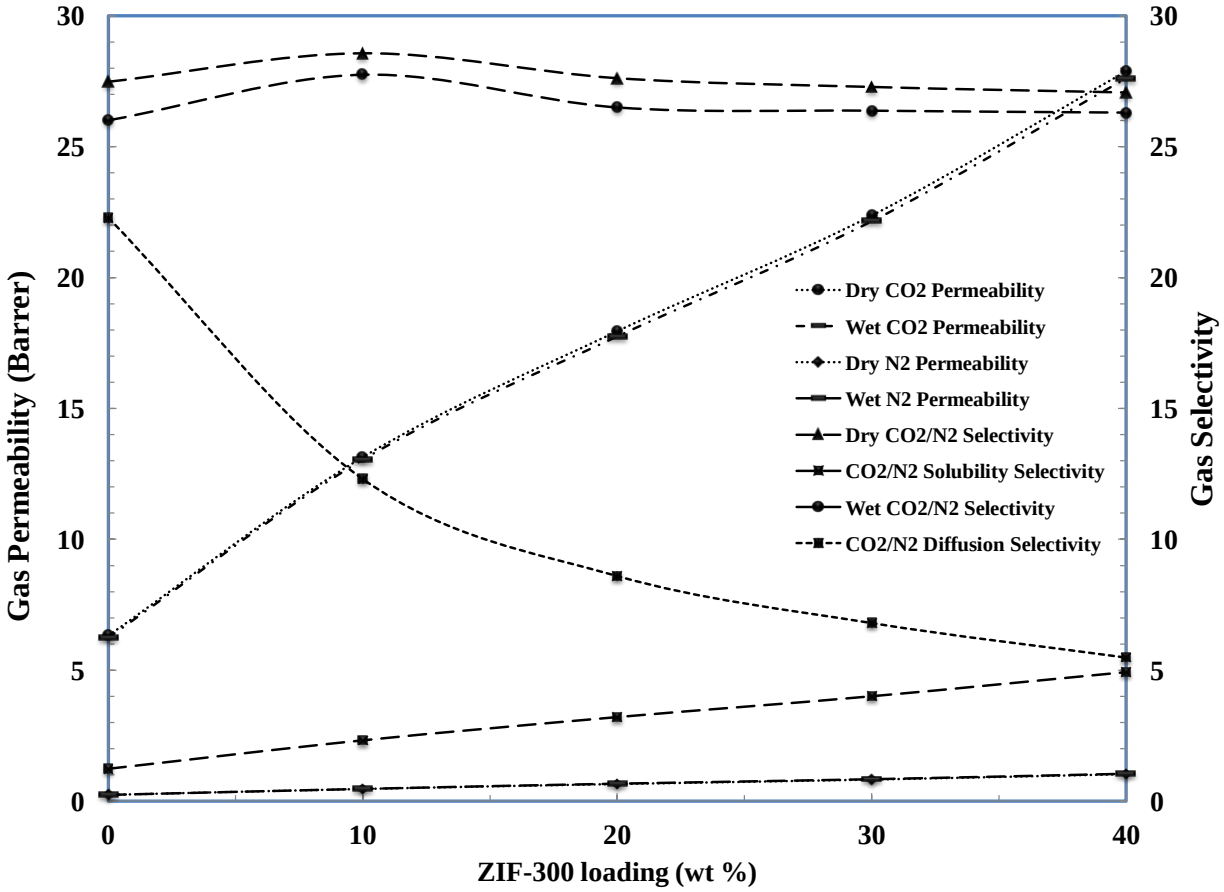

Fig. 2.5 Dry and wet gas CO_2 and N_2 permeabilities and CO_2/N_2 selectivity of pure PSF and ZIF-300/PSF MMMs with different ZIF loadings.

2.3.5.2 Diffusivity and solubility of MMMs. Gas permeation through a membrane occurs via solution-diffusion mechanism. The data for coefficients of diffusion (D) and solubility (S) along with their corresponding CO_2/N_2 selectivity values for bare PSF membrane and different ZIF-300/PSF MMMs are illustrated in Figs. 2.5 and 2.6.

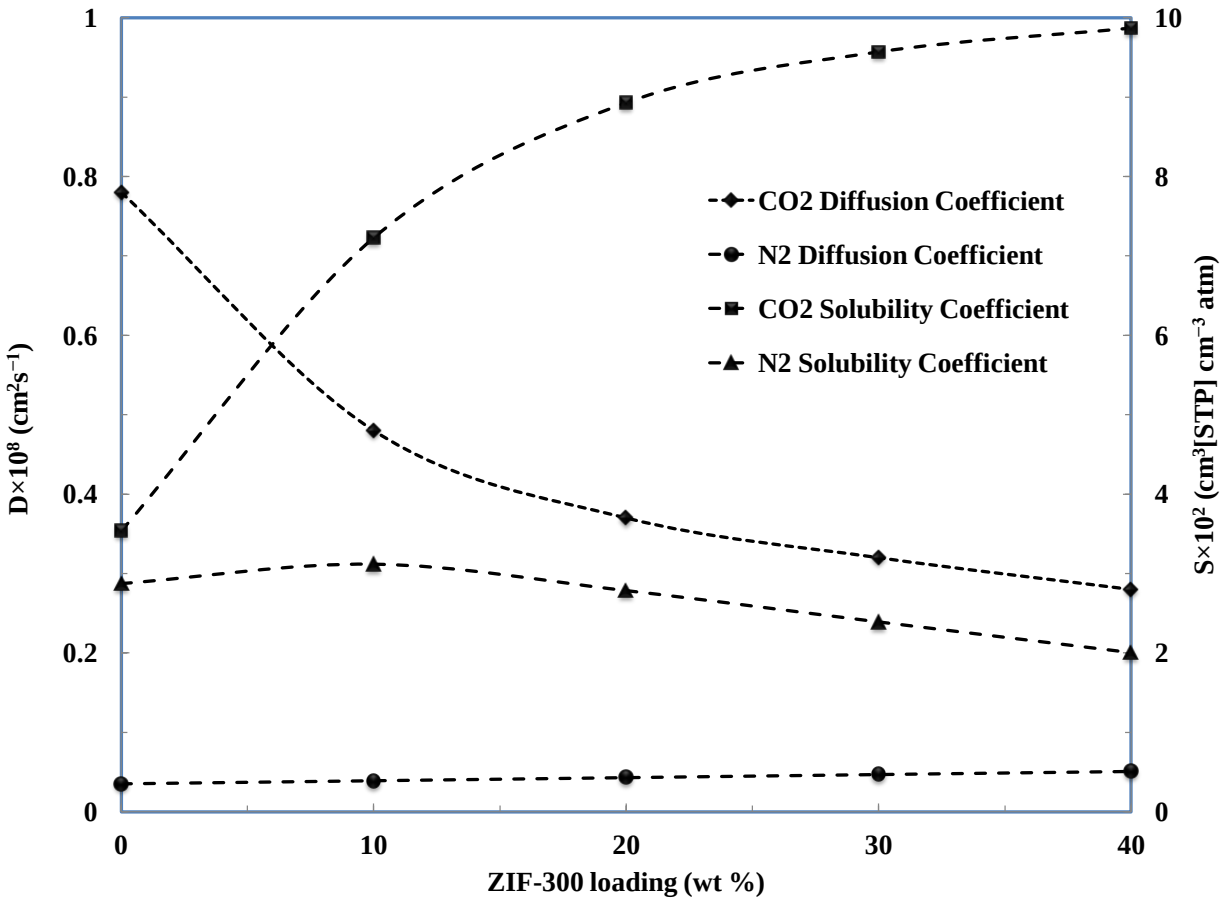

Fig. 2.6 Pure gas diffusion (D) and solubility (S) coefficients for bare PSF and selected MMMs having different ZIF-300 loadings

The time-lag method (eq. 6) was used to determine the values of diffusion coefficients. CO_2 and N_2 adsorption isotherms obtained at 25 ^oC under varying pressure helped to

calculate Langmuir parameters to determine the correction parameters (bracketed term in eq. 3). The D values thus determined were used to calculate solubility coefficients of the membranes under the same conditions of temperature and pressure using eq. 4. Comparatively the values of gas diffusivity coefficient selectivity (D_{CO2}/D_{N2}) successively decline and those of gas solubility coefficient selectivity (S_{CO2}/S_{N2}) in turn increase for all MMMs with increasing ZIF-300 contents as shown in Fig. 2.5.

The pore size reduction of ZIF-filled MMMs led to restricted N_2 adsorption as compared to CO_2. Also the selective solubility of CO_2 into ZIF-300 nanocrystals greatly enhanced its permeation through the MMMs. In general the improved CO_2/N_2 ideal selectivities of MMMs can be ascribed to controlled N_2 diffusion and preferential CO_2 solubility. The overall analysis based on improved CO_2 permeabilities and reduced N_2 diffusivities in ZIF-300/PSF MMMs strongly support the development of a genuine mixed matrix membrane. The membranes permeation time lag characteristic also implied good interfacial adhesion and homogeneous distribution of ZIF-300 entities into PSF matrix.

Since a membrane possessing high perm-selectivity values meets industrial applications, it appears that ZIF-300 is a competent material to fabricate MMMs for post combustion carbon capture on account of its high CO_2 permeability coupled with reasonable CO_2/N_2 selectivity.

2.3.5.3 Comparison of experimental data with mathematical models. Two- and three-phase permeability models were employed to predict CO_2 permeability through the prepared MMMs (Fig. 2.7). The two-phase Maxwell and Singh models well predict the permeability at low filler loadings, while the three-phase modified Felske and Bruggeman

models more accurately describe the MMMs behavior at higher filler concentration. The error in three-phase models is lower than two-phase models thus dictating non-ideal morphology of the MMMs.

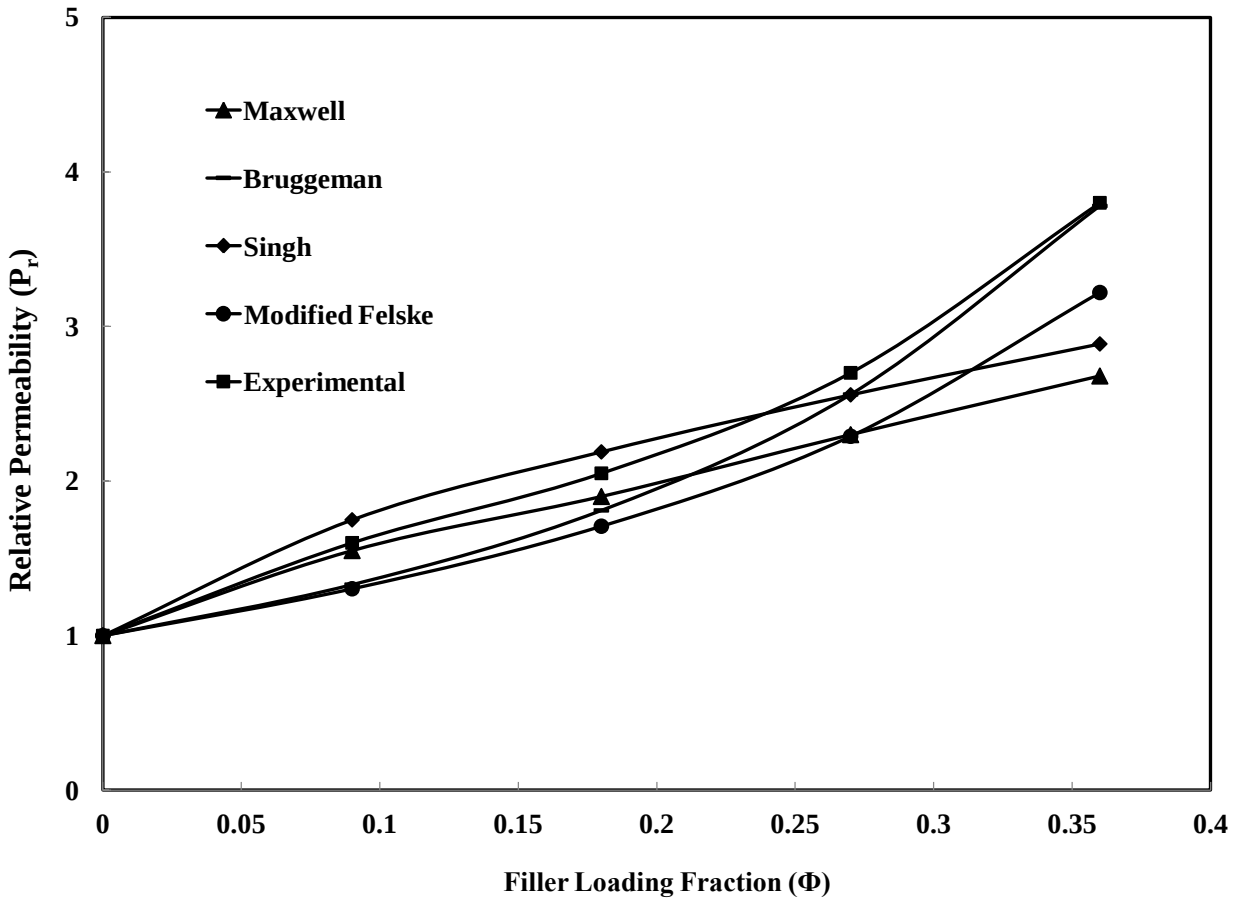

Fig. 2.7 Comparison between experimentally determined CO_2 permeability and that predicted by Maxwell, Bruggeman, Singh, and modified Felske models.

2.3.5.4 Comparison with Robeson upper bounds. A comparison of the CO_2/N_2 gas pair separation performance of MOF-based MMMs, along with Robeson 1991 and 2008 upper bounds [14], is depicted on a permeability-selectivity chart as shown in Fig. 2.8. The diagram indicates that the incorporation of ZIF-300 nanofiller into PSF matrix has

enhanced the perm-selectivity of the MMMs as compared to neat polysulfone membrane. The perm-selectivity value of MMM containing 10 wt% ZIF-300 is located very close to the 1991-upper bound line while those of MMMs containing 10-40 wt% ZIF-300 loadings lie on this line, an important achievement of this work. ZIF-300 loadings higher than 40 wt % are susceptible to poor filler-matrix interface adhesion and inhomogeneous dispersion of filler in polymer matrix.

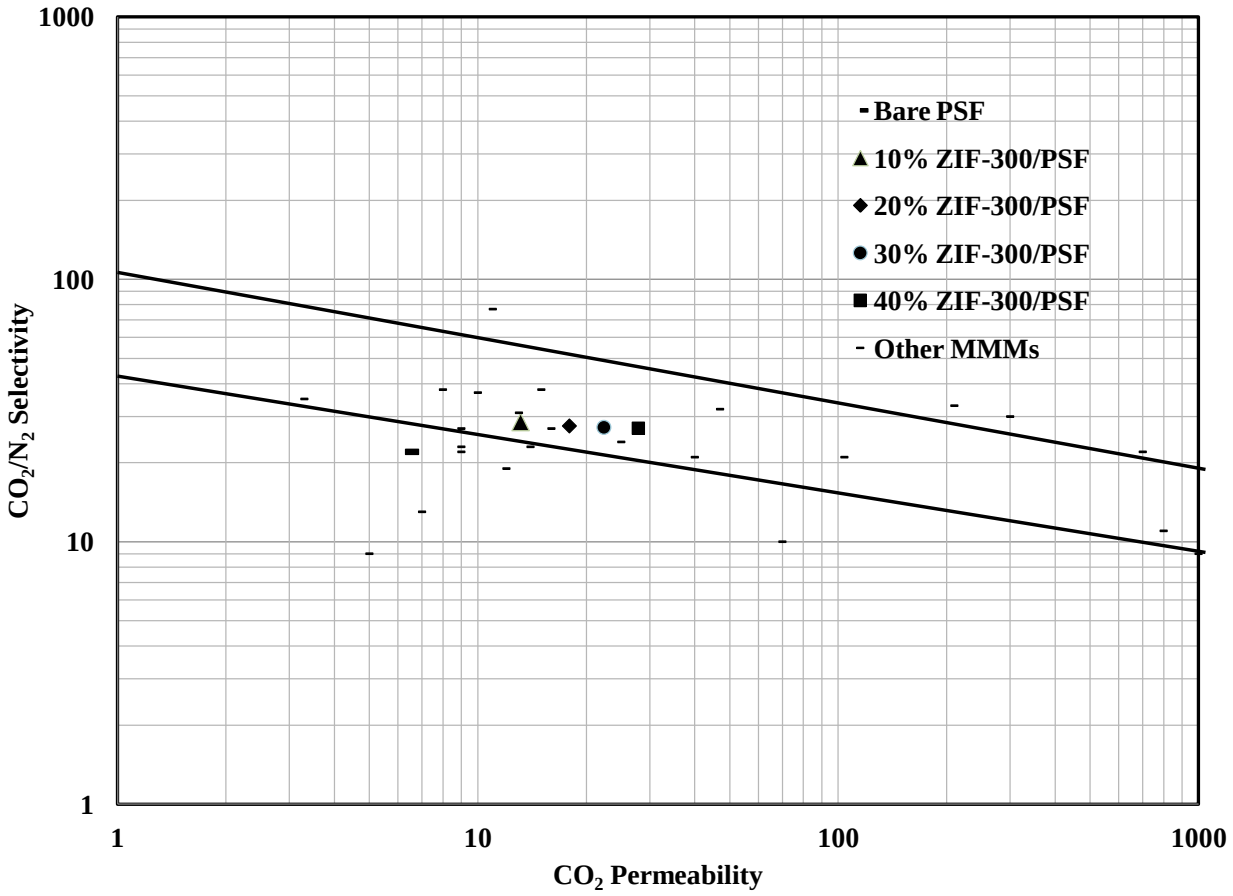

Fig. 2.8 Comparison of CO_2/N_2 separation performance of ZIF-300/PSF MMMs with other ZIF or MOF containing MMMs obtained from literature data. The Robeson upper bound 2008 for polymer separation performance is also shown.

2.4 Conclusions

ZIF-300 nanocrystals with narrow particle size distribution were incorporated into PSF to fabricate hydrothermally stable high performance mixed-matrix membranes for selective CO_2 separation from post combustion flue gases. Characterization of the MMMs done by XRD, TGA, SEM and gas sorption experiments indicated that they are thermally stable, mesoporous, crystalline materials possessing homogeneous filler dispersion and good interfacial filler-matrix adhesion without adding any compatibilizing agent. The MMMs developed in this work demonstrated four times increment in CO_2 permeability as compared to that of pure PSF membrane while the CO_2/N_2 ideal selectivity remained almost undeteriorated. The separation performance of the MMMs produced in this work coincided with the Robeson 1991 upper bound and the CO_2/N_2 ideal selectivity is considered to be high enough to meet industrial applications.

Acknowledgement

The authors are thankful to KACST- Technology Innovation Center on Carbon Capture and Sequestration (CCS), King Fahd University of Petroleum and Minerals, Dhahran, Kingdom of Saudi Arabia for providing support for this work.

References

[1] D. M. D'Alessandro, B. Smit, J. R. Long, Carbon Dioxide Capture: Prospects for New Materials, Angew. Chem. Int. Ed. 49 (2010) 6058-6082.

[2] M. Z. Jacobson, Review of Solutions to Global Warming, Air Pollution, and Energy Security, Energy Environ. Sci. 2 (2009) 148-173.

[3] N. MacDowell, N. Florin, A. Buchard, J. Hallett, A. Galindo, G. Jackson, C. S. Adjiman, C. K. Williams, N. Shah, P. Fennell, An Overview of CO_2 Capture Technologies, Energy Environ. Sci. 3 (2010) 1645-1669.

[4] H. Herzog, D. Golomb, Carbon capture and storage from fossil fuel use, Encyc. Energy 1 (2004) 277-287.

[5] A. Hussain, M.B. Hägg, A feasibility study of CO_2 capture from flue gas by a facilitated transport membrane, J. Membr. Sci. 359 (2010) 140-148.

[6] J. Zhao, Z. Wang, J.X. Wang, S.C. Wang, Influence of heat-treatment on CO_2 separation performance of novel fixed carrier composite membranes prepared by interfacial polymerization, J. Membr. Sci. 283 (2006) 346-356.

[7] P. Pandey, R.S. Chauhan, Membranes for gas separation, Prog. Polym. Sci. 26 (2001) 853-893.

[8] R. Mahajan, W.J. Koros, Factors controlling successful formation of mixed-matrix gas separation materials, Ind. Eng. Chem. Res. 39 (2000) 2692–2696.

[9] E.P. Fawas, G.C. Kapantaidakis, J.W. Nolan, A.C. Mitropoulos, N.K. Kanellopoulos, Preparation, characterization and gas permeation properties of carbon hollow fiber membranes based on Matrimid® 5218 precursor, J. Mater. Process. Technol. 186 (2007) 102–110.

[10] R.W. Baker, Future directions of membrane gas separation technology, J. Ind. Eng. Chem. Res. 41 (2002) 1393–1411.

[11] D.L. Gin, R.D. Noble, Designing the next generation of chemical separation membranes, Science 332 (2011) 674-676.

[12] Y. Xiao, T.-S. Chung, Grafting thermally labile molecules on cross-linkable polyimide to design membrane materials for natural gas purification and CO_2 capture. Energy Environ. Sci. 4 (2011) 201-208.

[13] C. Staudt-Bickel, W.J. Koros, Improvement of CO_2/CH_4 separation characteristics of polyimides by chemical crosslinking. J. Membr. Sci. 155 (1999) 145-154.

[14] L.M. Robeson, The upper bound revisited. J. Membr. Sci. 320 (2008) 390–400.

[15] T.-S. Chung, L.Y. Jiang, Y. Li, S. Kulprathipanja, Mixed matrix membranes (MMMs) comprising organic polymers with dispersed inorganic fillers for gas separation. Prog. Polym. Sci. 32 (2007) 483-507.

[16] C.E. Powell, G.G. Qiao, Polymeric CO_2/N_2 gas separation membranes for the capture of carbon dioxide from power plant flue gases. J. Membr. Sci. 279 (2006) 1-49.

[17] M. Rezakazemi, A.E. Amooghin, M.M. Montazer-Rahmati, A.F. Ismail, T. Matsuura, State-of-the-art membrane based CO_2 separation using mixed matrix membranes (MMMs): An overview on current status and future directions, Prog. Polym. Sci. 39 (2014) 817-861.

[18] J.D. Wind, D.R. Paul, W.J. Koros, Natural gas permeation in polyimide membranes, J. Membr. Sci. 228 (2004) 227-236.

[19] W. Qiu, C.C. Chen, L. Xu, L. Cui, D.R. Paul, W.J. Koros, Sub-T_g cross-linking of a polyimide membrane for enhanced CO_2 plasticization resistance for natural gas separation, Macromolecules 44 (2011) 6046-6056.

[20] J. Park, D. Paul, Correlation and prediction of gas permeability in glassy polymer membrane materials via a modified free volume based group contribution method, J. Membr. Sci. 125 (1997) 23-39.

[21] Y. Yampolskii, Polymeric gas separation membranes, Macromolecules 45 (2012) 3298-3311.

[22] L.M. Robeson, Correlation of separation factor versus permeability for polymeric membranes, J. Membr. Sci. 62 (1991) 165-185.

[23] C.H. Lau, P. Li, F. Li, T.-S. Chung, D.R. Paul, Reverse-selective polymeric membranes for gas separations, Prog. Polym. Sci. 38 (2013) 740-766.

[24] T.C. Merkel, B.D. Freeman, R.J. Spontak, Z. He, I. Pinnau, P. Meakin, A. Hill, J. Ultrapermeable, reverse-selective nanocomposite membranes, Science 296 (2002) 519-522.

[25] J. Ahn, W.-J. Chung, I. Pinnau, M.D. Guiver, Polysulfone/silica nanoparticle mixed-matrix membranes for gas separation, J. Membr. Sci. 314 (2008) 123-133.

[26] B.D. Reid, A. Ruiz-Trevino, I.H. Musselman, K.J. Balkus, J.P. Ferraris, Gas permeability properties of polysulfone membranes containing the mesoporous molecular sieve MCM-41, Chem. Mater. 13 (2001) 2366-2373.

[27] S. Kim, E. Marand, J. Ida, V.V. Guliants, Polysulfone and mesoporous molecular sieve MCM-48 mixed matrix membranes for gas separation, Chem. Mater. 18 (2006) 1149-1155.

[28] S. Kim, E. Marand, High permeability nano-composite membranes based on mesoporous MCM-41 nanoparticles in a polysulfone matrix, Microp. Mesop. Mater. 114 (2008) 129-136.

[29] D.Q. Vu, W.J. Koros, S.J. Miller, Mixed matrix membranes using carbon molecular sieves. II. Modeling permeation behavior, J. Membr. Sci. 211 (2003) 335-348.

[30] H.L. Cong, J.M. Zhang, M. Radosz, Y.Q. Shen, Carbon nanotube composite membranes of brominated poly(2,6-diphenyl-1,4-phenylene oxide) for gas separation, J. Membr. Sci. 294 (2007) 178–185.

[31] S. Kim, L. Chen, J.K. Johnson, E. Marand, Polysulfone and functionalized carbon nanotube mixed matrix membranes for gas separation: Theory and experiment, J. Membr. Sci. 294 (2007) 147–158.

[32] P. Gorgojo, S. Uriel, C. Tellez, J. Coronas, Development of mixed matrix membranes based on zeolite Nu-6(2) for gas separation, J. Microporous Mesoporous Mater. 115 (2008) 85–92.

[33] Y. Liu, D. Peng, G. He, S. Wang, Y. Li, H. Wu, Z. Jiang, Enhanced CO_2 permeability of membranes by incorporating polyzwitterion@CNT composite particles into polyimide matrix, ACS Appl. Mater. Interfaces 6 (2014) 13051-13060.

[34] B. Harold, T. Jeazet, C. Staudt, C. Janiak, Metal–organic frameworks in mixed-matrix membranes for gas separation, Dalton Trans. 41 (2012) 14003–14027.

[35] A. Car, C. Stropnik, K.-V. Peinemann, Hybrid membrane materials with different metal–organic frameworks (MOFs) for gas separation, Desalination 200 (2006) 424.

[36] B. Zornoza, S. Irusta, C. Tellez, J. Coronas, Mesoporous silica sphere-polysulfone mixed matrix membranes for gas separation, Langmuir 25 (2009) 5903–5909.

[37] B. Zornoza, B. Seoane, J. M. Zamaro, C. Téllez and J. Coronas, Combination of MOFs and zeolites for mixed-matrix membranes, Chem-PhysChem, 12 (2011) 2781–2785.

[38] B. Harold, T. Jeazet, T. Koschine, C. Staudt, K. Raetzke, C. Janiak, Correlation of gas permeability in a metal-organic framework MIL-101(Cr)–polysulfone mixed-matrix

membrane with free volume measurements by positron annihilation lifetime spectroscopy (PALS), Membranes 3 (2013) 331-353.

[39] T.T.N. Nhung, H. Furukawa, F. Gandara, H.T. Nguyen, K.E. Cordova, O.M. Yaghi, Selective capture of carbon dioxide under humid conditions by hydrophobic chabazite-type zeolitic imidazolate frameworks, Angew. Chem. 126 (2014) 10821–10824.

[40] L.A. El-Azzami, E.A. Grulke, Parametric study of CO_2 fixed carrier facilitated transport through swollen chitosan membranes. Ind. Eng. Chem. Res. 48 (2008) 894−902.

[41] J.U. Wieneke, C. Staudt, Thermal stability of 6FDA-(co-)polyimides containing carboxylic acid groups. Polym. Degrad. Stab. 95 (2010) 684–693.

[42] X.W. Yu, Z. Wang, Z.H. Wei, S.J. Yuan, J. Zhao, J.X. Wang, S.C. Wang, Novel tertiary amino containing thin film composite membranes prepared by interfacial polymerization for CO_2 capture, J. Membr. Sci. 362 (2010) 265-278.

[43] D.R. Paul, D.R. Kemp, The diffusion time lag in polymer membranes containing adsorptive fillers, J. Polym Sc: Polym. Symp. 41 (1973) 79–93.

[44] H. Vinh-Thang, S. Kaliaguine, Predictive Models for Mixed-Matrix Membrane Performance: A Review, J. ACS Publications, 113 (2012) 4980–5028.

[45] S.A. Hashemifard, A.F. Ismail, T. Matsuura, A new theoretical gas permeability model using resistance modeling for mixed matrix membrane systems, J. Membr. Sci., 350 (2010) 259-268.

[46] B. Shimekit, H. Mukhtar, T. Murugesan, Prediction of the relative permeability of gases in mixed matrix membranes", J. Membr. Sci., 373 (2011) 152-159.

[47] Y.C. Xiao, T.S. Chung, H.M. Guan, M.D. Guiver, Synthesis, cross-linking and carbonization of co-polyimides containing internal acetylene units for gas separation, J. Membr. Sci. 302 (2007) 254-264.

[48] A.C.C. Chang, S.S.C. Chuang, M. Gray, Y. Soong, In-situ infrared study of CO_2 adsorption on SBA-15 grafted with γ-(aminopropyl) triethoxysilane, Energy Fuels 17 (2003) 468-473.

CHAPTER 3

PURSUIT OF HIGH PERFORMANCE MMMS FOR CARBON DIOXIDE SEPARATION: COLLEGIAL INCORPORATION OF CNTS AND ZIF-300 NANOFILLERS INTO POLYSULFONE

Abstract

High performance mixed-matrix membranes (MMMs) for CO_2 separation were prepared by collegially incorporating carbon nanotubes (CNTs) and zeolitic imidazole frameworks (ZIF-300) nanocrystals into glassy polysulfone (PSF) matrix using solution-casting technique. Different loadings of the nanofillers were doped into PSF to optimize the CO_2 separation performance of MMMs. The flexible MMMs exhibiting homogeneous dispersion and good adhesion of nanofillers with polymer matrix were characterized by scanning electron microscopy (SEM), x-ray diffraction (XRD), and thermal gravimetric analysis (TGA). Pure gas sorption studies coupled with dry and wet gas permeation tests demonstrated that both CO_2 permeability and CO_2/N_2 selectivity of MMMs were enhanced due to synergistic effect of nanofillers. The MMM doped with 6 wt % CNTs and 18 wt % ZIF-300 nanofillers exhibited an optimal separation performance rendering a CO_2 permeability of 34 Barrers with CO_2/N_2 selectivity of 72.

Key Words

Hydrophobic MMMs, ZIF-300, CNTs, synergistic effect, CO_2 capture, permselectivity

3.1 Introduction

Global warming caused by carbon dioxide (CO_2) gas emissions from burning of fossil fuels has turned out to be a severe environmental issue throughout the globe [1-3]. CO_2 emissions can be reduced by its capture or sequestration via economically feasible methods [4-5]. As compared to other conventional processes, polymer-based mixed-matrix membrane (MMM) gas separation technology has received significant consideration on account of its low capital and operating costs, high efficiency, low energy requirement, simple function, flexible design, ease of scale up, and environmental kindliness [6-13].

To formulate efficient hybrid membranes having improved permselectivity characteristics as compared to unfilled polymer membranes, a lot of glassy polymers have been tailored to develop MMMs by incorporating inorganic fillers like nonporous silica [14-15], structured mesoporous silica [16-18], carbon molecular sieves [19], carbon nanotubes [20-21], zeolites [22], and microporous metal organic frameworks (MOFs) [23]. Some key benefits of MMMs prepared by incorporating CNTs and microporous MOF/ZIF nanocrystals into polymer matrix include the ability to integrate the ease of fabrication and processability, improved mechanical and chemical stability of polymers coupled with exceptional gas separation characteristics of microporous crystalline materials possessing tunable pore size, modifiable surface functionality, and high surface areas [24].

Microporous MOFs and ZIFs are appealing materials to engineer efficient MMMs for gas separation due to their high surface areas, tunable nano-sized pores, modifiable surface functionality, good wetting characteristics, improved thermal and chemical stability [25–27]. Hydrothermally stable microporous crystalline ZIF-300 [28] selectively captures CO_2 gas from post combustion flue gas and their incorporation into polymers helps to improve separation performance of MMMs.

On account of their smooth interior surfaces, nano-sized structure, high aspect ratios, large pore diameter, outstanding thermal and mechanical properties [29–31], gas permeation through CNTs are exceptionally higher as compared to other microporous materials. The selectivity of pure CNTs for different gas molecules is low and difficult to improve by functionalization due to their highly unreactive nature [32–34]. Although CNTs-based MMMs are highly efficient as compared to ZIF/MOF-based MMMs, good adhesion and proper distribution of nanofillers in the polymer matrix is the main challenge. A more sophisticated approach to develop a MMM with enhanced permselectivity is to collectively incorporate naonfillers of different nature, morphology and dimensions into a polymer matrix [35].

Various combinations of MOFs (HKUST-1), ZIFs (ZIF-8) and zeolites (S1C) were incorporated into PSF to develop different MMMs for gas permeation of CO_2, N_2, CH_4, O_2, and H_2 [36]. The CO_2/N_2 separation efficiency did not improve for S1C-ZIF-8/PSF MMMs. The CO_2 permeabilities of S1C/PSF, HKUST-1/PSF, ZIF-8/PSF and HKUST-1/ZIF-8/PSF MMMs were found to be 9.4, 9.5, 12.3 and 8.4 Barrers respectively with corresponding CO_2/N_2 selectivities of 23, 24, 19 and 38. The synergistic effect of combining (NH_2-MIL-53(Al)) and mesoporous silica MCM-41 into polymer-based

MMMs improved their gas separation performance [37]. Galve et al. [38] prepared MMMs by incorporating layered microporous titanosilicate JDF-L1 sheets and mesoporous silica MCM-41 spheres into polyimide matrix; JDF-L1 sheets facilitated to properly disperse MCM-41 spheres in the polymer matrix. Li and group studied the collective incorporation of CNTs and graphene oxide into PSF matrix to find the optimum filler loadings [39].

When incorporated separately in polymer matrices, both the CNTs and ZIFs impart improved gas separation performances. In the present study combination of CNTs and ZIF-300 nanocrystals have been incorporated into glassy PSF matrix for the first time to develop PSF/CNTs/ZIF-300 MMMs to efficiently separate CO_2 from CO_2-N_2 mixture. The main objective of this study is to systematically investigate the solubility-diffusivity separation mechanism and determine the optimum loadings of the two nanofillers to achieve high CO_2 permselectivity.

3.2 Experimental

3.2.1 Materials

Commercially available polysulfone, having density 1.25 g cm^{-3} and average molecular weight ~ 35000 by LS, was obtained from Sigma Aldrich. Hydroxyl modified multi-walled CNTs having average length and diameter of approximately 1.2 μm and 8 nm were obtained from Nanjing XFNANO Materials Tech. Co., Ltd. Zinc nitrate tetrahydrate and 2-methylimidazole were obtained from Merck Chemical Company. 5(6)-chlorobenzimidazole, methanol and N,N-dimethylformamide (DMF) were obtained from Aldrich Chemical Company. The polymer and chemicals were used as received without

additional treatment. Highly pure CO_2, N_2 and He gases were used for gas sorption and permeation experiments.

3.2.2 Synthesis of ZIF-300 nanocrystals

To synthesize ZIF-300 nanocrystals, 67.8 mg of $Zn(NO_3)_2 \cdot 6H_2O$ (the metal salt), 23.4 mg of 2-methylimidazole (primary organic linker), and 43.6 mg of 5(6)-chlorobenzimidazole (secondary organic linker) were dissolved in a mixture of 9.5 mL DMF and 0.5 mL distilled water by sonication in a 20-mL vial for 10 minutes. The resulting mixture was then moderately stirred on a hot plate at 50 °C for 70 hours to obtain light brown suspension. The suspended nanocrystals were separated from the mother liquor by centrifuge and washed with 7 mL of fresh DMF. This process was repeated 5 times to make them ready to incorporate into polymer matrix to prepare MMMs of varying composition.

3.2.3 Preparation of PSF/CNTs/ZIF-300 MMMs

To prepare bare PSF membrane and PSF/CNTs/ZIF-300 MMMs, the main constituents i.e., PSF, CNTs and ZIF-300 nanocrystals were degassed at 100 ^oC under vacuum for 20 h to remove any adsorbed gas or moisture. Bare polymer membrane was fabricated by dissolving 1g PSF in 10 mL DMF followed by stirring at room temperature for 24 hours until a thick viscous solution was formed. The MMMs containing varying quantities of CNTs and ZIF-300 nanocrystals were prepared as follows. 1 g PSF was added in 10 mL DMF and stirred at room temperature for 20 h. Also a weighed quantity of CNTs was dispersed in 4 mL DMF by sonicating for 1 h to get well dispersed homogeneous

suspension. In addition, a specified amount of ZIF-300 nanocrystals was redispersed in 7 mL DMF by stirring for 10 minutes. The three solutions were combined together and subjected to vigorous stirring for another 12 h until a thick viscous solution was obtained. All the membranes were knife casted on clean glass plates at a specified gate height using a flat sheet membrane casting system (FSMCS). After slowly evaporating the solvent under ambient conditions overnight, the membranes were detached from the glass plates and placed in a VO 200 vacuum oven to dry the MMMs at 80, 100 and 180 ^{o}C for 12, 20 and 60 hours respectively to ensure complete removal of the remaining solvent before subjecting it to gas permeation tests.

The prepared MMMs were designated as PSF/CNTs(X)/ZIF-300(Y), where X (ranging from 1-10) and Y (ranging from 6-30) represent loadings of CNTs and ZIF-300 by wt % respectively. For instance the MMM denoted by PSF/CNTs(6)/ZIF-300(18) respectively contains 6 and 18 wt % loadings of CNTs and ZIF-300 nanocrystals. The thicknesses of the membranes were determined in the range of 50-80 μm as measured by a digital micrometer.

3.2.4 Material Characterization Methods

The ZIF-300 nanocrystals, CNTs, bare PSF membrane and PSF/CNTs/ZIF-300 mixed-matrix membranes were characterized by x-ray diffraction, scanning electron microscopy, thermogravimetric analysis, and gas sorption measurement techniques. The fractional volume (Φ_D expressed in %) of CNTs and/or ZIF-300 in MMMs can be defined as:

$$\Phi_D = \frac{m_D/\rho_D}{m_D/\rho_D + m_C/\rho_C} \times 100 \qquad (1)$$

where m and ρ represent mass and density of PSF (continuous phase denoted by subscript C) and CNTs and/or ZIF-300 (dispersed phase denoted by subscript D) respectively. Normally the void volume of MMMs is negligible as supported by SEM images and gas sorption analysis. Hence the apparent volume fraction can safely be considered as the exact volume fraction of CNTs and/or ZIF-300 in MMMs.

Powder x-ray diffraction patterns of ZIF-300 nanocrystals, CNTs, bare PSF and PSF/CNTs/ZIF-300 MMMs were performed using a Bruker D8 X-ray diffractometer using Cu Kα radiation (λ = 1.5406 Å) operated at 45 mA and 40 kV with an increment of 0.02^o in 2θ and a step scan size of 0.02^o s^{-1}. The membrane sample was loaded on silicon substrate placed in a sample holder. The MMMs were characterized by XRD to check whether the polymeric matrix alters the crystalline patterns of CNTs and ZIF-300 nanocrystals or not.

Scanning electron microscopy images of all the samples were taken to explore the morphology of ZIF-300 nanocrystals, CNTs, bare PSF membrane and MMMs having different nanofillers loadings by Hitachi S-4300SE/N SEM instrument. Testing specimens were cryofractured in liquid nitrogen and their outer surfaces were covered with a thin gold film to avoid charging of electrons. The SEM machine was operated at an accelerating voltage of 20 kV.

Thermal properties and stability of ZIF-300 nanocrystals, CNTs, bare PSF membrane and their MMMs were assessed by thermal gravimetric analysis by using a TGA/SDTA 851

(Mettler Toledo) system in air by heating from ambient temperature to 700 ^{o}C at a rate of 10 ^{o}C min^{-1}.

Nitrogen and carbon dioxide adsorption isotherms measured at different temperatures using a Quantachrome Autosorb iQ gas sorption analyzer helped to determine various characteristics (e.g., specific BET and Langmuir surface areas, total microporous volume, CO_2 and N_2 gas uptakes) of ZIF-300 microporous nanoparticles, CNTs, PSF membrane and their composite membranes. The membrane samples were cut into small pieces and degassed at 100 ^{o}C under vacuum (<10^{-6} bar) for 5 hours. Physisorption data of CO_2 and N_2 gases were measured at 298 K under a gas pressure ranging from 10^{-6} -1 bar.

3.2.5 Gas Permeation Measurements

Pure gas (CO_2 and N_2) transport properties (i.e., permeability, ideal selectivity, and separation performance) of the MMMs were estimated using single gas permeation cell following the variable pressure (constant volume) method at room temperature [40]. After measuring its average thickness and effective cross sectional area, the membrane was affixed into the cell. While keeping the feed side valve closed, both the upstream (feed side) and downstream (permeate side) lines of the cell were evacuated. The valve between the permeate side line and the vacuum pump was then closed followed by opening the feed side valve to maintain a low feed pressure (e.g., 0.1 bars) for a specific time (i.e., 2 h) to record the permeation measurements. The feed pressure was then intermittently increased and data were collected after at least 1 h of stabilization for each interval. In order to estimate error and identify imperfect membranes, at least three replicas were prepared and tested corresponding to each composition of the MMMs.

Gas permeability (P_i, *Barrer*) of the membrane was computed using eq. (2):

$$P_i = \frac{22414}{A} \times \frac{V}{RT} \times \frac{l}{\Delta P_i} \frac{dP_i}{dt} \qquad (2)$$

where *l, A, V, R, T,* ΔP and $\Delta P_i/dt$ are respectively membrane thickness (*cm*), membrane effective area (cm^2), downstream volume (cm^3), universal gas constant (6236.56 cm^3 *cmHg/mol/K*), absolute temperature (*K*), pressure difference across the membrane (*psi*), and permeation rate (*psi/s*) of component i.

Time-lag method, suggested by Paul and Kemp [41], was used to determine diffusion coefficient (D) by using *diffusivity vs. time-lag* (D-θ) relationship for MMMs:

$$D = \frac{l^2}{6\theta} \left[1 + \frac{6K}{y^3} \left\{\frac{y^2}{2} + y - (1+y)\ln(1+y)\right\} \left(\frac{V_d}{V_p}\right)\right] \qquad (3)$$

where V_d and V_p are respectively the volume fractions of filler and polymer phases; K and y are adsorption parameters determined from Langmuir adsorption isotherm.

The solubility coefficient (S) can be calculated from Eq. (4):

$$S = \frac{P}{D} \qquad (4)$$

The ideal selectivity (α_{ij}) for gases i and j can be determined using Eq. (5):

$$\alpha_{ij} = \frac{P_i}{P_j} = \left(\frac{D_i}{D_j}\right)\left(\frac{S_i}{S_j}\right) \qquad (5)$$

Here (D_i/Dj) and (S_i/S_j) represent diffusion- and solubility-based selectivity terms respectively.

3.3 Results and discussion

The end results of different characterization techniques i.e., XRD, SEM, TGA, gas sorption and gas permeation are briefly described here.

3.3.1 Powder X-ray Diffraction

Powder x-ray diffraction is a good practice to probe the effect of nanofillers on the polymer chains configuration in MMMs and to confirm the existence of crystalline particles in amorphous matrices. XRD measurements ranging from 2^o to 50^o were recorded to determine and confirm the existence of CNTs and ZIF-300 crystalline structure in composite membranes as shown in Fig. 3.1. The characteristic peak intensities appearing at 2θ of 10.6^o, 13.1^o and 22.8^o in XRD patterns of MMMs correspond to ZIF-300 nanocrystals [28], while those emerging at 25.8^o and 44.1^o corroborated the dispersion of CNTs within PSF matrix [42]. The fine coincidence of XRD patterns of MMMs with those of CNTs and ZIF-300 nanocrystals suggests their crystallinities preservation even after incorporation into the polymer matrix as shown in Fig. 3.1. Also the addition of different loading levels of nanofillers in MMMs proportionally heightens their corresponding peak intensities at the specified 2θ positions. All the membranes displayed a characteristic broad peak of PSF centered at an angle of $2\theta = 17.2^o$. Furthermore the slight shift of broad peak position (2θ) of bare PSF from 17.2° (d-spacing = 5.21 Å) to 17.4° (d-spacing = 5.15 Å) can be attributed to the strong filler-polymer interactions thus reducing the polymer inter-chain distance.

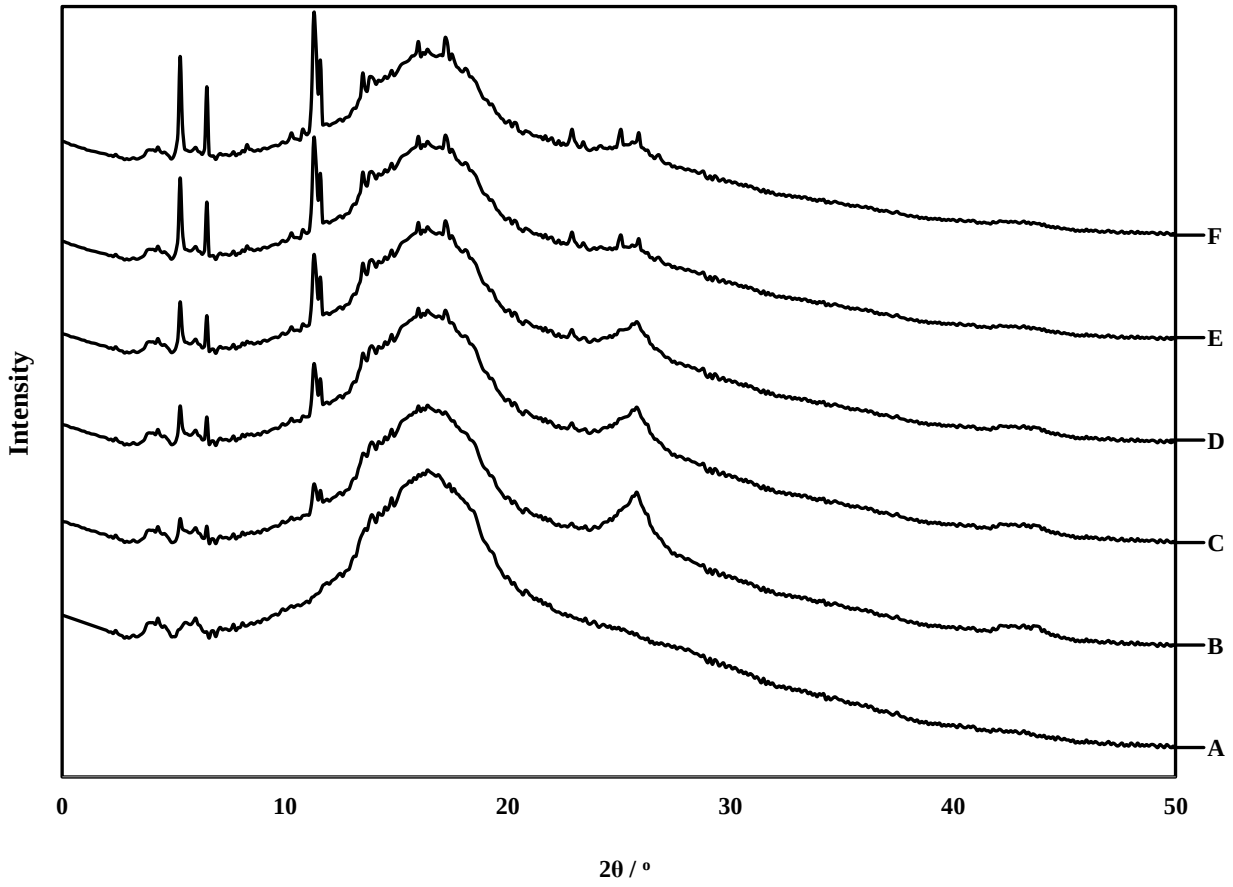

Fig. 3.1 Powder x-ray patterns of bare PSF [A], PSF/CNTs(10)/ZIF-300(6) [B], PSF/CNTs(8)/ZIF-300(12) [C], PSF/CNTs(6)/ZIF-300(18) [D], PSF/CNTs(4)/ZIF-300(24) [E], and PSF/CNTs(2)/ZIF-300(30) [F] MMMs containing different loadings of CNTs and ZIF-300 nanocrystals.

3.3.2 Morphology of PSF/CNTs/ZIF-300 MMMs

The morphology and structural characteristics of the MMMs strongly depend on the nature of organic polymer matrix and the incorporated inorganic filler(s). To explore the morphology, adhesion and dispersion of CNTs and ZIF-300 nanoparticles within the polymer matrix cross sectional micrographs of the MMMs were probed by SEM as

depicted in Fig. 3.2. All MMMs having different loadings of nanofillers exhibit continuous phases, almost free of interfacial voids.

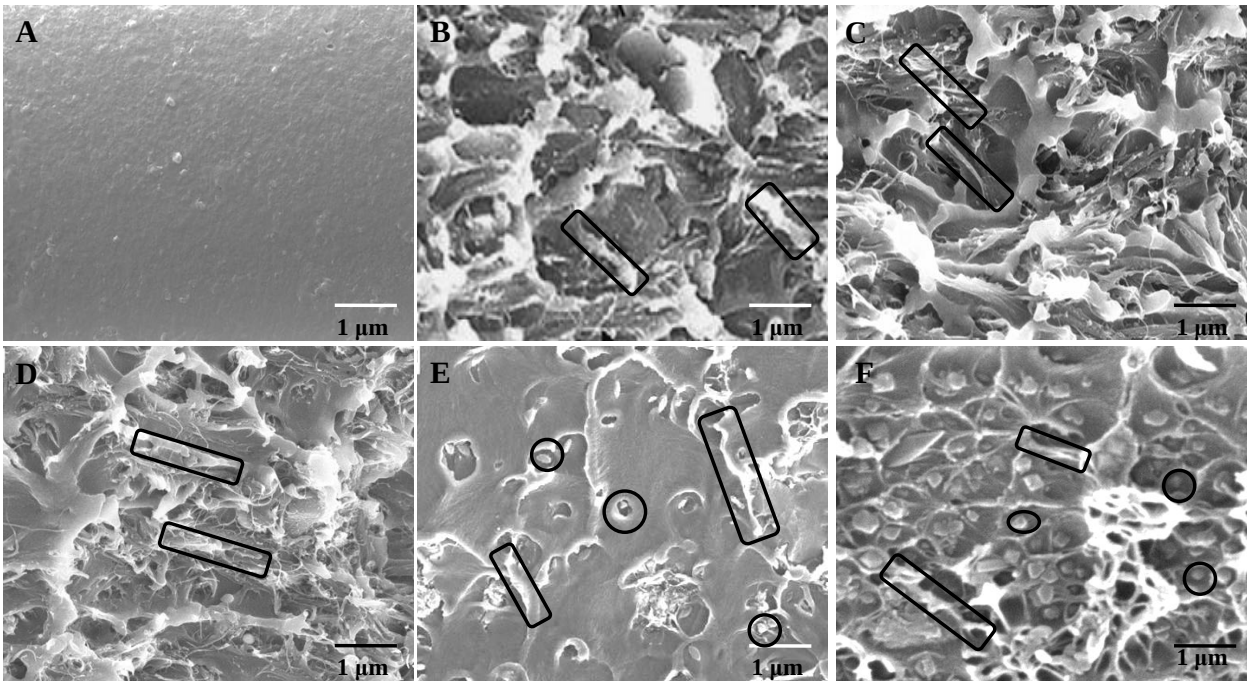

Fig. 3.2 Scanning electron micrographs of bare PSF [A], PSF/CNTs(10)/ZIF-300(6) [B], PSF/CNTs(8)/ZIF-300(12) [C], PSF/CNTs(6)/ZIF-300(18) [D], PSF/CNTs(4)/ZIF-300(24) [E], and PSF/CNTs(2)/ZIF-300(30) [F] MMMs containing different loadings of CNTs (enclosed by rectangles) and ZIF-300 nanocrystals (surrounded by circles).

For MMMs containing high CNTs loadings (8 and 10 wt %) and low ZIF-300 contents (6 and 12 wt %), the CNTs are agglomerated owing to their large surface energy while ZIF-300 nanocrystals show uniform dispersion and good filler-polymer adhesion on account of their tiny particle size (Fig. 3.2 [B] and [C]). MMMs incorporated with high ZIF-300 (24 and 30 wt %) and low CNTs (2 and 4 wt %) loadings revealed consistent CNTs

distribution but improper dispersion and poor adhesion of ZIF-300 nanoparticles (Fig. 3.2 [E] and [F]). The MMM filled with optimum nanofillers loading (6 wt % CNTs and 18 wt % ZIF-300) demonstrated uniform dispersion and good interfacial adhesion of the nanofillers with polymer matrix as the cross sectional view of MMM exhibits defect-free interconnected network morphology (Fig. 3.2 [D]). The controlled morphology of ZIF-300 nanoparticles dispersed in the optimized MMM rendered substantial steric effect to mitigate CNTs aggregation; conversely the strong polymer-filler interaction led to the consistent scattering of ZIF-300 nanoparticles. The collegial impact of CNTs and ZIF-300 nanoparticles oriented some of the CNTs in parallel to gas permeation pathways through the MMM.

3.3.3 Thermal Gravimetric Analysis

In order to study the effect of CNTs and ZIF-300 nanofillers on thermal stability, phase transitions, physical and chemical phenomena of MMMs, TGA-DTG analyses of bare PSF membrane and PSF/CNTs/ZIF-300 MMMs having different loadings were conducted from room temperature to a final temperature of 700 ^{o}C. The TGA curves of the prepared membranes show a consistent decomposition profile indicating a two-step weight loss at around 100-270 ^{o}C (desolvation) and 460-660 ^{o}C (pyrolysis) as depicted in Fig. 3.3 [A]. The weight loss corresponding to first peak can be attributed to the liberation of volatile solvent molecules (water, DMF, CCl_4 etc.) trapped within the pores of MMMs. The weight loss related to second peak can be attributed to the decomposition of organic ligands (2-methylimidazole and 5(6)-bromobenzimidazole) of the imidazole framework and complete degradation of CNTs and PSF constituting entities (C, SO_2,

benzene, phenol, toluene, styrene, xylene etc.). The residual weight at the end of analyses helped to verify the nominal mass contents of the filled CNTs and ZIF-300 nanocrystals in corresponding MMMs.

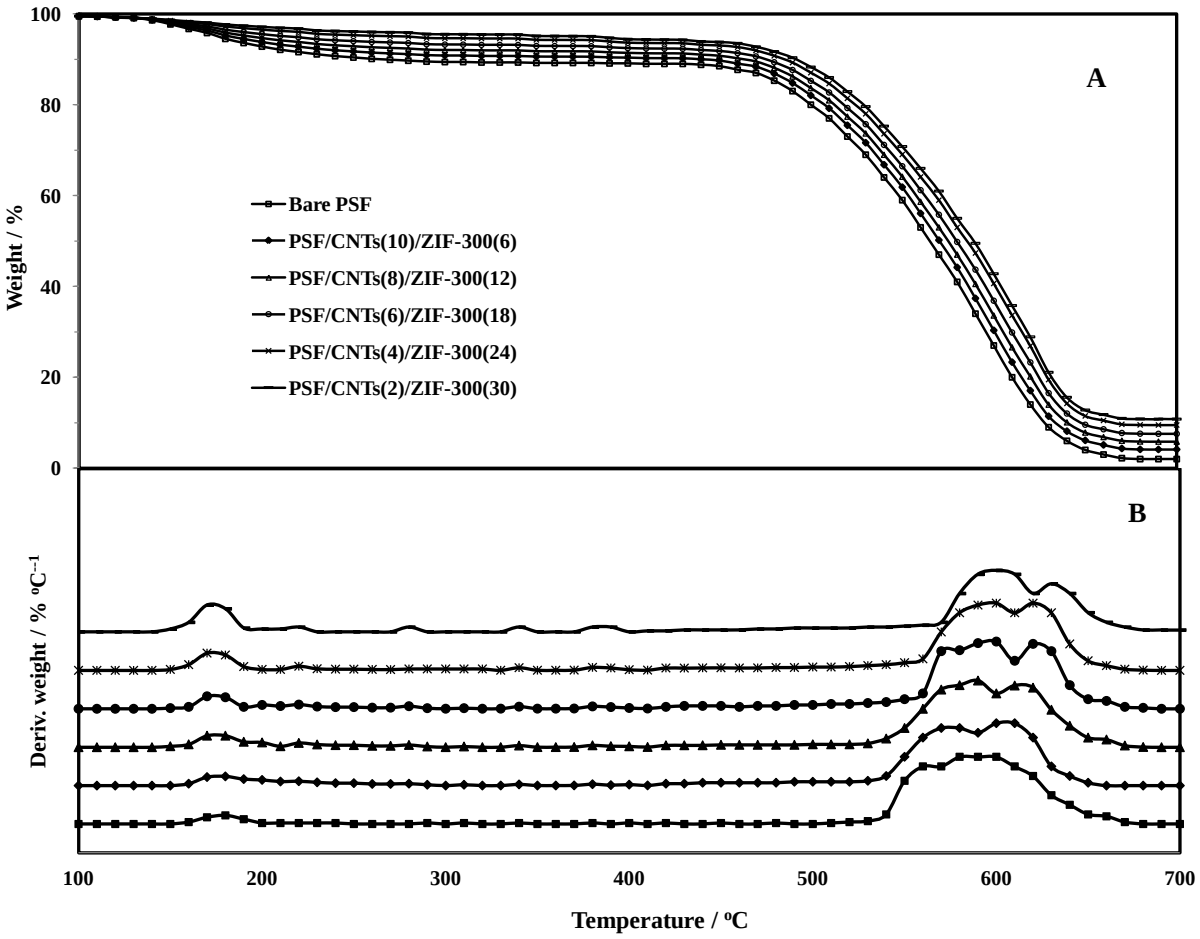

Fig. 3.3 TGA-DTG curves: TGA [A] and DTG [B] bare PSF and MMMs containing different loadings of CNTs and ZIF-300 nanocrystals.

The temperatures at which testing specimen loses its 5 and 10 percent weight, denoted by $T_{d5\%}$ and $T_{d10\%}$ respectively, in TGA analysis determine the thermal stability of a material [43]. Table 3.1 summarizes some important thermal parameters of the synthesized materials. Both parameters being increasing function of nanofillers, $T_{d5\%}$ and $T_{d10\%}$

values occur between 176-382 °C and 264-492 °C respectively. The DTG curves illustrated in Fig. 3.3 [B] also give information on pyrolysis rates; the residual masses of all the materials are enlisted in Table 1. The degree of rigidification of the polymer chains in MMMs can be determined in terms of T_g, 1st and 2nd DTG peak values. The advancement in these values with increased nanofiller loadings (Table 1) indicate improved rigidity of MMMs due to the constrained motion of polymer chains resulting from mutual interactions among polymer chains and nanofiller entities.

Table 3.1 Characteristic temperatures of membrane materials acquired from TGA-DTG data

Sample Designation	$T_{d5\%}$ (^oC)	$T_{d10\%}$ (^oC)	**Residual mass** (%)	**1st DTG peak** (^oC)	**2nd DTG peak** (^oC)
Bare PSF	176	264	2.1	178	587
PSF/CNTs(10)/ZIF-300(6)	183	441	4.1	181	591
PSF/CNTs(8)/ZIF-300(12)	194	463	5.3	185	593
PSF/CNTs(6)/ZIF-300(18)	213	476	6.7	188	598
PSF/CNTs(4)/ZIF-300(24)	280	484	8.2	183	596
PSF/CNTs(2)/ZIF-300(30)	382	492	9.3	182	595

The thermal decomposition of MMMs, as compared to that of bare PSF membrane, occurring at higher temperatures can be ascribed to strong filler-polymer interactions

along with good thermal stability of CNTs and ZIF-300. The thermal stability of PSF/CNTs(6)/ZIF-300(18) MMM was the highest due to synergistic effect of CNTs and ZIF-300 nanofillers. As indicated by weight loss curves the thermal stability of MMMs, determined in terms of 2nd DTG peaks, improved with increasing nanofiller contents. Since the maximum temperature experienced in different gas separation and combustion processes falls in the range of 30 to 350 °C, these MMMs can safely be used in gas separation applications [44].

3.3.4 Gas Sorption Analysis

Low pressure CO_2 and N_2 adsorption isotherms with increasing pressure up to 1 bar were measured at 298 K for bare PSF membrane and PSF/CNTs/ZIF-300 MMMs containing varying contents of nanofillers (see Fig. 3.4).

Main physical macroscopic properties (density, fractional volume of nanofillers) and microporous characteristics such as Brunauer-Emmett-Teller (S_{BET}) and Langmuir (S_{Lang}) surface areas, total micropore volume, CO_2 and N_2 uptakes, and CO_2/N_2 adsorption selectivity, of the specimen are enhanced with nanofillers loading as summarized in Table 3.2. These findings directly validate the existence of homogeneous dispersion, improved adhesion and interfaces between nanoparticles and PSF matrix leading to good quality membranes.

CO_2 uptake for all the samples appreciably increased with pressure due to the chemical affinity of both the nanofillers for quadro-polar CO_2 molecules. MMM containing 6 wt % CNTs and 18 wt % ZIF-300 had the highest CO_2 loading ca. 26 cm^3/g (≈1.3 mmol/g) at 25 ^oC which can be further increased by lowering the temperature. The N_2 adsorption

isotherms for all the membranes almost followed a proportional correlation with pressure up to 1 bar. In addition all the membranes showed preferably high adsorption affinity for CO_2 as compared to N_2, especially at low CO_2 partial pressure. The CO_2/N_2 sorption selectivities of the MMMs significantly increased with nanofillers (especially ZIF-300) loadings. These facts suggest potential applications for the separation of CO_2/N_2 mixture from post combustion flue gases.

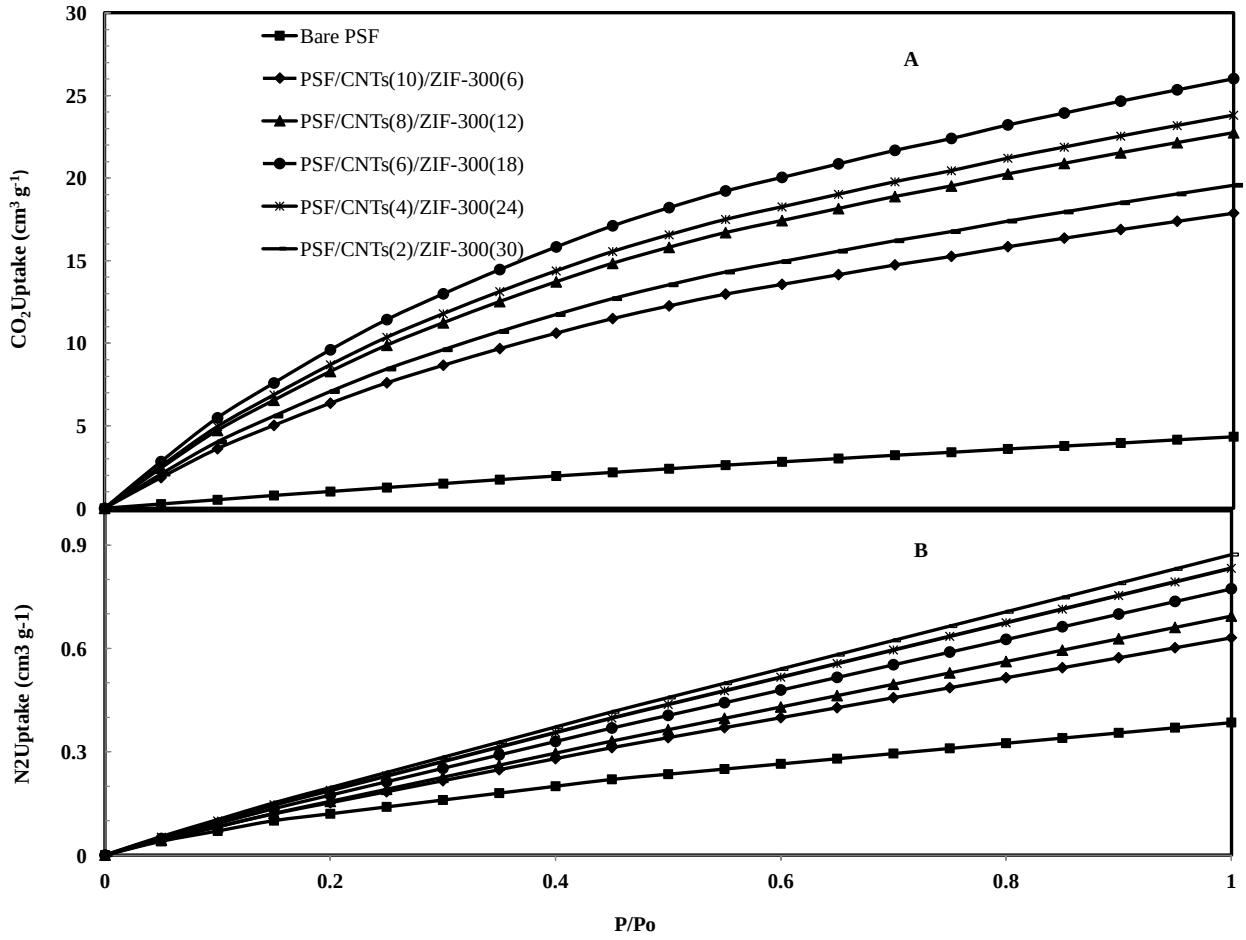

Fig. 3.4 CO_2 [A] and N_2 [B] adsorption isotherms for bare PSF and PSF/CNTs/ZIF-300 MMMs containing varying loadings of CNTs and ZIF-300 nanocrystals at 298 ^oC.

Table 3.2 Physical and microporous properties of bare PSF and PSF/CNTs/ZIF-300 MMMs

Sample Designation	**Density** ($g\ cm^{-3}$)	**Φ_d** (%)	**S_{BET}** (m^2g^{-1})	**S_{Lang}** (m^2g^{-1})	**V_{micro}** (m^3g^{-1})	**CO_2 uptake** (cm^3g^{-1})	**N_2 uptake** (cm^3g^{-1})	α_{CO_2/N_2}
Bare PSF	1.25	0.00	12	20	0.02	4.34	0.39	11
PSF/CNTs(10)/ZIF-300(6)	1.347	11.7	120	170	0.22	17.88	0.63	28
PSF/CNTs(8)/ZIF-300(12)	1.342	15.9	150	210	0.26	22.74	0.69	33
PSF/CNTs(6)/ZIF-300(18)	1.337	20.1	170	240	0.31	26.02	0.77	34
PSF/CNTs(4)/ZIF-300(24)	1.332	24.3	160	220	0.28	23.80	0.83	29
PSF/CNTs(2)/ZIF-300(30)	1.327	28.5	130	200	0.23	19.56	0.87	22

3.3.5 Gas Permeation Properties of MMMs

Single gas (CO_2 and N_2) dry and wet permeation experiments for PSF/CNTs/ZIF-300 MMMs containing different CNTs and ZIF-300 loadings were performed at 25 °C under an upstream pressure of 2 bar. Owing to its strong affinity for the nanofillers, CO_2 permeability and CO_2/N_2 selectivity of the MMMs were substantially enhanced with CNTs and ZIF-300 contents as represented in Fig. 3.5. The permeation experiments accomplished using humid gases did not affect the transport properties of CO_2 and N_2.

Owing to their large pore size and smooth internal surfaces, doping of CNTs into the polymer matrix significantly enhanced CO_2 permeability at the expense of reduced CO_2/N_2 selectivity. The incorporation of ZIF-300 nanocrystals into MMMs moderately enhanced both CO_2 permeability and CO_2/N_2 selectivity due to the presence of amine

functional groups. The CO_2 permeability and CO_2/N_2 selectivity of the MMMs were significantly improved by the synergistic effect of adding CNTs and ZIF-300 nanofillers as shown in Fig. 3.5. The optimum filler loading was found to be 6 wt % CNTs and 18 wt % ZIF-300 nanocrystals. At the optimal filler loading the CO_2 permeability of the MMM was determined to be 33 Barrer with CO_2/N_2 selectivity of 72. The most preferable loading favored homogeneous distribution of the nanofillers so as to exploit the pathways of CNTs pores to amplify CO_2 permeability and the CO_2/N_2 selective affinity of amine-functionalized ZIF-300 nanocrystals to render high selectivity.

Gas permeation through a membrane occurring via solution-diffusion mechanism can be better explained by evaluating diffusion (D) and solubility (S) coefficients of CO_2 and N_2 in MMMs. The data for coefficients of diffusion (D) and solubility (S) along with their corresponding CO_2/N_2 selectivity values for bare PSF membrane and different PSF/CNTs/ZIF-300 MMMs are illustrated in Figs. 3.5 and 3.6. The diffusivity coefficients of CO_2 and N_2 slightly changed with different levels of filler loading and were maximized at the optimal filler loading. The gas diffusivities were improved due to preferential orientation and close packing of smooth-walled CNTs within the polymer matrix. At the optimum loading the solubility coefficient of CO_2, in contrast to that of N_2, was significantly enhanced. The solubility coefficient, in general, depends on both chemical constitution and structural arrangement of the membrane. The basic nature of both CNTs hydroxyl groups and ZIF-300 amine groups generated a synergistic impact to preferably adsorb the acidic CO_2 molecules as compared to non-polar N_2 molecules. This phenomenon resulted in high CO_2 solubility and restricted that of N_2, consequently improving CO_2/N_2 solubility selectivity. The improved permselectivity of CO_2 over N_2

can also be attributed to the increased number of interaction sites, functional and basic groups by incorporating CNTs and ZIF-300 nanocrystals into PSF matrix.

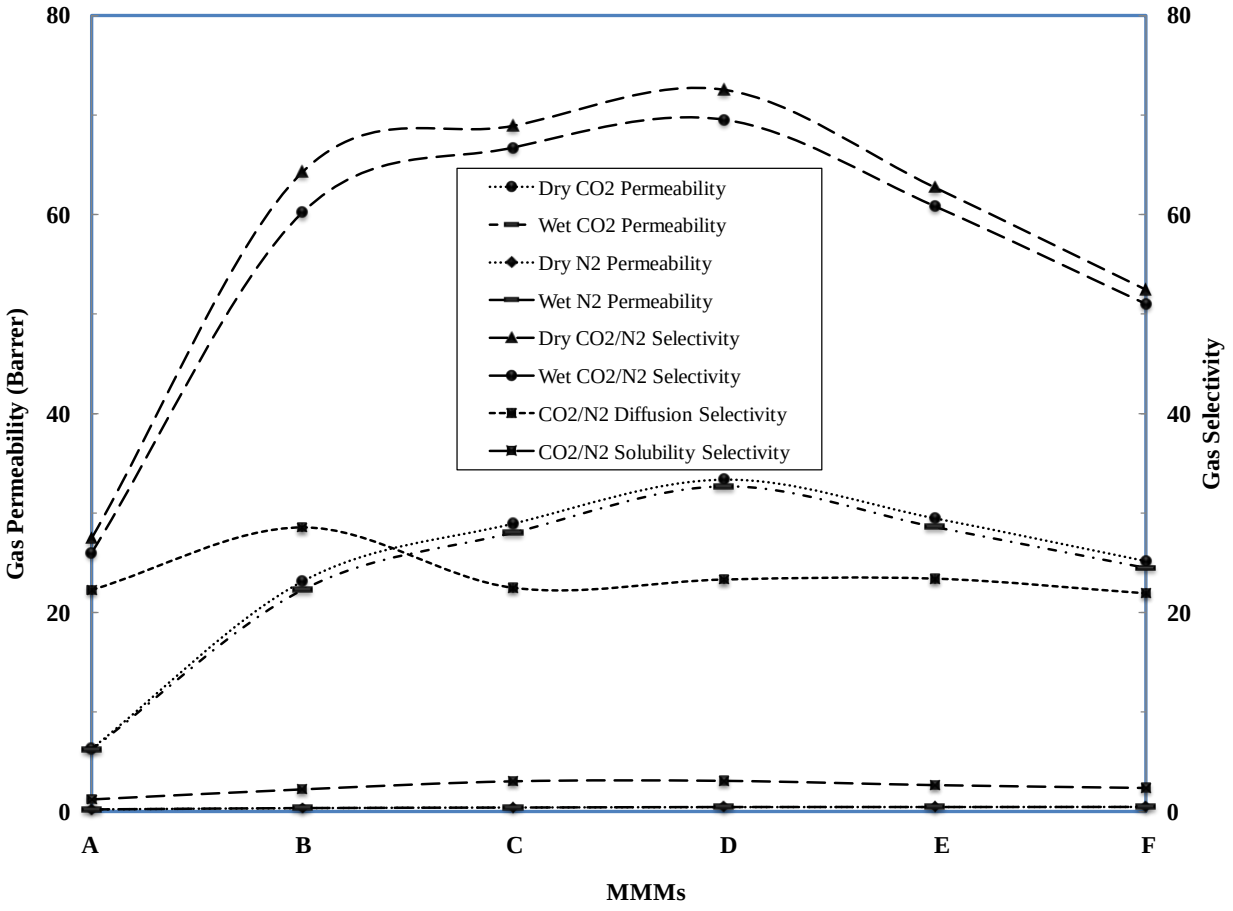

Fig. 3.5 Dry and wet gas CO_2 and N_2 permeabilities and CO_2/N_2 selectivity of bare PSF [A], PSF/CNTs(10)/ZIF-300(6) [B], PSF/CNTs(8)/ZIF-300(12) [C], PSF/CNTs(6)/ZIF-300(18) [D], PSF/CNTs(4)/ZIF-300(24) [E], and PSF/CNTs(2)/ZIF-300(30) [F] MMMs containing different loadings of CNTs and ZIF-300 nanocrystals.

The time-lag method (eq. 6) was used to determine the values of diffusion coefficients. CO_2 and N_2 adsorption isotherms obtained at 25 ^oC under varying pressure helped to calculate Langmuir parameters to determine the correction parameters (bracketed term in eq. 3). The D values thus determined were used to calculate solubility coefficients of the membranes under the same conditions of temperature and pressure using eq. 4. The values of gas diffusivity coefficient selectivity (D_{CO2}/D_{N2}) slightly varied with different nanofiller loadings, while the gas solubility coefficient selectivity (S_{CO2}/S_{N2}) significantly changed for all MMMs achieving a maximum value for the MMM containing 6 wt % CNTs and 18 wt % ZIF-300 as shown in Fig. 3.5.

Almost defect-free CNTs allowed both type of gas molecules to diffuse quickly through the internally smooth-walled channels. Since the well dispersed CNTs in PSF matrix acted as pathways to efficiently carry gas molecules, the overall gas permeability was highly improved. Also the selective solubility of CO_2 into ZIF-300 nanocrystals greatly enhanced its permeation through the MMMs. The pore size reduction of MMMs occurred by doping of ZIF-300 nanocrystals led to restricted N_2 adsorption as compared to CO_2. In general the improved CO_2/N_2 ideal selectivities of MMMs can be ascribed to controlled N_2 diffusion and preferential CO_2 solubility. Both the nanofillers mutually interacted so as to render controlled passages for improved CO_2 permeability and CO_2/N_2 selectivity in MMMs. The overall analysis based on improved CO_2 permeability and reduced N_2 diffusivities in PSF/CNTs/ZIF-300 MMMs strongly support the development of a genuine mixed matrix membrane. The membranes permeation time lag characteristic also implied good interfacial adhesion and homogeneous distribution of the nanofillers in PSF matrix.

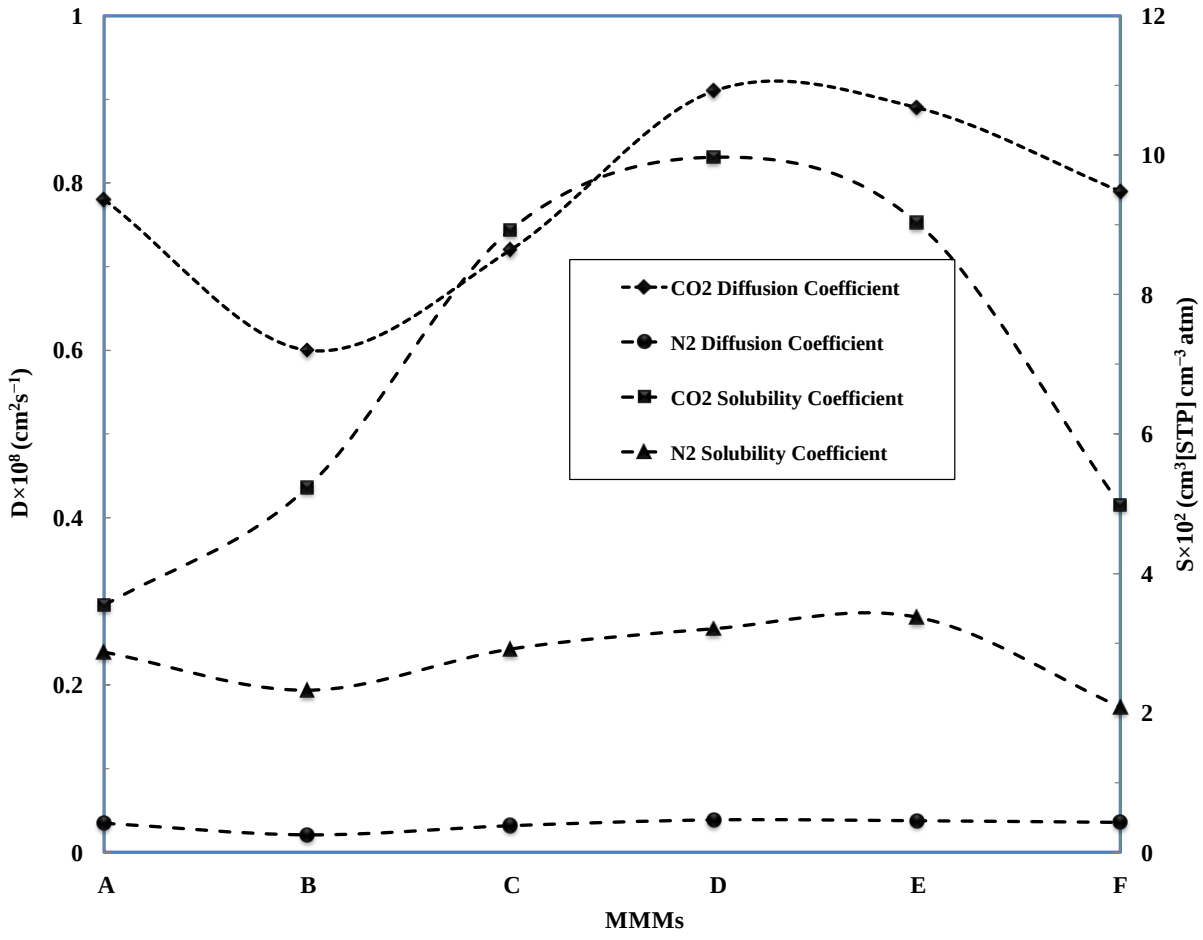

Fig. 3.6 Pure gas diffusion (D) and solubility (S) coefficients for bare PSF [A], PSF/CNTs(10)/ZIF-300(6) [B], PSF/CNTs(8)/ZIF-300(12) [C], PSF/CNTs(6)/ZIF-300(18) [D], PSF/CNTs(4)/ZIF-300(24) [E], and PSF/CNTs(2)/ZIF-300(30) [F] MMMs containing different loadings of CNTs and ZIF-300 nanocrystals.

Since a membrane possessing high perm-selectivity values meets industrial applications, it appears that CNTs and ZIF-300 nanofillers are competent materials to fabricate MMMs

for post combustion carbon capture on account of its high CO_2 permeability coupled with reasonable CO_2/N_2 selectivity.

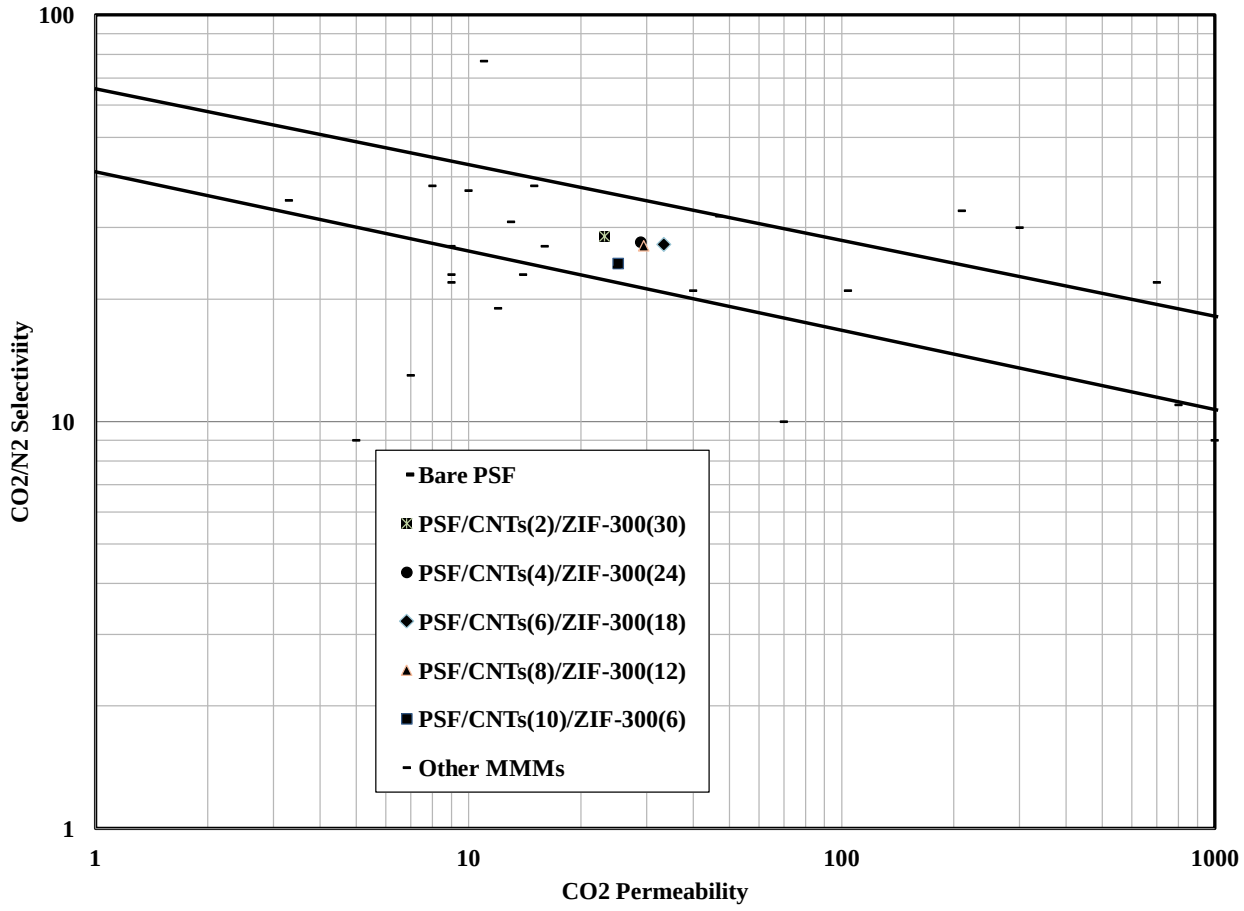

Fig. 3.7 Comparison of CO_2/N_2 separation performance of PSF/CNTs/ZIF-300 MMMs with other ZIF or MOF containing MMMs obtained from literature data. The Robeson 1991 and 2008 upper bounds for polymer separation performance are also shown.

A comparison of the CO_2/N_2 gas pair separation performance of nanofilled MMMs, along with Robeson 1991 and 2008 upper bounds [14], is depicted on a permeability-selectivity chart as shown in Fig. 3.7. The diagram indicates that the incorporation of CNTs and

ZIF-300 nanofillers into PSF matrix has enhanced the perm-selectivity of the MMMs as compared to neat polysulfone membrane. The perm-selectivity values of all the MMMs containing different nanofiller loadings are located in between 1991- and 2008-upper bound lines, an important achievement of this work.

3.4 Conclusions

Multiwalled CNTs and ZIF-300 nanofillers were incorporated into PSF to fabricate hydrothermally stable high performance mixed-matrix membranes for selective CO_2 separation from post combustion flue gases. Characterization of the MMMs done by XRD, TGA, SEM and gas sorption experiments indicated that they are thermally stable, microporous, crystalline materials possessing homogeneous filler dispersion and good interfacial filler-matrix adhesion without adding any compatibilizing agent. The MMMs developed in this work demonstrated more than 5 times increment in CO_2 permeability as compared to that of pure PSF membrane while the CO_2/N_2 ideal selectivity was enhanced by 3 times. The separation performance of the MMMs produced in this work were above the Robeson 1991 upper bound and the CO_2/N_2 ideal selectivity is considered to be high enough to meet industrial applications.

Acknowledgement

The authors are thankful to KACST-TIC on Carbon Capture and Sequestration (CCS), King Fahd University of Petroleum and Minerals, Dhahran, Kingdom of Saudi Arabia for providing support for this work.

References

[1] D. M. D'Alessandro, B. Smit, J. R. Long, Carbon Dioxide Capture: Prospects for New Materials, Angew. Chem. Int. Ed. 49 (2010) 6058-6082.

[2] M. Z. Jacobson, Review of Solutions to Global Warming, Air Pollution, and Energy Security, Energy Environ. Sci. 2 (2009) 148-173.

[3] N. MacDowell, N. Florin, A. Buchard, J. Hallett, A. Galindo, G. Jackson, C. S. Adjiman, C. K. Williams, N. Shah, P. Fennell, An Overview of CO_2 Capture Technologies, Energy Environ. Sci. 3 (2010) 1645-1669.

[4] H. Herzog, D. Golomb, Carbon capture and storage from fossil fuel use, Encyc. Energy 1 (2004) 277-287.

[5] A. Hussain, M.B. Hägg, A feasibility study of CO_2 capture from flue gas by a facilitated transport membrane, J. Membr. Sci. 359 (2010) 140-148.

[6] J. Zhao, Z. Wang, J.X. Wang, S.C. Wang, Influence of heat-treatment on CO_2 separation performance of novel fixed carrier composite membranes prepared by interfacial polymerization, J. Membr. Sci. 283 (2006) 346-356.

[7] P. Pandey, R.S. Chauhan, Membranes for gas separation, Prog. Polym. Sci. 26 (2001) 853-893.

[8] R. Mahajan, W.J. Koros, Factors controlling successful formation of mixed-matrix gas separation materials, Ind. Eng. Chem. Res. 39 (2000) 2692–2696.

[9] E.P. Fawas, G.C. Kapantaidakis, J.W. Nolan, A.C. Mitropoulos, N.K. Kanellopoulos, Preparation, characterization and gas permeation properties of carbon hollow fiber membranes based on Matrimid® 5218 precursor, J. Mater. Process. Technol. 186 (2007) 102–110.

[10] R.W. Baker, Future directions of membrane gas separation technology, J. Ind. Eng. Chem. Res. 41 (2002) 1393–1411.

[11] D.L. Gin, R.D. Noble, Designing the next generation of chemical separation membranes, Science 332 (2011) 674-676.

[12] Y. Xiao, T.-S. Chung, Grafting thermally labile molecules on cross-linkable polyimide to design membrane materials for natural gas purification and CO_2 capture. Energy Environ. Sci. 4 (2011) 201-208.

[13] C. Staudt-Bickel, W.J. Koros, Improvement of CO_2/CH_4 separation characteristics of polyimides by chemical crosslinking. J. Membr. Sci. 155 (1999) 145-154.

[14] T.C. Merkel, B.D. Freeman, R.J. Spontak, Z. He, I. Pinnau, P. Meakin, A. Hill, J. Ultrapermeable, reverse-selective nanocomposite membranes, Science 296 (2002) 519-522.

[15] J. Ahn, W.-J. Chung, I. Pinnau, M.D. Guiver, Polysulfone/silica nanoparticle mixed-matrix membranes for gas separation, J. Membr. Sci. 314 (2008) 123-133.

[16] B.D. Reid, A. Ruiz-Trevino, I.H. Musselman, K.J. Balkus, J.P. Ferraris, Gas permeability properties of polysulfone membranes containing the mesoporous molecular sieve MCM-41, Chem. Mater. 13 (2001) 2366-2373.

[17] S. Kim, E. Marand, J. Ida, V.V. Guliants, Polysulfone and mesoporous molecular sieve MCM-48 mixed matrix membranes for gas separation, Chem. Mater. 18 (2006) 1149-1155.

[18] S. Kim, E. Marand, High permeability nano-composite membranes based on mesoporous MCM-41 nanoparticles in a polysulfone matrix, Microp. Mesop. Mater. 114 (2008) 129-136.

[19] D.Q. Vu, W.J. Koros, S.J. Miller, Mixed matrix membranes using carbon molecular sieves. II. Modeling permeation behavior, J. Membr. Sci. 211 (2003) 335-348.

[20] H.L. Cong, J.M. Zhang, M. Radosz, Y.Q. Shen, Carbon nanotube composite membranes of brominated poly(2,6-diphenyl-1,4-phenylene oxide) for gas separation, J. Membr. Sci. 294 (2007) 178–185.

[21] S. Kim, L. Chen, J.K. Johnson, E. Marand, Polysulfone and functionalized carbon nanotube mixed matrix membranes for gas separation: Theory and experiment, J. Membr. Sci. 294 (2007) 147–158.

[22] P. Gorgojo, S. Uriel, C. Tellez, J. Coronas, Development of mixed matrix membranes based on zeolite Nu-6(2) for gas separation, J. Microporous Mesoporous Mater. 115 (2008) 85–92.

[23] Y. Liu, D. Peng, G. He, S. Wang, Y. Li, H. Wu, Z. Jiang, Enhanced CO_2 permeability of membranes by incorporating polyzwitterion@CNT composite particles into polyimide matrix, ACS Appl. Mater. Interfaces 6 (2014) 13051-13060.

[24] B. Harold, T. Jeazet, C. Staudt, C. Janiak, Metal–organic frameworks in mixed-matrix membranes for gas separation, Dalton Trans. 41 (2012) 14003–14027.

[25] T. Li, Y. Pan, K.V. Peinemann, Z. Lai, Carbon dioxide selective mixed matrix composite membrane containing ZIF-7 nano-fillers, J. Membr. Sci. 425–426 (2013) 235–242.

[26] Chen Zhang, Kuang Zhang, Liren Xu, Ying Labreche, Brian Kraftschik, W.J. Koros, Highly scalable ZIF-based mixed-matrix hollow fiber membranes for advanced hydrocarbon separations, AIChE J. 60 (2014) 2625–2635.

[27] Mohammad Askari, T.S. Chung, Natural gas purification and olefin/paraffin separation using thermal cross-link ableco-polyimide/ZIF-8 mixed matrix membranes, J. Membr. Sci. 444 (2013) 173–183.

[28] T.T.N. Nhung, H. Furukawa, F. Gandara, H.T. Nguyen, K.E. Cordova, O.M. Yaghi, Selective capture of carbon dioxide under humid conditions by hydrophobic chabazite-type zeolitic imidazolate frameworks, Angew. Chem. 126 (2014) 10821–10824.

[29] H. Chen, D.S. Sholl, Predictions of selectivity and flux for CH_4/H_2 separations using single walled carbon nanotubes as membranes, J. Membr. Sci. 269 (2006) 152–160.

[30] D.S. Sholl, J.K. Johnson, Making high-flux membranes with carbon nanotubes, Science 312 (2006) 1003–1004.

[31] A.I. Skoulidas, D.S. Sholl, J.K. Johnson, Adsorption and diffusion of carbon dioxide and nitrogen through single-walled carbon nanotube membranes, J. Chem. Phys. 124 (2006) 054708.

[32] S. Kim, J.R. Jinschek, H. Chen, D.S. Sholl, E. Marand, Scalable fabrication of carbon nanotube/polymer nanocomposite membranes for high flux gas transport, Nano Lett. 7 (2007) 2806–2811.

[33] T.W. Chamberlain, J.C. Meyer, J. Biskupek, J. Leschner, A. Santana, N.A. Besley, E. Bichoutskaia, U. Kaiser, A.N. Khlobystov, Reactions of the inner surface of carbon nanotubes and nanoprotrusion processes imaged at the atomic scale, Nat. Chem. 3 (2011) 732–737.

[34] A.F. Ismail, P.S. Goh, S.M. Sanip, M. Aziz, Transport and separation properties of carbon nanotube-mixed matrix membrane, Sep. Purif. Technol. 70 (2009) 12–26.

[35] L. Ge, L. Wang, V. Rudolph, Z. Zhu, Hierarchically structured metal-organic framework/vertically-aligned carbon nanotubes hybrids for CO_2 capture, RSC Adv. 3 (2013) 25360–25366.

[36] B. Zornoza, B. Seoane, J. M. Zamaro, C. Téllez and J. Coronas, Combination of MOFs and zeolites for mixed-matrix membranes, Chem-PhysChem, 12 (2011) 2781–2785.

[37] M. Valero, B. Zornoza, C. Téllez, J. Coronas, Mixed matrix membranes for gas separation by combination of silica MCM-41 and MOF NH2-MIL-53 (Al) in glassy polymers, Microporous Mesoporous Mater. 192 (2013) 23–28.

[38] A. Galve, D. Sieffert, C. Staudt, M. Ferrando, C. Güell, C. Téllez, J. Coronas, Combination of ordered mesoporous silica MCM-41 and layered titanosilicate JDF-L1 fillers for 6FDA-based copolyimide mixed matrix membranes, J. Membr. Sci. 431 (2013) 163-170.

[39] X. Li, L. Ma, H. Zhang, S. Wang, Z. Jiang, R. Guo, H. Wu, X.Z. Cao, J. Yang, B. Wang, Synergistic effect of combining carbon nanotubes and grapheme oxide in mixed matrix membranes for efficient CO_2 separation, J. Memb. Sc. 479 (2015) 1-10

[40] X.W. Yu, Z. Wang, Z.H. Wei, S.J. Yuan, J. Zhao, J.X. Wang, S.C. Wang, Novel tertiary amino containing thin film composite membranes prepared by interfacial polymerization for CO_2 capture, J. Membr. Sci. 362 (2010) 265-278.

[41] D.R. Paul, D.R. Kemp, The diffusion time lag in polymer membranes containing adsorptive fillers, J. Polym Sc: Polym. Symp. 41 (1973) 79–93.

[42] V. Gupta, T. Saleh, Synthesis of Carbon Nanotube-Metal Oxides Composites; Adsorption and Photo-Degradation, Carbon 59 (2013)308–314.

[43] Y.C. Xiao, T.S. Chung, H.M. Guan, M.D. Guiver, Synthesis, cross-linking and carbonization of co-polyimides containing internal acetylene units for gas separation, J. Membr. Sci. 302 (2007) 254-264.

[44] A.C.C. Chang, S.S.C. Chuang, M. Gray, Y. Soong, In-situ infrared study of CO_2 adsorption on SBA-15 grafted with γ-(aminopropyl) triethoxysilane, Energy Fuels 17 (2003) 468-473.

CHAPTER 4

A NOVEL ZEOLITIC IMIDAZOLATE FRAMEWORK BASED MIXED-MATRIX MEMBRANE FOR EFFICIENT CO_2 SEPARATION UNDER WET CONDITIONS

Abstract

Polymer-based mixed-matrix membranes (MMMs) were prepared by filling glassy polysulfone (PSF) with zeolitic imidazole framework ZIF-301 nanocrystals using solution-casting method. Different loadings of ZIF-301 nanocrystals were incorporated in PSF matrix for the first time to find the separation effectiveness of MMMs to remove carbon dioxide from dry and wet CO_2/N_2 gaseous mixture. Hydrothermally stable flexible MMMs demonstrating consistent distribution and fine adhesion of filler-matrix were characterized by x-ray diffraction (XRD), scanning electron microscopy (SEM), and thermal gravimetric analysis (TGA). Gas sorption analysis along with dry and wet gas permeation tests exhibited that CO_2 permeability of MMM containing 40 wt % ZIF-301 was increased by three times as compared to bare PSF without affecting CO_2/N_2 permselectivity.

4.1. Introduction

Carbon dioxide (CO_2) emissions from burning of fossil fuels cause global warming and has turned out to be a serious environmental concern throughout the sphere [1-3]. CO_2 emissions into the atmosphere can be reduced by its capture and/or sequestration via economically viable processes [4-5]. As compared to other convenient processes, gas separation technology using polymer-based mixed-matrix membranes (MMMs) has gained substantial importance due to their low capital and operating costs, improved efficiency, low energy requirement, uncomplicated function, flexible design, ease of scale up, and environmental kindliness [6-13].

The important considerations of a fine quality gas separation membrane comprise enhanced permselectivity and separation factor, good mechanical strength, improved chemical and thermal stability, and good operational permanence [14-20]. On account of its intrinsic structural limitations (inter-chain spacing and chain mobility), a glassy polymer membrane being highly permeable is generally less selective [15, 21-23]; it requires significant improvements for adaptable applications.

To prepare competent hybrid membranes with improved permselectivity features as compared to bare polymer membranes, a lot of glassy polymers have been modified to fabricate MMMs by integrating organic polymers with inorganic fillers like nonporous silica [24-25], structured mesoporous silica [26-28], carbon molecular sieves [29], carbon nanotubes [30-31], zeolites [32], and microporous metal organic frameworks (MOFs) [33]. Some key advantages of MMMs fabricated by incorporating microporous MOF or ZIF nanocrystals into polymer matrix include the ability to integrate the ease of production and processability, improved mechanical and chemical stability of polymers

coupled with enhanced gas separation attributes of microporous nanocrystalline materials possessing adjustable pore size, modifiable surface functionality, and high surface areas [34].

Polysulfone membrane, commonly used for CO_2 separation, has achieved significant research interests due to its high permselectivity values [34]. Useful strategies to enhance CO_2 permeability of a polymer membrane include either its chemical modification or development of a hybrid membrane by incorporating microporous particles into polymer matrix. Car et al. (2006) reported the development of HKUST-1/PSF MMMs by adding varying loadings of HKUST-1 into glassy polysulfone [35]. The CO_2 permeability of the MMMs gradually enhanced with increasing HKUST-1 contents up to 10 % by weight. The CO_2/N_2 permselectivity improved with HKUST-1 loadings, reached a maximum value of 25 at 5 wt % loading, and then started decreasing with further addition of HKUST-1. Zornoza and coworkers (2009) developed MMMs by incorporating mesoporous silica spheres into polysulfone Udel® matrix up to a maximum loading of 32 % by weight; the optimum CO_2/N_2 permselectivity was obtained at 8 wt % HKUST-1 loading [36]. Various combinations of MOFs (HKUST-1), ZIFs (ZIF-8) and zeolites (S1C) were incorporated into PSF to develop different MMMs for gas permeation of CO_2, N_2, CH_4, O_2, and H_2 molecules [37]. The CO_2/N_2 separation efficiency did not improve for S1C-ZIF-8/PSF MMMs. The CO_2 permeabilities of S1C/PSF, HKUST-1/PSF, ZIF-8/PSF and HKUST-1/ZIF-8/PSF MMMs were found to be 9.4, 9.5, 12.3 and 8.4 Barrers respectively with corresponding CO_2/N_2 permselectivities of 23, 24, 19 and 38. CO_2 permeability of MIL-101(Cr)/PSF membranes developed by Harold et al. (2013)

increased linearly with MIL-101(Cr) loading while CO_2/N_2 ideal selectivity was slightly improved with MIL-101(Cr) contents [38].

ZIF-301, a hydrothermally stable microporous crystalline material [39], is efficiently capable to selectively capture CO_2 gas under real post combustion conditions. A typical flue gas contains 75% N_2, 15% CO_2, 6% H_2O and 4% trace gases by volume [40]. In the present study ZIF-301 nanocrystals have been incorporated into glassy PSF matrix for the first time to develop ZIF-301/PSF MMMs to efficiently enhance CO_2 separation performance. The main objective of this study is to check the effect of moisture contents on permselectivity values of ZIF-301/PSF MMMs with increasing ZIF-301 contents by performing the permeation tests under dry and wet conditions. The experimentally obtained gas permeation data were assessed by two- and three-phase permeation models.

4.2 Experimental and Modeling

4.2.1 Materials

Polysulfone having density 1.25 g cm^{-3} and average molecular weight ~ 35000 by LS was obtained from Sigma Aldrich. Zinc nitrate tetrahydrate and 2-methylimidazole were obtained from Merck Chemical Company. 5(6)-chlorobenzimidazole and solvent N,N-dimethylformamide (DMF) were obtained from Aldrich Chemical Company. Organic solvents such as anhydrous methanol (for ZIF-301 washing) and chloroform (for polymer dissolution) were obtained from Fisher Scientific. The polymer and chemicals were used as received without any additional treatment. Highly pure CO_2, N_2 and He gases were used for gas sorption and permeation experiments.

4.2.2 Synthesis of ZIF-301 nanocrystals

ZIF-301 nanocrystals were synthesized via cold synthesis procedure by slightly modifying the process conditions originally report by Nhung T. et al. [39]. 67.8 mg of $Zn(NO_3)_2 \cdot 6H_2O$ (the metal salt), 23.4 mg of 2-methylimidazole (primary organic linker), and 43.6 mg of 5(6)-chlorobenzimidazole (secondary organic linker) were dissolved in a mixture of 9.5 mL DMF and 0.5 mL distilled water by sonication in a 20-mL vial for 10 minutes. The resulting mixture was then moderately stirred on a hot plate at 50 °C for 70 hours to obtain light brown suspension. The suspended nanocrystals were separated from the mother liquor by centrifuge and daily washed with 7 mL of fresh DMF followed by solvent exchange with anhydrous methanol thrice a day at room temperature for 3 days. After decanting the spent methanol, ZIF-301 nanocrystals were washed three times with chloroform, and lastly redispersed in fresh chloroform to incorporate them into polymer matrix to prepare MMMs of varying compositions.

4.2.3 Preparation of ZIF-301/PSF MMMs

To prepare bare PSF membrane and ZIF-301/PSF MMMs, PSF was degassed at 100 ^{o}C under vacuum for 5 h to remove any adsorbed gas or moisture. Bare polymer membrane was fabricated by dissolving 500 mg of PSF into 5 mL of chloroform followed by stirring at room temperature for 24 hours until a thick viscous solution was formed. The MMMs containing 10, 20, 30 and 40 weight % ZIF-301 nanocrystals were prepared by redispersing a weighed quantity of ZIF-301 nanocrystals in 5 mL of chloroform for 10 minutes, adding weighed quantity of PSF into the system, and stirring the whole mixture for 24 hours. All the membranes were knife casted on clean glass plates at fixed gate

height using Flat Sheet Membrane Casting System (FSMCS). After slowly evaporating the solvent under ambient conditions overnight, the membranes were detached from the glass plates and placed in a VO 200 vacuum oven at 100 ^{o}C under a pressure of 10 mbar for 24 hours to ensure complete removal of the remaining solvent and internal stresses at polymer-filler interface.

4.2.4 Material Characterization Methods

The ZIF-301 nanocrystals, bare polysulfone membrane and ZIF-301/PSF mixed-matrix membranes were characterized by x-ray diffraction, scanning electron microscopy, thermal gravimetric analysis, and gas sorption measurement techniques. The fractional volume (Φ_D expressed in %) of ZIF-301 in MMMs can be defined as:

$$\Phi_D = \frac{(m_D/\rho_D)}{(m_D/\rho_D)+(m_C/\rho_C)} \times 100 \qquad (1)$$

where m and ρ represent mass and density of PSF (continuous phase denoted by subscript C) and ZIF-301 (dispersed phase denoted by subscript D) respectively. Normally the void volume of MMMs is negligible as supported by SEM images and gas sorption analysis. Hence the apparent volume fraction can safely be considered as the exact volume fraction of ZIF-301 in MMMs.

Powder x-ray diffraction patterns of ZIF-301 nanocrystals, bare PSF and ZIF-301/PSF MMMs were performed using a Bruker D8 X-ray diffractometer using Cu Kα radiation (λ = 1.5406 Å) run at 45 mA and 40 kV with an increment of 0.02^{o} in 2θ and a step scan size of 0.02^{o} s^{-1}. The membrane sample was loaded on silicon substrate placed in a

sample holder. The MMMs were characterized by XRD to check whether the polymeric matrix alters the crystalline pattern of ZIF-301 or not.

SEM images of all the samples were taken to look into the morphology of ZIF-301 nanocrystals, bare PSF membrane and MMMs having different ZIF-301 loadings by Hitachi S-4300SE/N SEM instrument. Testing specimens were cryofractured in liquid nitrogen and their outer surfaces were covered with a thin gold film to avoid charging of electrons. The SEM machine was operated at an accelerating voltage of 20 kV.

Glass transition temperature (T_g) of ZIF-301 nanocrystals, bare PSF membrane and their MMMs were determined by differential scanning calorimetry (DSC) with a Netzsch DSC 200F3 calorimeter in the temperature range of 20−400 °C at a heating rate of 5°C/min, under a nitrogen atmosphere with a flow rate of 50 mL/min. Thermal gravimetric analysis were done using a TGA/SDTA 851 (Mettler Toledo) system in air by heating from ambient temperature to 700 ^{o}C at a rate of 5 ^{o}C min^{-1}.

Nitrogen and carbon dioxide adsorption isotherms measured at different temperatures using a Quantachrome Autosorb iQ gas sorption analyzer helped to determine various characteristics (e.g., specific BET and Langmuir surface areas, total microporous volume, CO_2 and N_2 gas uptakes) of ZIF-301 microporous nanoparticles, PSF membrane and their composite membranes. The membrane samples were cut into small pieces and degassed at 100 ^{o}C under vacuum (<10^{-6} bar) for 5 hours. Physisorption data of CO_2 and N_2 gases were measured at 298 K under a gas pressure ranging from 10^{-6} -1 bar.

4.2.5 Gas Permeation Measurements

Pure gas (CO_2 and N_2) transport properties (i.e., permeability, ideal selectivity, and separation factor) of the membranes were estimated using single gas permeation cell

following the variable pressure (constant volume) method at room temperature [41-42]. After measuring its average thickness and effective cross sectional area, the membrane was affixed into the cell. While keeping the feed side valve closed, both the upstream (feed side) and downstream (permeate side) lines of the cell were evacuated. The valve between the permeate side line and the vacuum pump was then closed followed by opening the feed side valve to maintain a low feed pressure (e.g., 1 bar) for a specific time (i.e., 2 h) to record the permeation measurements. In order to estimate error and identify imperfect membranes, at least three replicas were prepared and tested corresponding to each composition of the MMMs.

Gas permeability (P_i, *Barrer*) of the membrane was computed using eq. (2):

$$P_i = \frac{22414}{A} \times \frac{V}{RT} \times \frac{l}{\Delta P_i} \frac{dP_i}{dt} \qquad (2)$$

where *l, A, V, R, T,* ΔP and $\Delta P_i/dt$ are respectively membrane thickness (*cm*), membrane effective area (cm^2), downstream volume (cm^3), universal gas constant (6236.56 cm^3 *cmHg/mol/K*), absolute temperature (*K*), pressure difference across the membrane (*psi*), and permeation rate (*psi/s*) of component i.

Time-lag method, suggested by Paul and Kemp [43], was used to determine diffusion coefficient (D) by using *diffusivity vs. time-lag* (D-θ) relationship for MMMs:

$$D = \frac{l^2}{6\theta}\left[1 + \frac{6K}{y^3}\left\{\frac{y^2}{2} + y - (1+y)\ln(1+y)\right\}\left(\frac{V_d}{V_p}\right)\right] \qquad (3)$$

where V_d and V_p are respectively the volume fractions of filler and polymer phases; K and y are adsorption parameters determined from Langmuir adsorption isotherm.

The solubility coefficient (S) can be calculated from Eq. (4):

$$S = \frac{P}{D} \qquad (4)$$

The ideal selectivity (α_{ij}) for gases i and j can be determined using Eq. (5):

$$\alpha_{ij} = \frac{P_i}{P_j} = \left(\frac{D_i}{D_j}\right)\left(\frac{S_i}{S_j}\right) \qquad (5)$$

Here (D_i/Dj) and (S_i/S_j) represent diffusion- and solubility-based selectivity terms respectively.

4.2.6 Modeling in ZIF-301/PSF MMMs

Analogous to electrical/thermal conductivity models through composite materials, several hypothetical models [44-46] have been proposed to estimate gas permeation through ideal and non-ideal morphology of MMMs. A two-phase system comprising continuous polymer matrix and dispersed inorganic filler particles constitutes an ideal morphology without any distortion and defect at the polymer-filler interface. Occurrence of defects and imperfections at organic-inorganic interface leads to a three-phase non-ideal morphology which addresses the polymer-filler interface in addition to matrix and filler phases. The two-phase permeation models to predict gas permeability through MMMs can be presented by the following expressions.

Maxwell:

$$P_r = \frac{1 + 2\phi\left(\frac{\lambda_{dm} - 1}{\lambda_{dm} + 2}\right)}{1 - \phi\left(\frac{\lambda_{dm} - 1}{\lambda_{dm} + 2}\right)} \qquad (6)$$

Bruggeman:

$$P_r^{\frac{1}{3}}\left(\frac{\lambda_{dm} - 1}{\lambda_{dm} - P_r}\right) = (1 - \Phi)^{-1} \qquad (7)$$

where

$$P_r = \frac{P_{eff}}{P_m} = \frac{Effective\ permeability\ of\ MMM}{Permeability\ of\ polymer\ matrix}$$

$$\lambda_{dm} = \frac{P_d}{P_m} = \frac{Permeability\ of\ dispersed\ phase}{Permeability\ of\ polymer\ matrix}$$

$$\Psi = 1 + \left(\frac{1 - \Phi_m}{\Phi_m^2}\right)\Phi$$

$$\Phi_m = volume\ fraction\ of\ fillers\ at\ maximum\ packing = 0.64$$

Φ = volume fraction of fillers

The three-phase modified Felske model can be expressed as follows.

Modified Felske:

$$P_r = \frac{1 + \frac{2\Phi(\beta - \gamma)}{(\beta + 2\gamma)}}{1 - \frac{\Phi\Psi(\beta - \gamma)}{(\beta + 2\gamma)}} \qquad (9)$$

where

$$\beta = (2 + \delta^3)\lambda_{dm} - 2(1 - \delta^3)\lambda_{im}$$

$$\gamma = 1 + 2\delta^3 - (1 - \delta^3)\lambda_{di}$$

$$\lambda_{di} = \frac{P_d}{P_i} = \frac{Permeability\ of\ dispersed\ phase}{Permeability\ of\ interphase}$$

$$\lambda_{im} = \frac{P_i}{P_m} = \frac{Permeability\ of\ interphase}{Permeability\ of\ matrix\ phase}$$

$$\lambda_{dm} = \lambda_{di}\lambda_{im} = \frac{\beta}{\gamma}$$

$$\delta = ratio\ of\ the\ interphase\ radius\ to\ the\ particle\ radius$$

4.3 Results and discussion

The end results of different characterization techniques i.e., XRD, SEM, TGA, gas sorption and gas permeation are briefly described here.

4.3.1 Powder X-ray Diffraction

Powder x-ray diffraction can be used to corroborate the survival of crystalline particles of ZIF-301 after their incorporation into amorphous PSF matrix. XRD measurements in the range of 2^o to 50^o were taken to establish and verify the existence of ZIF-301 crystalline structure in the prepared MMMs [see Fig. 4.1].

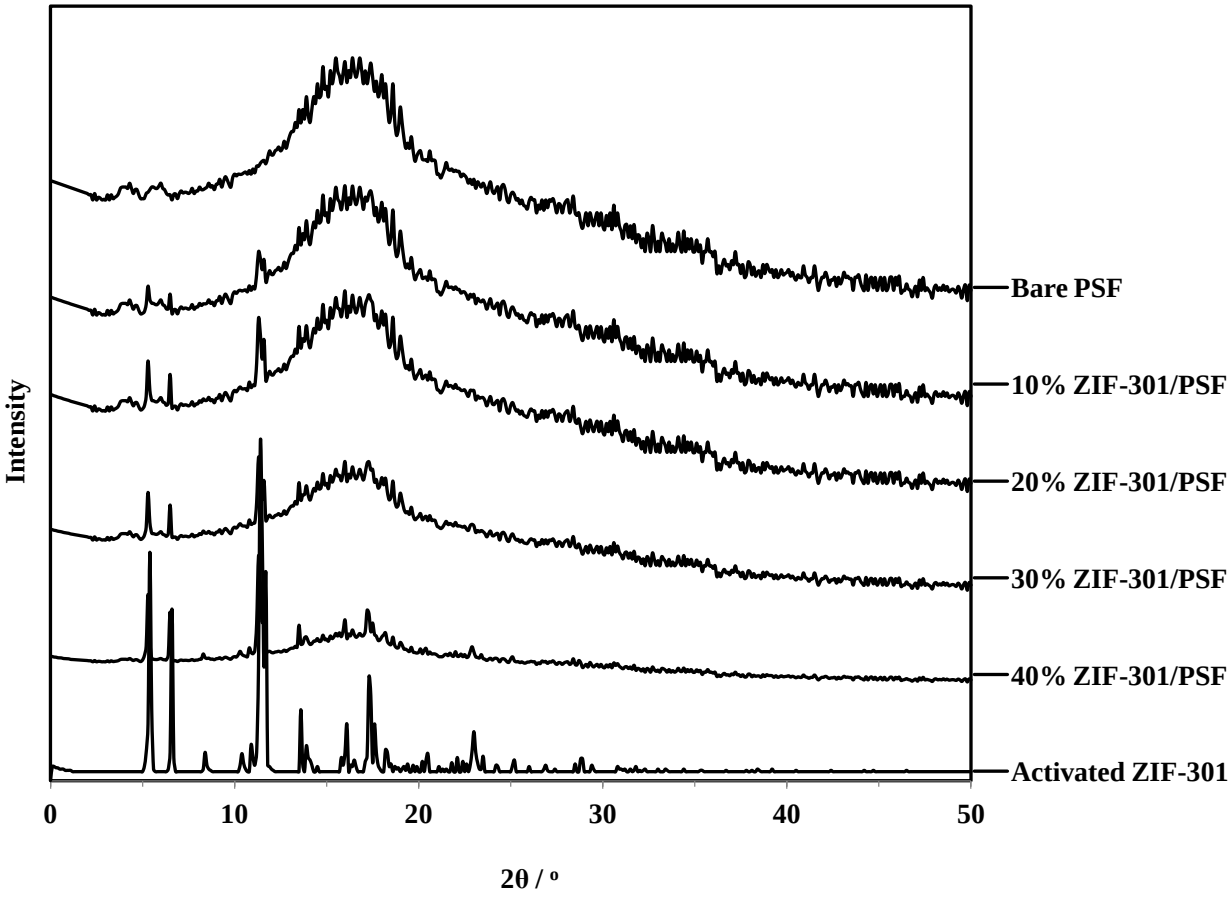

Fig. 4.1 XRD patterns of pure ZIF-301, pure PSF, and ZIF-301/PSF MMMs containing 10, 20, 30 and 40 % by weight of ZIF-301.

The peak intensities appearing at angles of 10.6^{o}, 13.1^{o} and 22.8^{o} correspond to the trigonal crystalline structure of microporous ZIF-301 nanoparticles. The perfect concurrence of specific XRD peaks of MMMs with those of activated ZIF-301 nanocrystals implies the preservation of ZIF-301 crystal structure after their addition into the PSF matrix. Moreover the slight shift of broad peak position (2θ) of bare PSF from ~ 17.3° (d-spacing = 5.1 Å) to ~ 17.1° (d-spacing = 5.15 Å) can be ascribed to the filler-

polymer interaction thus slightly changing the polymer inter-chain distance. Furthermore the addition of ZIF-301 nanoparticles in different MMMs successively heightens their corresponding peak intensities at the specified 2θ positions.

4.3.2 Morphology of ZIF-301/PSF MMMs

The nature of the dispersed inorganic filler and organic polymer matrix determines the structural characteristics and morphology of the MMMs. Generally the glassy polymers exhibit a rigid structure, typically create interfacial voids between the two phases, and influence the free volume of MMMs. To further investigate the morphology, adhesion and dispersion of ZIF-301 nanoparticles within PSF matrix, surface and cross sectional micrographs of the membranes were examined by SEM as illustrated in Fig. 4.2.

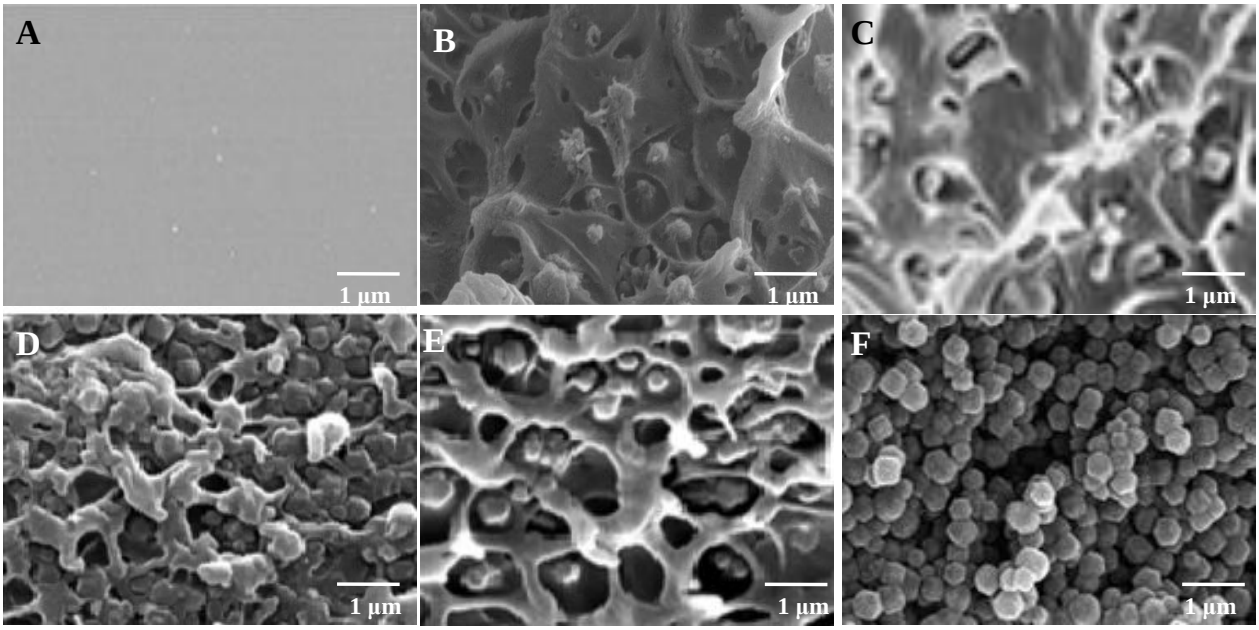

Fig. 4.2 Scanning electron micrographs of pure ZIF-301 [F], pure PSF [A], and ZIF-301/PSF MMMs containing 10 [B], 20 [C], 30 [D] and 40 [E] % by weight of ZIF-301.

Continuous ZIF-301/PSF phases are obtained for all MMMS having different loadings of the nanofiller. Owing to their fairly small particle size the dispersion of ZIF-301 nanocrystals is rationally consistent and homogeneous (Fig. 2), sparse on 10 wt % ZIF-301 loading (Fig. 2 B), and a minute aggregation and slightly rough cross section in 40 wt % ZIF-301/PSF MMM (Fig. 2 E). Also the interfacial voids are not observable in all the MMMs. The ZIF-301 nanocrystals exhibited strong interfacial adhesion and contact with PSF matrix as the cross sectional view of MMMs exhibits defect-free interconnected network morphology.

4.3.3 Thermal Gravimetric Analysis

In order to study their phase transitions, thermal stability, physical and chemical phenomena, DSC and TGA-DTG analyses of all the materials were carried out in the range of 100-700 ^{o}C as outlined in Table 4.1. The improvement in glass transition temperature (T_g) and rigidity of MMMs with increasing ZIF-301 contents can be correlated to the restricted movement of polymer chains owing to mutual interactions occurring among polymer chains and ZIF-301 nanocrystals. This can be associated with the similar heat resistances of both the continuous polymer matrix and dispersed nanofiller phases.

The TGA curves of all the prepared samples indicate a two step weight loss corresponding to desolvation (100-200 ^{o}C) and pyrolysis (510-640 ^{o}C) as shown in Fig. 4.3 (A). The weight loss corresponding to first peak can be attributed to the liberation of volatile solvent molecules while that related to second peak can be ascribed to the decomposition of organic ligands of the imidazole framework and complete degradation

of PSF. The residual weight at the end of analyses helped to verify the nominal mass contents of the filled ZIF-301 nanocrystals in corresponding MMMs.

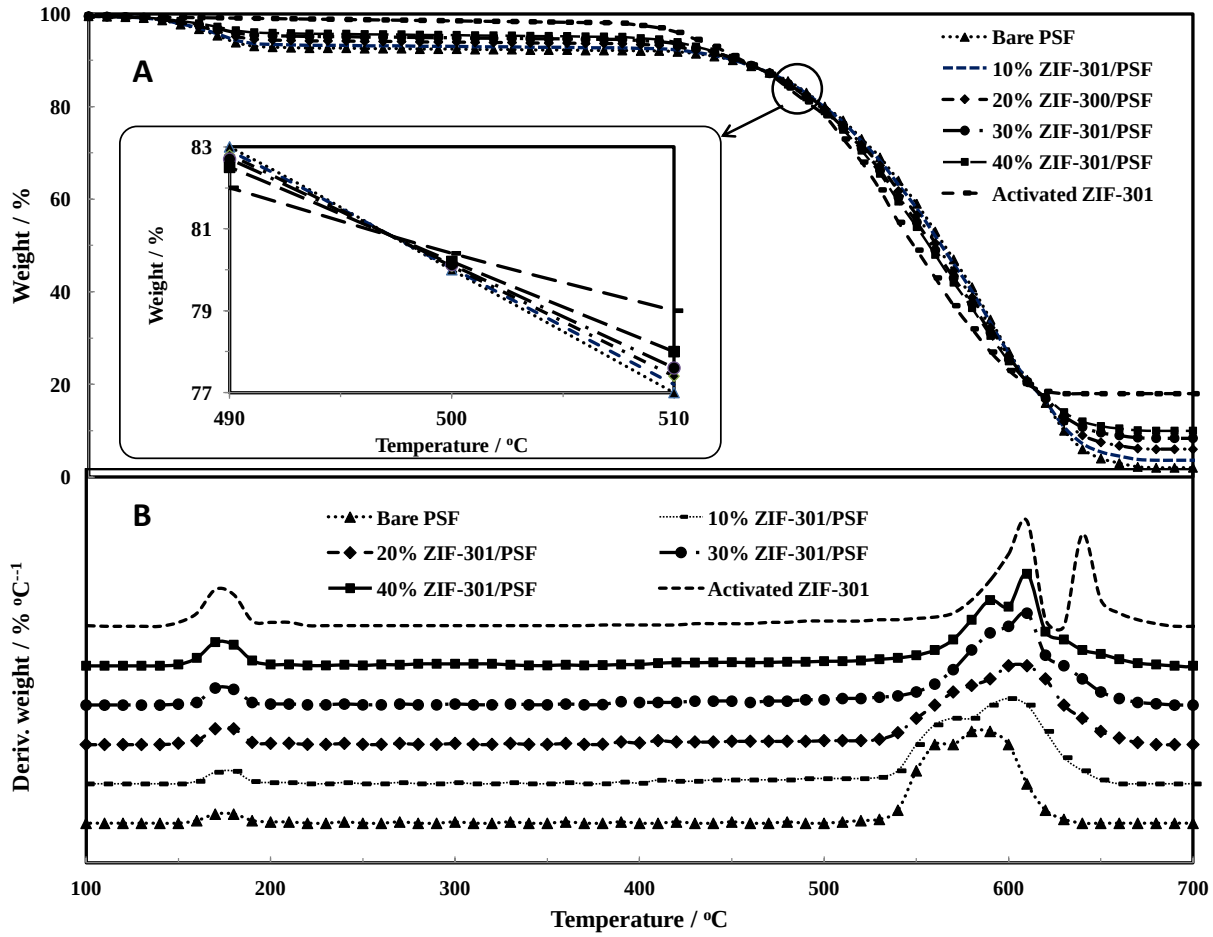

Fig. 4.3 TGA-DTG curves: TGA (A) and DTG (B) of pure ZIF-301, pure PSF, and ZIF-301/PSF MMMs containing 10, 20, 30 and 40 % by weight of ZIF-301.

The temperatures at which testing specimen loses its 5 and 10 percent weight, denoted by $T_{d5\%}$ and $T_{d10\%}$ respectively, in TGA analysis determine the thermal stability of a material [47]. Table 4.1 summarizes some important thermal parameters of the synthesized

materials. Both parameters being decreasing function of ZIF-301 contents, values of $T_{d5\%}$ and $T_{d10\%}$ occur between 172-423 °C and 449-458 °C respectively. The DTG curves illustrated in Fig. 3(B) also give information on pyrolysis rates; the residual masses of all the materials are enlisted in Table 4.1.

Table 4.1 Characteristic temperatures of membrane materials acquired from TGA-DTG data

Sample Designation	**T_g** (^oC)	**$T_{d5\%}$** (^oC)	**$T_{d10\%}$** (^oC)	**1st DTG peak** (^oC)	**2nd DTG peak** (^oC)	**Residual mass** (%)
Bare PSF	178	172	449	177	588	2.1
10% ZIF-301/PSF	180	175	451	176	597	3.6
20% ZIF-301/PSF	182	183	453	175	601	5.8
30% ZIF-301/PSF	183	248	454	174	602	8.4
40% ZIF-301/PSF	184	392	456	172	605	9.7
Activated ZIF-301	-	423	458	170	608	17.8

As indicated by weight loss curves the thermal stability of MMMs, determined in terms of 2nd DTG peaks, improved with increasing ZIF-301 contents. Since the maximum temperature experienced in different gas separation and combustion processes falls in the range of 30 to 500 °C, these MMMs can safely be used in gas separation applications [48].

4.3.4 Gas Sorption Analysis

Low pressure adsorption isotherms for CO_2 and N_2 in the pressure range of 10^{-6}-1 bar were measured at 298 K for activated ZIF-301 nanocrystals and all membranes (see Fig. 4.4).

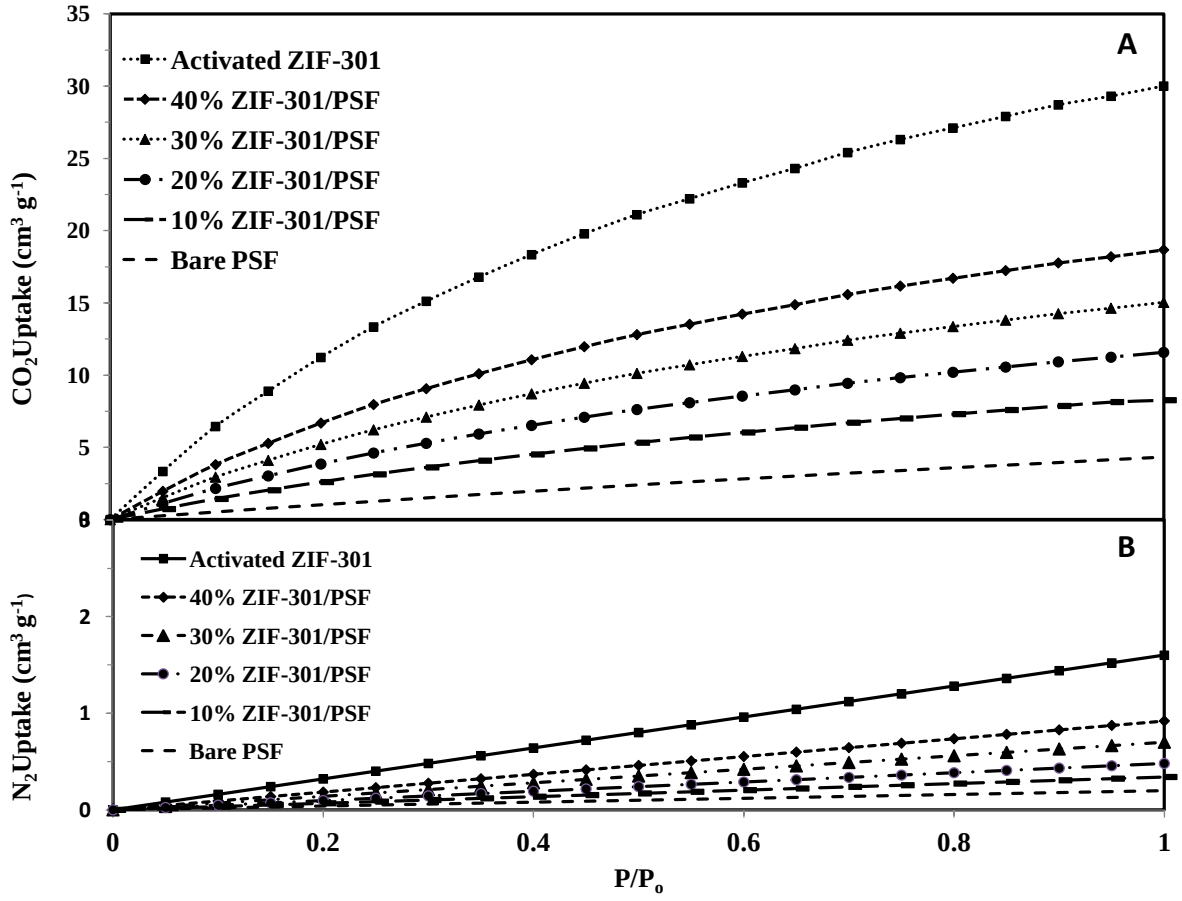

Fig. 4.4 CO_2 and N_2 adsorption isotherms for pure ZIF-301, pure PSF, and ZIF-301/PSF MMMs containing 10, 20, 30 and 40 % by weight of ZIF-301 at 298 ^{o}C.

Important physical properties (such as density, volume fraction of ZIF-301 nanocrystals) and microporous attributes (e.g. Brunauer-Emmett-Teller (S_{BET}) and Langmuir (S_{Lang})

surface areas, total micropore volume, CO_2 and N_2 uptakes, and CO_2/N_2 adsorption ideal selectivity) of the prepared membranes are enhanced with ZIF-301 contents as summarized in Table 4.2. These findings directly validate good adhesion, homogeneous dispersion and good-quality interfaces between ZIF-301 nanoparticles and PSF matrix leading to superior membranes.

Table 4.2 Microporous properties of ZIF-301, PSF, and ZIF-301/PSF MMMs

Sample Designation	**Density** ($g\ cm^{-3}$)	Φ_d (%)	S_{BET} (m^2g^{-1})	S_{Lang} (m^2g^{-1})	V_{micro} (m^3g^{-1})	**CO_2 uptake** ($cm^3\ g^{-1}$)	**N_2 uptake** ($cm^3\ g^{-1}$)	**CO_2/N_2 selectivity**
Bare PSF	1.25	0.0	12	19	0.019	4.3	0.23	18
10% ZIF-301/PSF	1.27	8.68	50	60	0.071	6.4	0.28	23
20% ZIF-301/PSF	1.28	17.48	90	110	0.123	8.6	0.33	26
30% ZIF-301/PSF	1.30	26.40	130	160	0.175	10.8	0.38	28
40% ZIF-301/PSF	1.31	35.46	170	200	0.228	12.8	0.41	32
Activated ZIF-301	1.45	100	400	470	0.538	26.4	1.18	22

CO_2 adsorption capacity for the membrane samples substantially increased with pressure due to the chemical affinity of chabazite-topologic ZIF-301 frameworks for quadro-polar CO_2 molecules. The CO_2 loading successively increased with increasing adsorption pressure. Activated ZIF-301 nanocrystals adsorbed the highest loading of CO_2 [~27 cm^3/g (≈1.3 mmol/g) at 298 K] which can be further increased by lowering the temperature. The N_2 adsorption isotherms for all the materials almost followed a proportional correlation with pressure up to 1 bar. In addition all the samples showed

preferably high adsorption affinity for CO_2 as compared to N_2, especially at low CO_2 partial pressure. The CO_2/N_2 sorption selectivities of the MMMs gradually increased with ZIF-301 contents. These facts suggest potential applications for the separation of CO_2/N_2 mixture from post combustion flue gases.

4.3.5 Gas Permeation Properties of MMMs

4.3.5.1 Dry and Wet gas permeation. Single gas dry and wet permeation experiments for CO_2 and N_2 through the membranes were performed at 298 K under an upstream pressure of 2 bar. Owing to its strong affinity for microporous ZIF-301 nanocrystals, CO_2 permeability and CO_2/N_2 selectivity values of the MMMs were considerably enhanced with increasing ZIF-301 contents up to 20 wt % loading and then started to decrease with ZIF-301 contents as represented in Fig. 5. The gas transport properties of both CO_2 and N_2 slightly improved under humid conditions on account of specific interactions among permeating gas, water molecules and MMMs structure.

4.3.5.2 Diffusivity and solubility of MMMs. Gas permeation through a membrane occurs via solution-diffusion mechanism. The data for coefficients of diffusion (D) and solubility (S) along with their corresponding CO_2/N_2 selectivity values for different membranes as illustrated in Figs. 4.5 and 4.6.

The time-lag method (eq. 6) was used to determine the values of diffusion coefficients using CO_2 and N_2 adsorption isotherms obtained at 298 K under varying pressure. The D values thus determined were used to calculate solubility coefficients of the membranes under the same conditions of temperature and pressure using eq. 4. Comparatively the

values of gas diffusivity coefficient selectivity (D_{CO2}/D_{N2}) successively declined and those of gas solubility coefficient selectivity (S_{CO2}/S_{N2}) in turn increase for all membranes with increasing ZIF-301 contents as shown in Fig. 4.5.

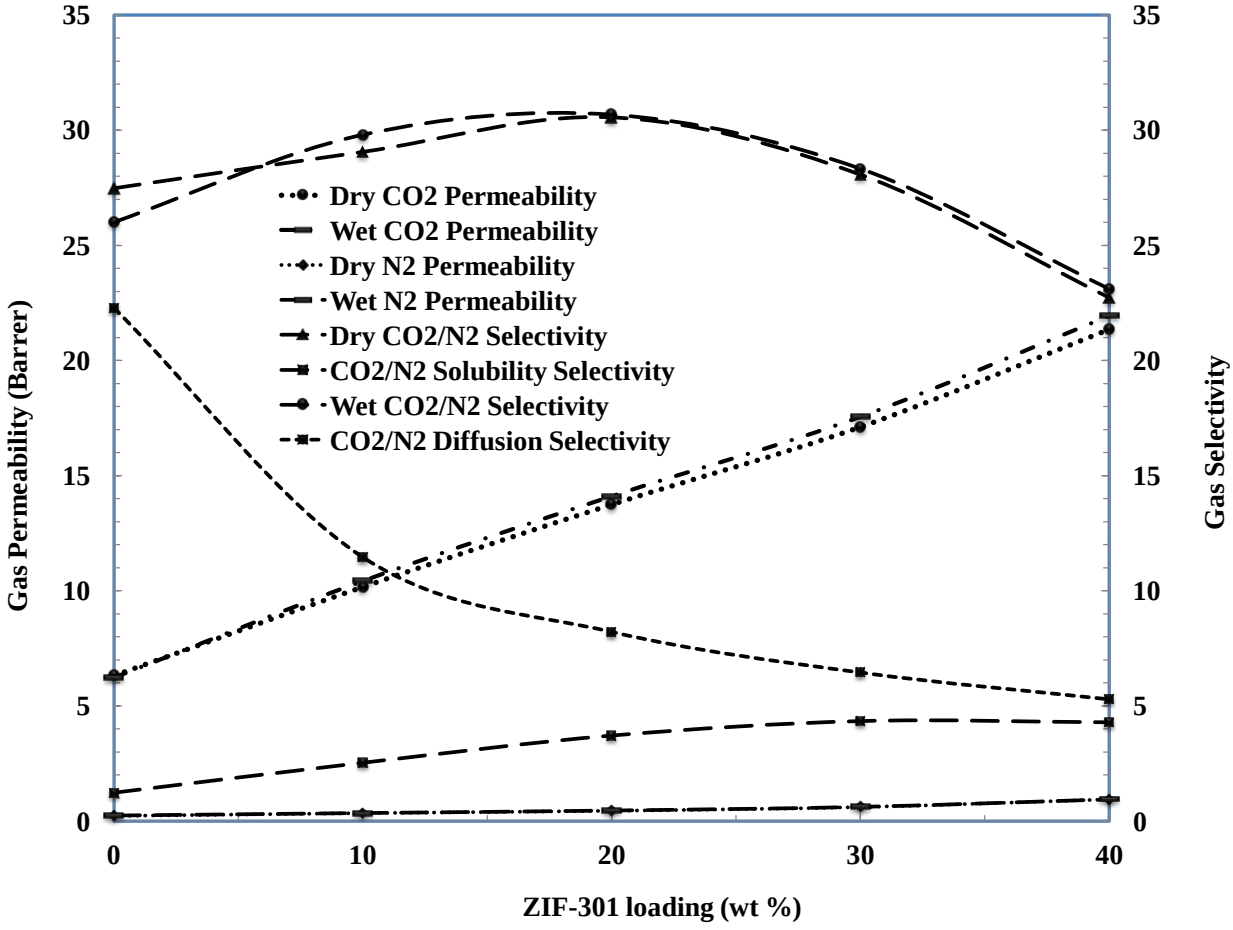

Fig. 4.5 Dry and wet gas CO_2 and N_2 permeabilities and CO_2/N_2 selectivity of pure PSF and ZIF-301/PSF MMMs with different ZIF loadings.

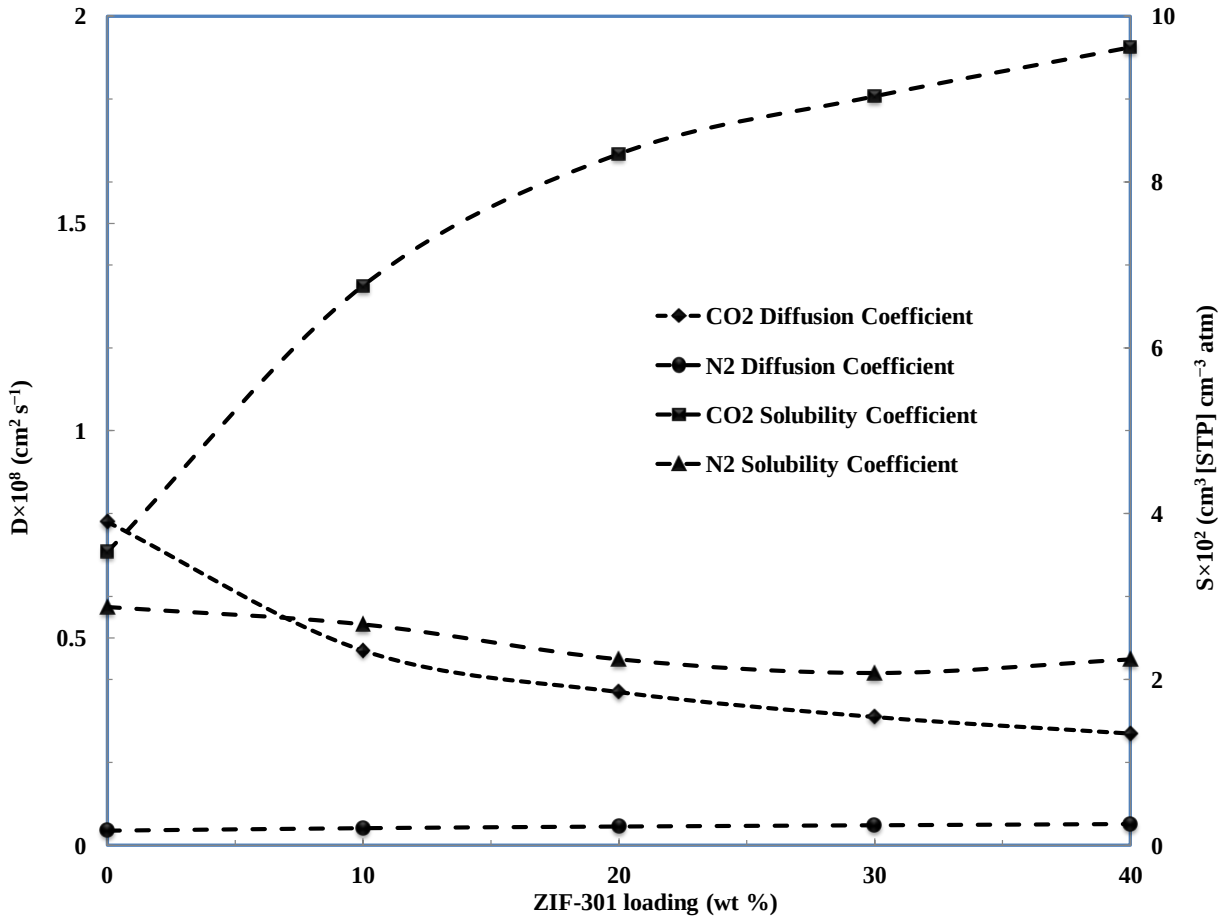

Fig. 4.6 Pure gas diffusion (D) and solubility (S) coefficients for bare PSF and selected MMMs having different ZIF-301 loadings.

The pore size reduction of ZIF-filled MMMs led to restricted N_2 adsorption as compared to CO_2. Also the selective solubility of CO_2 into ZIF-301 nanocrystals greatly enhanced its permeation through the MMMs. In general the improved CO_2/N_2 ideal selectivities of MMMs can be ascribed to controlled N_2 diffusion and preferential CO_2 solubility. The overall analysis based on improved CO_2 permeabilities and reduced N_2 diffusivities in ZIF-301/PSF MMMs strongly support the development of a genuine mixed matrix

membrane. The membranes permeation time lag characteristic also implied good interfacial adhesion and homogeneous distribution of ZIF-301 entities into PSF matrix. Since a membrane possessing high perm-selectivity values meets industrial applications, it appears that ZIF-301 is a competent material to fabricate MMMs for post combustion carbon capture on account of its high CO_2 permeability coupled with reasonable CO_2/N_2 selectivity.

4.3.5.3 Comparison of experimental data with mathematical models. Two- and three-phase permeability models were employed to predict CO_2 permeability through the prepared MMMs (Fig. 4.7). The two-phase Maxwell model well predict the permeability at low filler loadings; while the two-phase Bruggeman and three-phase modified Felske models more accurately described the MMMs behavior at higher filler concentration. The error in two-phase Bruggeman model is lower than other models thus dictating non-ideal morphology of the MMMs.

4.3.5.4 Comparison with Robeson upper bounds. A comparison of the CO_2/N_2 gas pair separation performance of MOF-based MMMs, along with Robeson 1991 and 2008 upper bounds [14], is depicted on a permeability-selectivity chart as shown in Fig. 4.8. The diagram indicates that the incorporation of ZIF-301 nanofiller into PSF matrix has enhanced the permselectivity of the MMMs as compared to neat polysulfone membrane. The permselectivity value of MMM containing 10 wt% ZIF-301 is located very close to the 1991-upper bound line while those of MMMs containing 20-40 wt% ZIF-301 loadings lie above this line, an important achievement of this work. ZIF-301 loadings

higher than 40 wt % are susceptible to poor filler-matrix interface adhesion and inhomogeneous dispersion of filler in polymer matrix.

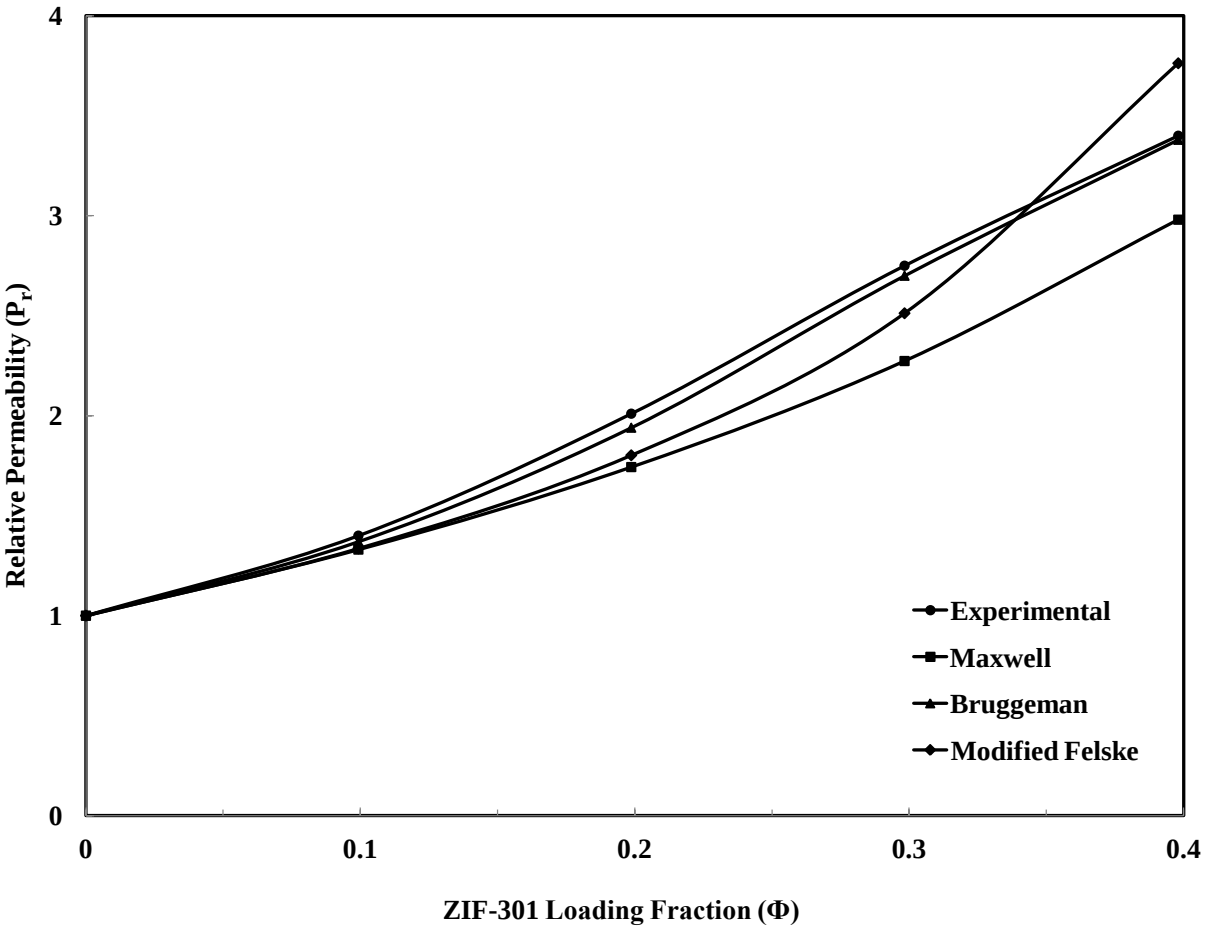

Fig. 4.7 Comparison between experimentally determined CO_2 permeability and that predicted by Maxwell, Bruggeman, and modified Felske models.

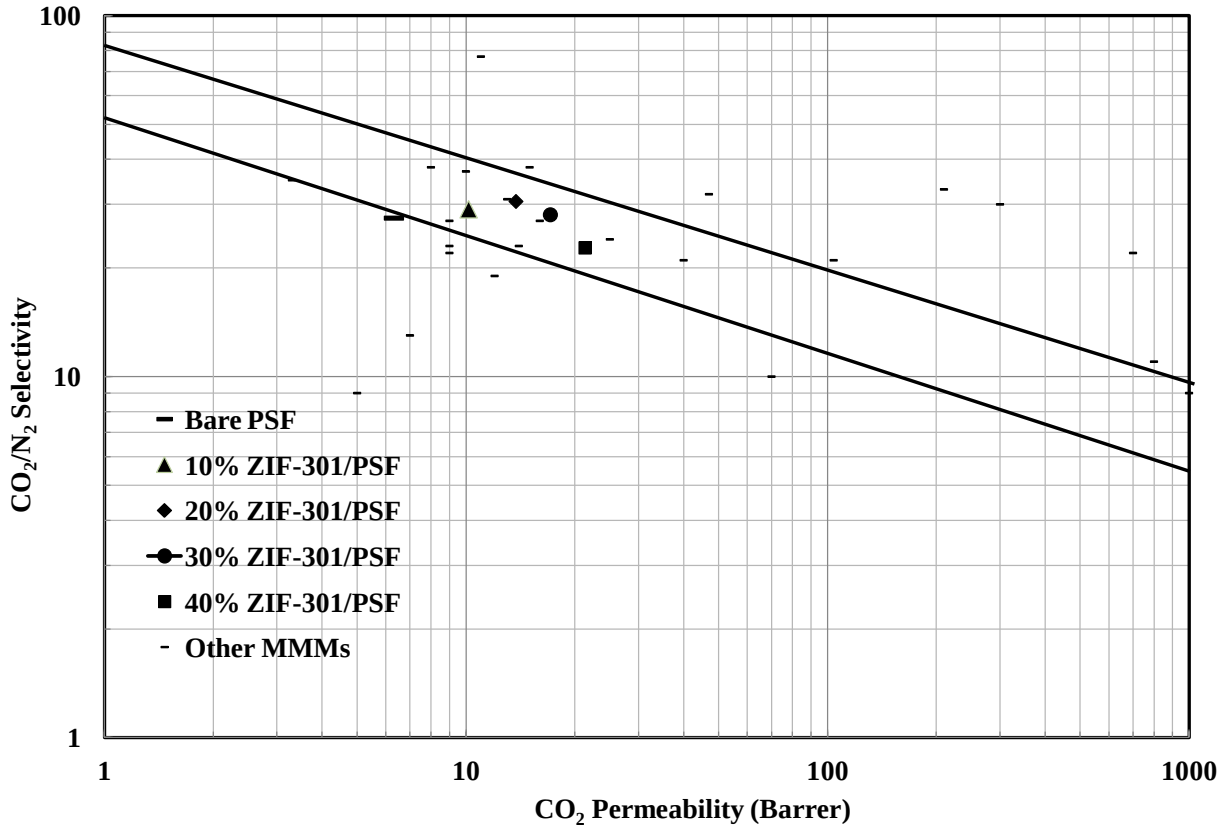

Fig. 4.8 Comparison of CO_2/N_2 separation performance of ZIF-301/PSF MMMs with other ZIF or MOF containing MMMs obtained from literature data. The Robeson upper bound 2008 for polymer separation performance is also shown.

4.4 Conclusions

ZIF-301 nanocrystals with narrow particle size distribution were incorporated into PSF for the first time to fabricate hydrothermally stable high performance mixed-matrix membranes for selective CO_2 separation from post combustion flue gases. Characterization of the MMMs done by XRD, TGA, SEM and gas sorption experiments indicated that they are thermally stable, mesoporous, crystalline materials possessing

homogeneous filler dispersion and good interfacial filler-matrix adhesion without adding any compatibilizing agent. The MMMs developed in this work demonstrated three times increment in CO_2 permeability as compared to that of bare PSF membrane while the CO_2/N_2 ideal selectivity increased up to 31 for 20 wt % ZIF-301 loading. The separation performance of the MMMs produced in this work coincided with the Robeson 1991 upper bound and the CO_2/N_2 ideal selectivity is considered to be high enough to meet industrial applications.

Acknowledgement

The authors are thankful to KACST- Technology Innovation Center on Carbon Capture and Sequestration (CCS), King Fahd University of Petroleum and Minerals, Dhahran, Kingdom of Saudi Arabia for providing support for this work.

References

[1] D. M. D'Alessandro, B. Smit, J. R. Long, Carbon Dioxide Capture: Prospects for New Materials, Angew. Chem. Int. Ed. 49 (2010) 6058-6082.

[2] M. Z. Jacobson, Review of Solutions to Global Warming, Air Pollution, and Energy Security, Energy Environ. Sci. 2 (2009) 148-173.

[3] N. MacDowell, N. Florin, A. Buchard, J. Hallett, A. Galindo, G. Jackson, C. S. Adjiman, C. K. Williams, N. Shah, P. Fennell, An Overview of CO_2 Capture Technologies, Energy Environ. Sci. 3 (2010) 1645-1669.

[4] H. Herzog, D. Golomb, Carbon capture and storage from fossil fuel use, Encyc. Energy 1 (2004) 277-287.

[5] A. Hussain, M.B. Hägg, A feasibility study of CO_2 capture from flue gas by a facilitated transport membrane, J. Membr. Sci. 359 (2010) 140-148.

[6] J. Zhao, Z. Wang, J.X. Wang, S.C. Wang, Influence of heat-treatment on CO_2 separation performance of novel fixed carrier composite membranes prepared by interfacial polymerization, J. Membr. Sci. 283 (2006) 346-356.

[7] P. Pandey, R.S. Chauhan, Membranes for gas separation, Prog. Polym. Sci. 26 (2001) 853-893.

[8] R. Mahajan, W.J. Koros, Factors controlling successful formation of mixed-matrix gas separation materials, Ind. Eng. Chem. Res. 39 (2000) 2692–2696.

[9] E.P. Fawas, G.C. Kapantaidakis, J.W. Nolan, A.C. Mitropoulos, N.K. Kanellopoulos, Preparation, characterization and gas permeation properties of carbon hollow fiber membranes based on Matrimid® 5218 precursor, J. Mater. Process. Technol. 186 (2007) 102–110.

[10] R.W. Baker, Future directions of membrane gas separation technology, J. Ind. Eng. Chem. Res. 41 (2002) 1393–1411.

[11] D.L. Gin, R.D. Noble, Designing the next generation of chemical separation membranes, Science 332 (2011) 674-676.

[12] Y. Xiao, T.-S. Chung, Grafting thermally labile molecules on cross-linkable polyimide to design membrane materials for natural gas purification and CO_2 capture. Energy Environ. Sci. 4 (2011) 201-208.

[13] C. Staudt-Bickel, W.J. Koros, Improvement of CO_2/CH_4 separation characteristics of polyimides by chemical crosslinking. J. Membr. Sci. 155 (1999) 145-154.

[14] L.M. Robeson, The upper bound revisited. J. Membr. Sci. 320 (2008) 390–400.

[15] T.-S. Chung, L.Y. Jiang, Y. Li, S. Kulprathipanja, Mixed matrix membranes (MMMs) comprising organic polymers with dispersed inorganic fillers for gas separation. Prog. Polym. Sci. 32 (2007) 483-507.

[16] C.E. Powell, G.G. Qiao, Polymeric CO_2/N_2 gas separation membranes for the capture of carbon dioxide from power plant flue gases. J. Membr. Sci. 279 (2006) 1-49.

[17] M. Rezakazemi, A.E. Amooghin, M.M. Montazer-Rahmati, A.F. Ismail, T. Matsuura, State-of-the-art membrane based CO_2 separation using mixed matrix membranes (MMMs): An overview on current status and future directions, Prog. Polym. Sci. 39 (2014) 817-861.

[18] J.D. Wind, D.R. Paul, W.J. Koros, Natural gas permeation in polyimide membranes, J. Membr. Sci. 228 (2004) 227-236.

[19] W. Qiu, C.C. Chen, L. Xu, L. Cui, D.R. Paul, W.J. Koros, Sub-T_g cross-linking of a polyimide membrane for enhanced CO_2 plasticization resistance for natural gas separation, Macromolecules 44 (2011) 6046-6056.

[20] J. Park, D. Paul, Correlation and prediction of gas permeability in glassy polymer membrane materials via a modified free volume based group contribution method, J. Membr. Sci. 125 (1997) 23-39.

[21] Y. Yampolskii, Polymeric gas separation membranes, Macromolecules 45 (2012) 3298-3311.

[22] L.M. Robeson, Correlation of separation factor versus permeability for polymeric membranes, J. Membr. Sci. 62 (1991) 165-185.

[23] C.H. Lau, P. Li, F. Li, T.-S. Chung, D.R. Paul, Reverse-selective polymeric membranes for gas separations, Prog. Polym. Sci. 38 (2013) 740-766.

[24] T.C. Merkel, B.D. Freeman, R.J. Spontak, Z. He, I. Pinnau, P. Meakin, A. Hill, J. Ultrapermeable, reverse-selective nanocomposite membranes, Science 296 (2002) 519-522.

[25] J. Ahn, W.-J. Chung, I. Pinnau, M.D. Guiver, Polysulfone/silica nanoparticle mixed-matrix membranes for gas separation, J. Membr. Sci. 314 (2008) 123-133.

[26] B.D. Reid, A. Ruiz-Trevino, I.H. Musselman, K.J. Balkus, J.P. Ferraris, Gas permeability properties of polysulfone membranes containing the mesoporous molecular sieve MCM-41, Chem. Mater. 13 (2001) 2366-2373.

[27] S. Kim, E. Marand, J. Ida, V.V. Guliants, Polysulfone and mesoporous molecular sieve MCM-48 mixed matrix membranes for gas separation, Chem. Mater. 18 (2006) 1149-1155.

[28] S. Kim, E. Marand, High permeability nano-composite membranes based on mesoporous MCM-41 nanoparticles in a polysulfone matrix, Microp. Mesop. Mater. 114 (2008) 129-136.

[29] D.Q. Vu, W.J. Koros, S.J. Miller, Mixed matrix membranes using carbon molecular sieves. II. Modeling permeation behavior, J. Membr. Sci. 211 (2003) 335-348.

[30] H.L. Cong, J.M. Zhang, M. Radosz, Y.Q. Shen, Carbon nanotube composite membranes of brominated poly(2,6-diphenyl-1,4-phenylene oxide) for gas separation, J. Membr. Sci. 294 (2007) 178–185.

[31] S. Kim, L. Chen, J.K. Johnson, E. Marand, Polysulfone and functionalized carbon nanotube mixed matrix membranes for gas separation: Theory and experiment, J. Membr. Sci. 294 (2007) 147–158.

[32] P. Gorgojo, S. Uriel, C. Tellez, J. Coronas, Development of mixed matrix membranes based on zeolite Nu-6(2) for gas separation, J. Microporous Mesoporous Mater. 115 (2008) 85–92.

[33] Y. Liu, D. Peng, G. He, S. Wang, Y. Li, H. Wu, Z. Jiang, Enhanced CO_2 permeability of membranes by incorporating polyzwitterion@CNT composite particles into polyimide matrix, ACS Appl. Mater. Interfaces 6 (2014) 13051-13060.

[34] B. Harold, T. Jeazet, C. Staudt, C. Janiak, Metal–organic frameworks in mixed-matrix membranes for gas separation, Dalton Trans. 41 (2012) 14003–14027.

[35] A. Car, C. Stropnik, K.-V. Peinemann, Hybrid membrane materials with different metal–organic frameworks (MOFs) for gas separation, Desalination 200 (2006) 424.

[36] B. Zornoza, S. Irusta, C. Tellez, J. Coronas, Mesoporous silica sphere-polysulfone mixed matrix membranes for gas separation, Langmuir 25 (2009) 5903–5909.

[37] B. Zornoza, B. Seoane, J. M. Zamaro, C. Téllez and J. Coronas, Combination of MOFs and zeolites for mixed-matrix membranes, Chem-PhysChem, 12 (2011) 2781–2785.

[38] B. Harold, T. Jeazet, T. Koschine, C. Staudt, K. Raetzke, C. Janiak, Correlation of gas permeability in a metal-organic framework MIL-101(Cr)–polysulfone mixed-matrix membrane with free volume measurements by positron annihilation lifetime spectroscopy (PALS), Membranes 3 (2013) 331-353.

[39] T.T.N. Nhung, H. Furukawa, F. Gandara, H.T. Nguyen, K.E. Cordova, O.M. Yaghi, Selective capture of carbon dioxide under humid conditions by hydrophobic chabazite-type zeolitic imidazolate frameworks, Angew. Chem. 126 (2014) 10821–10824.

[40] L.A. El-Azzami, E.A. Grulke, Parametric study of CO_2 fixed carrier facilitated transport through swollen chitosan membranes. Ind. Eng. Chem. Res. 48 (2008) 894−902.

[41] J.U. Wieneke, C. Staudt, Thermal stability of 6FDA-(co-)polyimides containing carboxylic acid groups. Polym. Degrad. Stab. 95 (2010) 684–693.

[42] X.W. Yu, Z. Wang, Z.H. Wei, S.J. Yuan, J. Zhao, J.X. Wang, S.C. Wang, Novel tertiary amino containing thin film composite membranes prepared by interfacial polymerization for CO_2 capture, J. Membr. Sci. 362 (2010) 265-278.

[43] D.R. Paul, D.R. Kemp, The diffusion time lag in polymer membranes containing adsorptive fillers, J. Polym Sc: Polym. Symp. 41 (1973) 79–93.

[44] H. Vinh-Thang, S. Kaliaguine, Predictive Models for Mixed-Matrix Membrane Performance: A Review, J. ACS Publications, 113 (2012) 4980–5028.

[45] S.A. Hashemifard, A.F. Ismail, T. Matsuura, A new theoretical gas permeability model using resistance modeling for mixed matrix membrane systems, J. Membr. Sci., 350 (2010) 259-268.

[46] B. Shimekit, H. Mukhtar, T. Murugesan, Prediction of the relative permeability of gases in mixed matrix membranes", J. Membr. Sci., 373 (2011) 152-159.

[47] Y.C. Xiao, T.S. Chung, H.M. Guan, M.D. Guiver, Synthesis, cross-linking and carbonization of co-polyimides containing internal acetylene units for gas separation, J. Membr. Sci. 302 (2007) 254-264.

[48] A.C.C. Chang, S.S.C. Chuang, M. Gray, Y. Soong, In-situ infrared study of CO_2 adsorption on SBA-15 grafted with γ-(aminopropyl) triethoxysilane, Energy Fuels 17 (2003) 468-473.

CHAPTER 5

HARMONIOUS INTERACTION OF INCORPORATING MULTIWALLED CNTS AND ZEOLITIC IMIDAZOLE FRAMEWORKS INTO POLYSULFONE TO PREPARE HIGH PERFORMANCE MMMS FOR CO_2 SEPARATION FROM POST COMBUSTION GASES

Abstract

Multiwalled CNTs and zeolitic imidazole frameworks (ZIF-301) were collegially incorporated into glassy polysulfone (PSF) to prepare mixed-matrix membranes (MMMs) to separate CO_2 from post combustion flue gases. Varying loadings of both nanofillers were incorporated into PSF using solution-casting technique to engineer CO_2 separation performance of MMMs. The flexible MMMs rendering consistent distribution and improved adhesion of nanofillers with polymer matrix were characterized by scanning electron microscopy (SEM), x-ray diffraction (XRD) and thermal gravimetric analysis (TGA). Gas sorption analysis along with dry and wet gas permeation experiments exhibited that both CO_2 permeability and CO_2/N_2 selectivity of MMMs were improved owing to collegial effect of nanofillers. The MMM filled with 18 wt % ZIF-301

nanofillers and 6 wt % CNTs showed an optimum separation performance by providing a CO_2 permeability of 19 Barrers with CO_2/N_2 selectivity of 48.

Key Words

Hydrophobic MMMs, ZIF-301, CNTs, synergistic effect, CO_2 capture, permselectivity

5.1 Introduction

CO_2 emissions from burning of fossil fuels induce environmental warming concerns throughout the globe [1-3]. Economically viable processes to reduce CO_2 releases include its sequestration or capture from a mixture of CO_2-containing gases [4-5]. On account of its flexible design, ease of scale up, high efficiency, low energy requirement, simple function, low capital and operating costs, and environmental friendliness, polymer-based mixed-matrix membrane gas separation technology, among other conventional processes, has gained momentous attention [6-13].

Majority of glassy polymers have been adapted to fabricate MMMs by adding inorganic fillers like nonporous silica [14-15], structured mesoporous silica [16-18], carbon molecular sieves [19], carbon nanotubes [20-21], zeolites [22], and microporous metal organic frameworks (MOFs) [23] in order to design efficient mix membranes showing better permselectivity characteristics as compared to unfilled polymer membranes. Advantages of adding microporous nanomaterials (such as ZIFs/MOFs and/or CNTs/graphenes etc.) into polymer matrix to form MMMs comprise the ability to combine the simplicity of casting and processability, enhanced mechanical and chemical performance of polymers conjoined with improved gas separation efficiency of

nanocrystals possessing adjustable pore dimensions, modifiable surface functionality, and high surface areas [24].

Nanocrystals of microporous zeolitic imidazolate frameworks are interesting materials to fabricate efficient MMMs for gas separation on account of their high surface areas, tunable nano-sized pores, modifiable surface functionality, good wetting characteristics, improved thermal and chemical stability [25–27]. Hydrothermally stable ZIF-301 crystals [28] selectively captures CO_2 gas from $CO_2/N_2/H_2O$ wet gaseous mixture and their inclusion into polymer matrices is expected to improve separation performance of MMMs under wet conditions.

Owing to their internal smooth walls, nano-sized configuration, large pore diameter, high aspect ratio, excellent mechanical and thermal properties [29–31], gas permeation through CNTs are exceptionally higher as compared to other microporous materials. The selectivity of as-synthesized CNTs for various gas molecules is comparatively low and tricky to recover by chemical modification/functionalization due to their inert nature [32–34]. Although CNTs-filled MMMs are significantly efficient as compared to MOF/ZIF-based MMMs, good adhesion and uniform dispersion of nanofillers in polymer matrices is the central challenge. A more refined strategy to engineer MMMs with enhanced permselectivity is the collegial incorporation of naonfillers possessing diversified morphology, nature, and dimensions into a polymer matrix [35].

Different types of zeolites (e.g. S1C), MOFs (e.g. HKUST-1), MILs (e.g. NH_2-MIL-53(Al)) and ZIFs (e.g. ZIF-8) were added into PSF to prepare MMMs to study the permeation of CO_2, N_2, CH_4, O_2, and H_2 gases [36]. The CO_2/N_2 permselectivity did not ameliorate for S1C-ZIF-8/PSF MMMs. The CO_2 permeation characteristics of HKUST-

1/ZIF-8/PSF, S1C/PSF, HKUST-1/PSF, and ZIF-8/PSF MMMs were found to be 8.4, 9.4, 9.5 and 12.3 Barrers respectively with corresponding CO_2/N_2 permselectivities of 38, 23, 24, and 19. The collegial impact of adding mesoporous silica MCM-41 and amine-functionalized MIL-53(Al) nanofillers into polymer-based MMMs improved their gas separation efficiency [37]. Galve and group [38] fabricated hybrid membranes by introducing mesoporous silica MCM-41 spheres and layered microporous titanosilicate JDF-L1 sheets into glassy polyimide matrix; the uniform distribution of MCM-41 spheres in the polymer matrix were facilitated by JDF-L1 sheets. Li et al. [39] investigated the combined inclusion of graphene oxide and CNTs into PSF to determine optimal loadings of the nanofillers.

The exclusive incorporation of CNTs and ZIFs into PSF matrix helped to improve gas separation efficiency of CO_2. The current work focuses on combined inclusion of CNTs and ZIF-301 nanocrystals into glassy PSF matrix for the first time to fabricate PSF/CNTs/ZIF-301 MMMs to efficiently separate CO_2 from CO_2/N_2 mixture. The main objective of this study is to determine the optimum loadings of both the nanofillers to attain high CO_2 permselectivity and to systematically investigate the solubility-diffusivity separation mechanism under dry and wet conditions.

5.2 Experimental

5.2.1 Materials

Glassy polysulfone having average molecular weight ~ 35000 by LS and density 1.25 g cm^{-3}, was purchased from Sigma Aldrich. Hydroxyl modified multi-walled CNTs having average length 1.2 μm and diameter 8 nm were obtained from Nanjing XFNANO

Materials Tech. Co., Ltd. Zinc nitrate hexahydrate and 2-methylimidazole were obtained from Merck Chemical Company. 5(6)-chlorobenzimidazole, methanol and N,N-dimethylformamide (DMF) were obtained from Aldrich Chemical Company. All the chemicals and polymer were used as received without further treatment. Highly pure CO_2, N_2 and He gases were used for gas sorption and permeation experiments.

5.2.2 Synthesis of ZIF-301 nanocrystals

ZIF-301 nanocrystals were synthesized by dissolving 67.8 mg of $Zn(NO_3)_2 \cdot 6H_2O$ (the metal salt), 23.4 mg of 2-methylimidazole (primary organic linker), and 43.6 mg of 5(6)-chlorobenzimidazole (secondary organic linker) in a mixture of 9.5 mL DMF and 0.5 mL distilled water by sonication in a 20-mL vial for 10 minutes. The ensuing solution was then subjected to moderate stirring on a hot plate at 50 °C for 70 hours to obtain colorless suspension of ZIF-301 nanocrystals. The suspended nanocrystals were separated from the mother liquor by centrifuge and washed with 7 mL of fresh DMF. This process was repeated 5 times to make them ready to prepare MMMs of varying composition.

5.2.3 Preparation of PSF/CNTs/ZIF-301 MMMs

Bare PSF membrane and PSF/CNTs/ZIF-301 MMMs were prepared by degassing the main constituents i.e., PSF, CNTs and ZIF-301 nanocrystals at 100 ^oC under vacuum for 20 h to remove adsorbed gases and/or moisture. Bare PSF membrane was prepared by dissolving 1g PSF in 10 mL DMF followed by stirring at room temperature for 24 hours until a thick viscous solution was formed. The MMMs containing different amounts of CNTs and ZIF-301 nanocrystals were prepared as follows. 1 g PSF was added in 10 mL

DMF and stirred at room temperature for 20 h. Then a weighed quantity of CNTs was dispersed in 4 mL DMF by sonicating for 1 h to get well dispersed homogeneous suspension. In addition, a specified amount of ZIF-301 nanocrystals was redispersed in 7 mL DMF by stirring for 10 minutes. The three solutions were mixed together and subjected to vigorous stirring for another 12 h until a thick viscous solution was obtained. All the membranes were knife casted on clean glass plates at a specified gate height using a flat sheet membrane casting system (FSMCS). After allowing the solvent to slowly evaporate from the membranes under ambient conditions overnight, the membranes were detached from the glass plates and placed in a VO 200 vacuum oven to dry the MMMs at 80, 100 and 180 ^{o}C for 12, 20 and 60 hours respectively to ensure complete removal of the traces of solvent before subjecting them to gas permeation experiments.

The prepared MMMs were designated as PSF/CNTs(X)/ZIF-301(Y), where X (ranging from 1-10), and Y (ranging from 6-30) represent loadings of CNTs and ZIF-301 by wt % respectively. As an illustration the MMM denoted by PSF/CNTs(6)/ZIF-301(18) contains 6 and 18 wt % loadings of CNTs and ZIF-301 nanocrystals respectively. The thicknesses of the membranes were determined in the range of 50-80 μm as measured by a digital micrometer.

5.2.4 Materials Characterization Methods

The measurement techniques used to characterize ZIF-301 nanocrystals, CNTs, bare PSF and PSF/CNTs/ZIF-301 MMMs include x-ray diffraction, scanning electron microscopy, thermal gravimetric analysis, and gas sorption analyses. The volume fraction of nanofillers added in MMMs can be defined as:

$$\Phi_D = \frac{m_D/\rho_D}{m_D/\rho_D + m_C/\rho_C} \times 100 \qquad (1)$$

where m and ρ represent mass and density of PSF (continuous phase denoted by subscript C) and CNTs and/or ZIF-301 nanofillers (dispersed phase denoted by subscript D) respectively. Normally the void volume of MMMs is insignificant as maintained by SEM micrographs and gas sorption analyses. Hence the apparent volume fraction of nanofillers can safely be considered as the exact volume fraction of CNTs and/or ZIF-301 nanocrystals collectively doped in MMMs.

Powder x-ray diffraction (XRD) patterns of all the materials were performed using a Bruker D8 X-ray diffractometer using Cu Kα radiation (λ = 1.5406 Å) operated at 45 mA and 40 kV with a step increment of 0.02^o in 2θ and a scan size of 0.02^o s^{-1}. The membrane samples were loaded in a sample holder placed on silicon substrate. The MMMs were characterized by XRD to check whether the polymeric matrix alters the crystalline patterns of CNTs and ZIF-301 nanocrystals or not.

Scanning electron microscopy images were taken to investigate the morphology of MMMs by Hitachi S-4300SE/N SEM instrument. Testing specimens were cryofractured in liquid nitrogen and their outer surfaces were covered with a thin gold film to avoid charging of electrons. The SEM machine was operated at an accelerating voltage of 20 kV.

Thermal stability and related properties of the membranes were assessed by thermogravimetric analysis using a TGA/SDTA 851 (Mettler Toledo) system in air by heating from ambient temperature to 700 ^oC at a heating rate of 10 ^oC min^{-1}.

CO_2 and N_2 adsorption isotherms evaluated at 77 and 298 K using a Quantachrome Autosorb iQ gas sorption analyzer helped to assess various microporous characteristics (e.g., specific BET and Langmuir surface areas, total microporous volume, CO_2 and N_2 gas uptakes) of the membranes. The membrane samples were chopped into tiny pieces and degassed at 100 ^oC under vacuum ($<10^{-6}$ bar) for 5 hours. Physisorption data of CO_2 and N_2 gases were measured at 298 K under a gas pressure ranging from 10^{-6} -1 bar.

5.2.5 Gas Permeation Measurements

Pure gas (CO_2 and N_2) transport properties (i.e., permeability, ideal selectivity, and separation performance) of the MMMs were assessed using single gas permeation cell following the variable pressure (constant volume) method at a temperature of 298 K [40]. After measuring its average thickness the membrane was fixed in the permeation cell. While keeping the feed side valve closed, both the upstream (feed side) and downstream (permeate side) lines of the cell were evacuated. The valve between the permeate side line and the vacuum pump was then closed followed by opening the feed side valve to maintain a low feed pressure (e.g., 0.1 bars) for a specific time (i.e., 2 h) to record the permeation measurements. The feed pressure was then intermittently increased and data were collected after at least 1 h of stabilization for each interval. At least three replicas were prepared and tested corresponding to each composition of the MMMs in order to assess error and identify imperfect membranes.

Gas permeability (P_i, *Barrer*) of the membrane was computed using eq. (2):

$$P_i = \frac{22414}{A} \times \frac{V}{RT} \times \frac{l}{\Delta P_i} \frac{dP_i}{dt} \qquad (2)$$

where *l, A, V, R, T,* ΔP and $\Delta P_i/dt$ are respectively membrane thickness (*cm*), membrane active area (cm^2), downstream volume (cm^3), universal gas constant (6236.56 cm^3 *cmHg/mol/K*), absolute temperature (*K*), pressure difference across the membrane (*psi*), and permeation rate (*psi/s*) of component i.

Time-lag method, suggested by Paul and Kemp [41], was used to determine diffusion coefficient (D) by using *diffusivity vs. time-lag* (D-θ) relationship for MMMs:

$$D = \frac{l^2}{6\theta}\left[1 + \frac{6K}{y^3}\left\{\frac{y^2}{2} + y - (1+y)\ln(1+y)\right\}\left(\frac{V_d}{V_p}\right)\right] \qquad (3)$$

where V_d and V_p are respectively the volume fractions of filler and polymer phases; K and y are adsorption parameters determined from Langmuir adsorption isotherm.

The solubility coefficient (S) can be calculated from Eq. (4):

$$S = \frac{P}{D} \qquad (4)$$

The ideal selectivity of gas i over j (α_{ij}) can be determined using Eq. (5):

$$\alpha_{ij} = \frac{P_i}{P_j} = \left(\frac{D_i}{D_j}\right)\left(\frac{S_i}{S_j}\right) \qquad (5)$$

Here (D_i/Dj) and (S_i/S_j) represent diffusion- and solubility-based selectivity terms respectively.

5.3 Results and discussion

The experimentally obtained results of different characterization techniques i.e., XRD, SEM, TGA, gas sorption and gas permeation are briefly described here.

5.3.1 Powder X-ray Diffraction

Powder x-ray diffraction is an effective exercise to analyze the effect of nanofillers on the configuration of polymer chains in MMMs and to validate the existence of crystalline materials in amorphous polymer matrices. XRD measurements in the range of 2-50^{o} were registered to ensure the existence of CNTs and ZIF-301 crystalline structure in hybrid membranes (Fig. 5.1). The specific peak intensities emerging at 2θ positions of 10.6^{o}, 13.1^{o} and 22.8^{o} in XRD patterns of MMMs correspond to ZIF-301 nanocrystals [28], while those appearing at 25.8^{o} and 44.1^{o} confirmed the dispersion of CNTs within PSF matrix [42]. The fine coincidence of XRD patterns of MMMs with those of CNTs and ZIF-301 nanocrystals suggests their crystalline preservation after doping into polymer matrix. Furthermore the peak intensifications at the specified 2θ positions are proportional to the loading levels of respective nanofillers incorporated in composite membranes. All the membranes displayed a characteristic broad peak of PSF centered at an angle of 2θ = 17.2^{o}. In addition the slight shift of broad peak position (2θ) of bare PSF from 17.2° (d-spacing = 5.21 Å) to 17.4° (d-spacing = 5.14 Å) can be attributed to the strong filler-polymer interactions thus reducing the polymer inter-chain distance. The inter-chain size reduction behavior facilitates to improve CO_2/N_2 permselectivity due to size exclusion phenomenon.

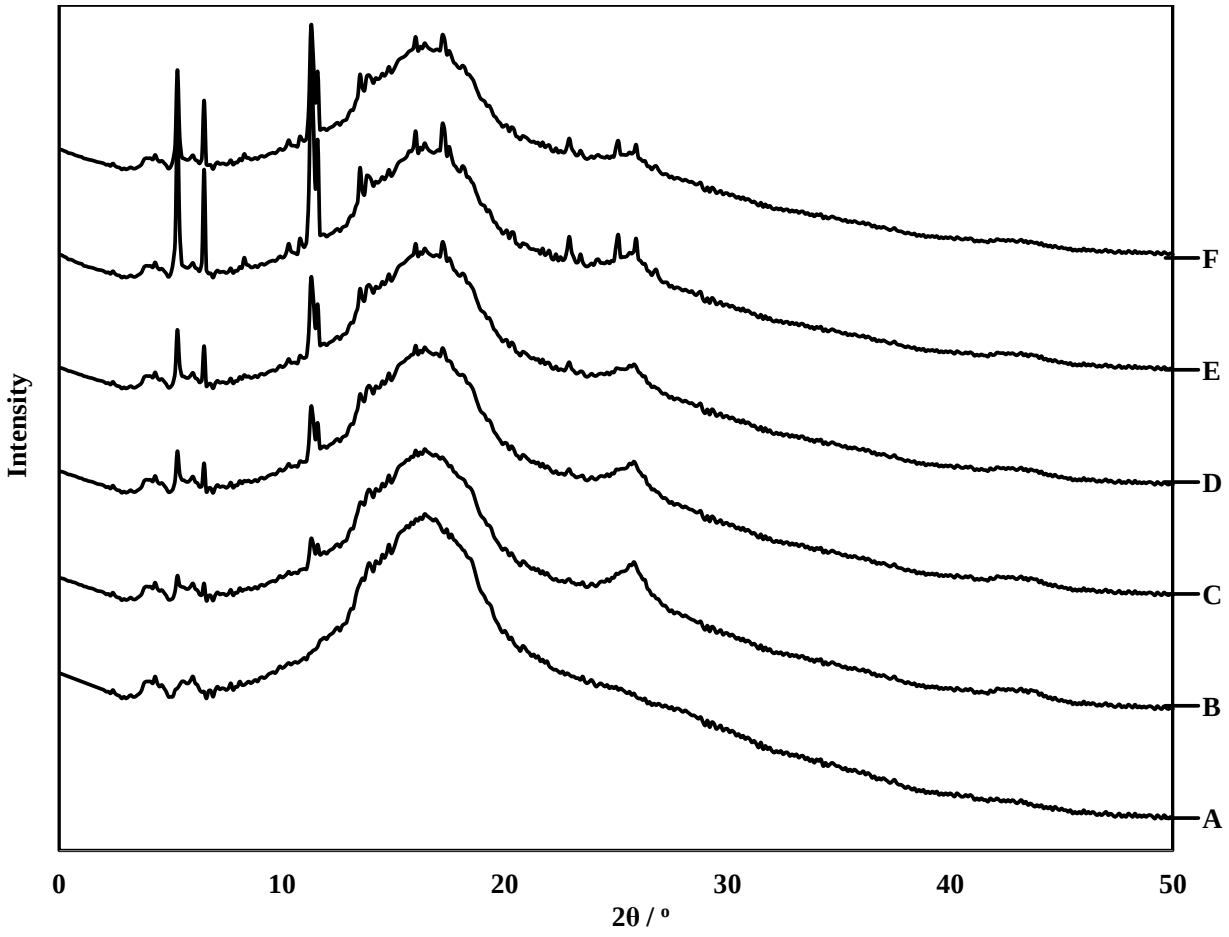

Fig. 5.1 Powder x-ray patterns of bare PSF [A], PSF/CNTs(10)/ZIF-301(6) [B], PSF/CNTs(8)/ZIF-301(12) [C], PSF/CNTs(6)/ZIF-301(18) [D], PSF/CNTs(4)/ZIF-301(24) [E], and PSF/CNTs(2)/ZIF-301(30) [F] MMMs containing different loadings of CNTs and ZIF-301 nanocrystals.

5.3.2 Morphology of PSF/CNTs/ZIF-301 MMMs

The morphology and structural characteristics of the hybrid membranes mainly depend upon the nature of organic polymer matrix and included inorganic filler(s). Cross sectional micrographs of MMMs were probed by SEM in order to investigate the

morphology of prepared MMMs, adhesion between filler-polymer interface and dispersion of CNTs and ZIF-301 nanoparticles within the polymer matrix as illustrated in Fig. 5.2. All MMMs filled with varying loadings of nanofillers exhibited continuous phases, almost free of interfacial voids.

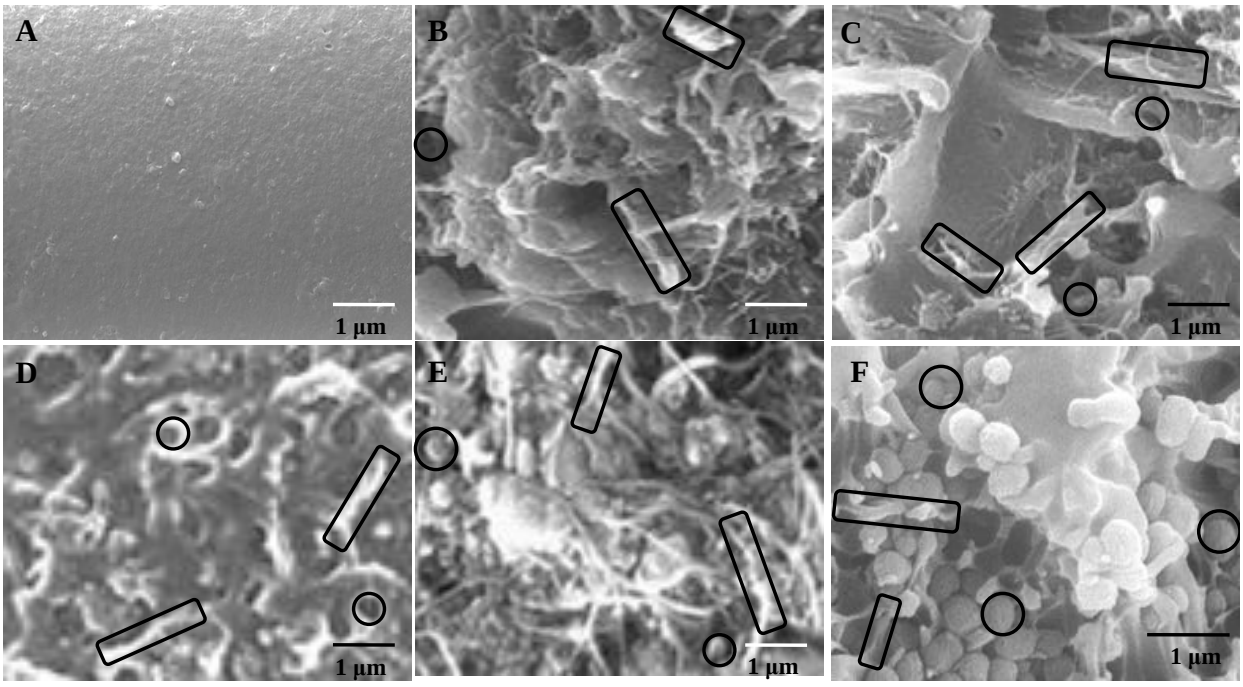

Fig. 5.2 Scanning electron micrographs of bare PSF [A], PSF/CNTs(10)/ZIF-301(6) [B], PSF/CNTs(8)/ZIF-301(12) [C], PSF/CNTs(6)/ZIF-301(18) [D], PSF/CNTs(4)/ZIF-301(24) [E], and PSF/CNTs(2)/ZIF-301(30) [F] MMMs containing different loadings of CNTs (enclosed by rectangles) and ZIF-301 nanocrystals (surrounded by circles).

In case of composite membranes containing high loadings of CNTs (ca. 8 and 10 wt %) and low ZIF-301 contents (i.e. 6 and 12 wt %), the CNTs agglomerated owing to their

large surface energy while ZIF-301 nanocrystals showed homogeneous dispersion and good polymer-filler adhesion on account of their tiny particle size (Figs. 5.2 [B] and [C]). The MMMs filled with high ZIF-301 (e.g. 24 and 30 wt %) and low CNTs (i.e. 2 and 4 wt %) loadings demonstrated uniform CNTs distribution but improper dispersion and poor adhesion of ZIF-301 nanoparticles with PSF matrix (Figs. 5.2 [E] and [F]). The mixed-matrix membrane containing optimal loading of nanofillers (6 wt % CNTs and 18 wt % ZIF-301) demonstrated uniform dispersion and good filler-polymer interfacial adhesion as the cross sectional view of MMM exhibits defect-free interconnected network morphology (Fig. 5.2 [D]). The controlled morphology of ZIF-301 nanocrystals dispersed in the optimized MMM provided significant steric effect to reduce CNTs aggregation; conversely the strong polymer-filler interaction led to homogeneous dispersion of ZIF-301 nanocrystals. The synergistic effect of ZIF-301 nanocrystals and CNTs helped to orient some of the CNTs parallel to gas permeation passages through the MMMs thickness.

5.3.3 Thermal Gravimetric Analysis

To assess the mutual effect of CNTs and ZIF-301 nanofillers on phase transitions, thermal stability, chemical and physical behavior of MMMs, TGA-DTG analyses of bare PSF and hybrid membranes were performed in the range of 100-700 ^{o}C. The TGA curves of the prepared membranes showed consistent decomposition profiles demonstrating a two-stage weight loss owing to desolvation (at around 100-180 ^{o}C) and pyrolysis (460-660 ^{o}C) processes as indicated in Fig. 5.3 [A]. The desolvation step refers to the release of volatile solvent molecules such as DMF, water, CCl_4 etc. confined within the pores of

MMMs while the decomposition of organic ligands of the imidazole frameworks and degradation of CNTs and PSF constituting entities occur during pyrolysis step. The residual ash left behind at the end of thermal test validated the nominal mass contents of nanofillers incorporated in corresponding MMMs.

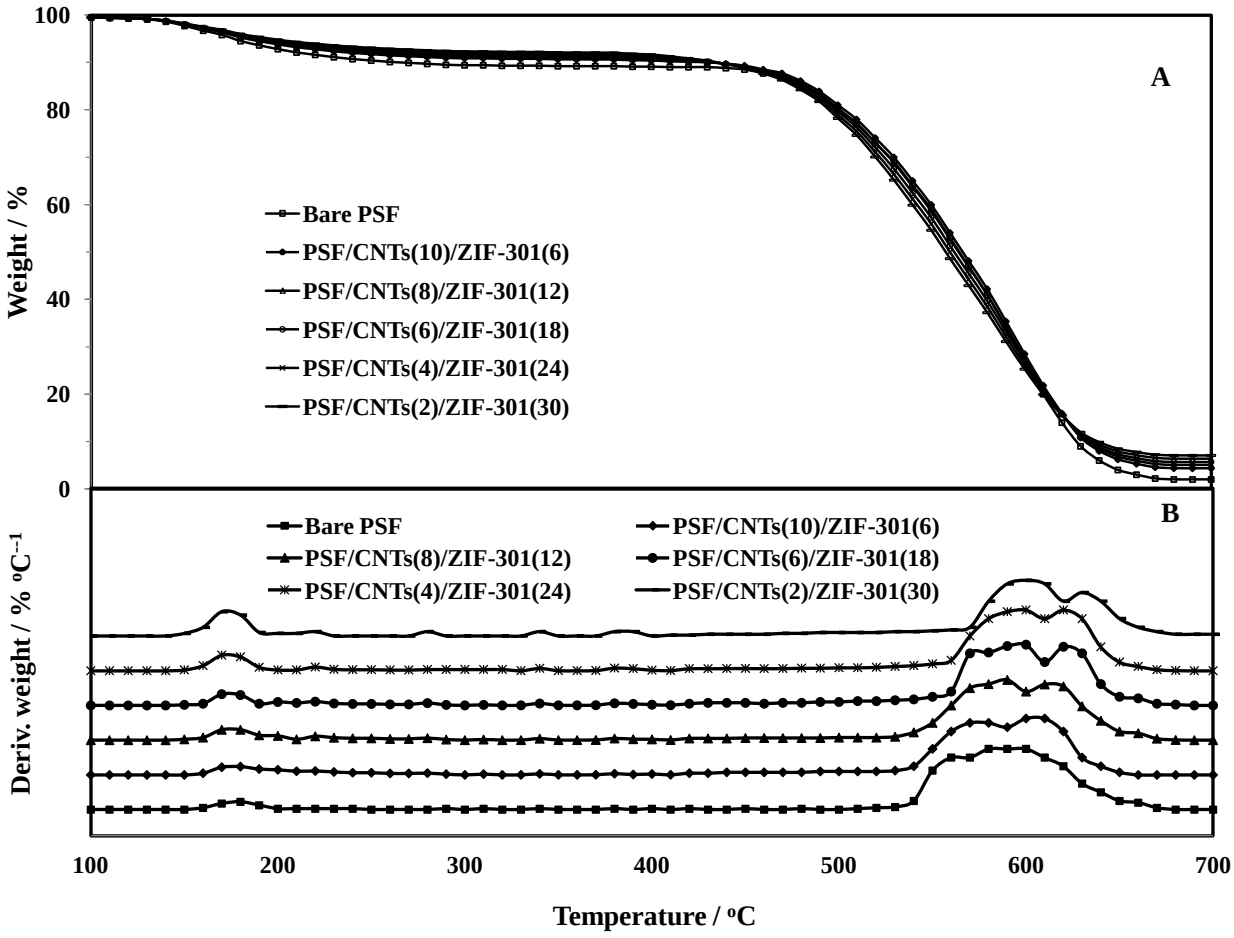

Fig. 5.3 TGA-DTG curves: TGA [A] and DTG [B] bare PSF and MMMs containing different loadings of CNTs and ZIF-301 nanocrystals.

The thermal stability of a material can be evaluated, via TGA analysis, in terms of $T_{d5\%}$ *and* $T_{d10\%}$ values- the temperatures at which testing specimen loses its 5 and 10 percent

weight respectively [43]. Being increasing function of nanofiller contents, values of $T_{d5\%}$ and $T_{d10\%}$ occur in the range of 177-188 °C and 591-599 °C respectively. Some of the notable thermal properties of hybrid membranes are outlined in Table 5.1. The derivative thermogravimetric (DTG) curves illustrated in Fig. 5.3 [B] provide essential data on pyrolysis rates in terms of 1st and 2nd DTG peaks. The degree of rigidity of the polymer chains in MMMs can be determined in terms of glass transition temperature (T_g), 1st and 2nd DTG peak values. The upgrading of these parameters, especially T_g, with increased nanofiller loadings (Table 5.1) signify improved rigidity of MMMs due to the constrained motion of polymer chains resulting from mutual interactions among polymer chains and nanofiller entities.

Table 5.1 Characteristic temperatures of membrane materials acquired from TGA-DTG data

Sample Designation	**T_g (^oC)**	**$T_{d5\%}$ (^oC)**	**$T_{d10\%}$ (^oC)**	**1st DTG peak (^oC)**	**2nd DTG peak (^oC)**	**Residual mass (%)**
Bare PSF	177	177	261	177	591	2.1
PSF/CNTs(10)/ZIF-301(6)	181	180	430	180	594	4.4
PSF/CNTs(8)/ZIF-301(12)	182	183	432	182	595	4.9
PSF/CNTs(6)/ZIF-301(18)	185	188	434	184	596	5.7
PSF/CNTs(4)/ZIF-301(24)	187	192	435	186	597	6.4
PSF/CNTs(2)/ZIF-301(30)	189	196	436	188	599	7.1

In contrast to bare PSF membrane, occurrence of thermal disintegration of hybrid membranes at higher temperatures can be attributed to improved polymer-filler

interactions and good thermal stability of CNTs and ZIF-301 nanocrystals. Thermal stability of hybrid membrane containing 6 wt % CNTs and 18 wt % ZIF-301, along with others, was found to be the highest due to harmonious effect of nanofillers. Thermal stability of mixed membranes determined in terms of 2^{nd} DTG peaks, improved with increasing nanofiller loadings as supported by weight loss curves. Since the maximum temperature observed in different gas separation and combustion processes occurs in the range of 30 to 350 °C, these MMMs can safely be used in gas separation applications [44].

5.3.4 Gas Sorption Analysis

N_2 adsorption isotherms, normally performed at 77 K under relative pressure of 0.3 bar, were applied to measure surface area and microporosity of the membranes. CO_2 and N_2 adsorption isotherms were obtained to determine their respective loading capacities under low pressure at 298 K as shown in Fig. 5.4.

Key physical macroscopic properties (density, fractional volume of nanofillers) and major microporous characteristics such as Brunauer-Emmett-Teller (S_{BET}) and Langmuir (S_{Lang}) surface areas, total micropore volume, CO_2 and N_2 uptakes, and CO_2/N_2 adsorption selectivity of the specimen were improved with the incorporation of nanofillers as summarized in Table 5.2. These outcomes precisely corroborated the existence of uniform distribution, improved adhesion and interfaces between PSF matrix and nanofillers resulting in fine quality MMMs.

Table 5.2 Physical and microporous properties of bare PSF and PSF/CNTs/ZIF-301 MMMs

Sample Designation	**Density** ($g\ cm^{-3}$)	**Φ_d** (%)	**S_{BET}** (m^2g^{-1})	**S_{Lang}** (m^2g^{-1})	**V_{micro}** (m^3g^{-1})	**CO_2 uptake** (cm^3g^{-1})	**N_2 uptake** (cm^3g^{-1})	α_{CO_2/N_2}
Bare PSF	1.25	0.00	12	18	0.02	4.3	0.39	11
PSF/CNTs(10)/ZIF-301(6)	1.347	12.41	130	170	0.23	9.1	0.63	14
PSF/CNTs(8)/ZIF-301(12)	1.342	17.24	160	190	0.27	11.3	0.76	15
PSF/CNTs(6)/ZIF-301(18)	1.337	21.99	180	220	0.32	13.7	0.91	15
PSF/CNTs(4)/ZIF-301(24)	1.332	26.67	200	250	0.28	11.8	1.1	11
PSF/CNTs(2)/ZIF-301(30)	1.327	31.28	230	280	0.23	10.3	1.2	9

As compared to bare PSF, CO_2 uptake for all the MMMs considerably improved with increasing pressure on account of specific chemical affinity of both the nanofillers for quadro-polar CO_2 molecules. The hybrid membrane filled with 6 wt % CNTs and 18 wt % ZIF-301 nanocrystals yielded the highest CO_2 loading ca. 14 cm^3/g (≈ 0.7 mmol/g) at 298 K which can be further improved by lowering the temperature. The N_2 gas was almost linearly adsorbed with pressure up to 1 bar for all the membranes indicating very poor chemical affinity for nanofillers. In addition all the membranes showed preferably high adsorption affinity for CO_2 as compared to N_2, especially at low CO_2 partial pressure. The CO_2/N_2 sorption selectivities of the MMMs significantly increased with nanofillers (especially ZIF-301) loadings. These findings suggest the fabricated MMMs as potential candidate to separate CO_2 from CO_2/N_2 mixture from post combustion flue gases.

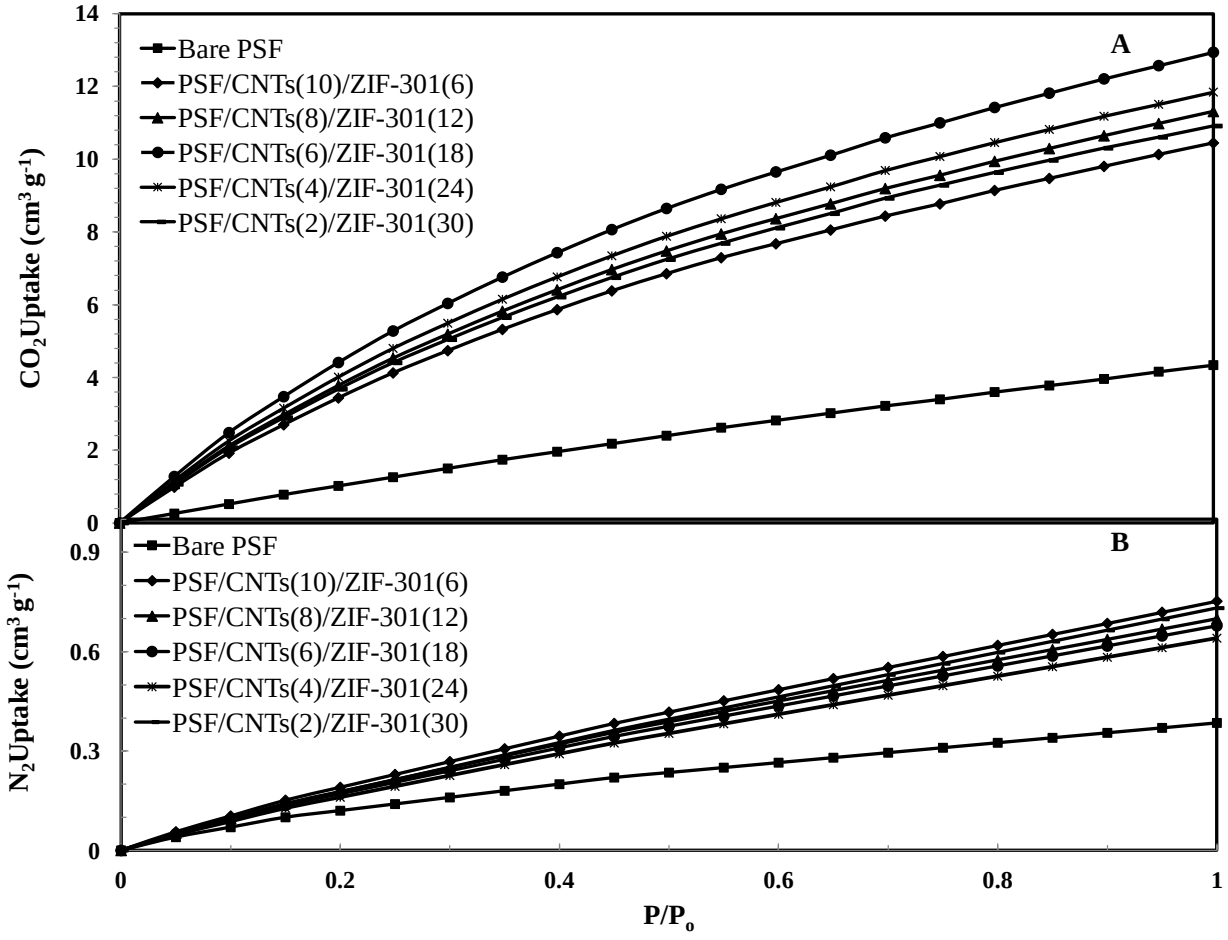

Fig. 5.4 CO_2 [A] and N_2 [B] adsorption isotherms for bare PSF and PSF/CNTs/ZIF-301 MMMs containing varying loadings of CNTs and ZIF-301 nanocrystals at 298 ^{o}C.

5.3.5 Gas Permeation Properties of MMMs

Single gas CO_2 and N_2 permeation experiments were performed to evaluate the permeability and ideal selectivity of the prepared membranes under dry and wet conditions at 25 °C subjected to an upstream pressure of 2 bar. On account of favorable CO_2-nanofillers mutual affinity, CO_2 permeability and CO_2/N_2 selectivity of the hybrid membranes were significantly improved by adding CNTs and ZIF-301 nanocrystals as

depicted in Fig. 5.5. The permeation experiments performed under wet conditions lead to slight improvement of CO_2 transport properties along with its separation from N_2.

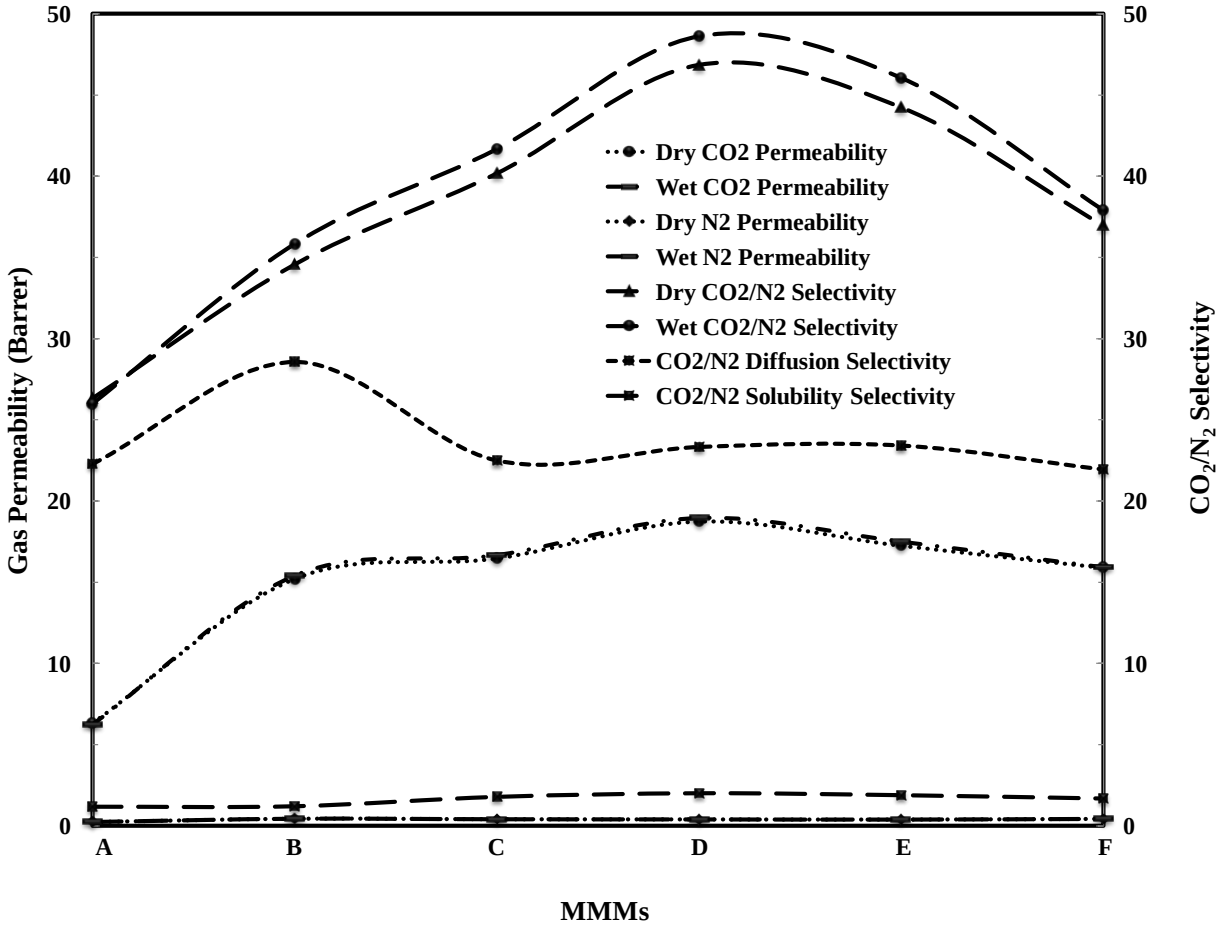

Fig. 5.5 Dry and wet gas CO_2 and N_2 permeabilities and CO_2/N_2 selectivity of bare PSF [A], PSF/CNTs(10)/ZIF-301(6) [B], PSF/CNTs(8)/ZIF-301(12) [C], PSF/CNTs(6)/ZIF-301(18) [D], PSF/CNTs(4)/ZIF-301(24) [E], and PSF/CNTs(2)/ZIF-301(30) [F] MMMs containing different loadings of CNTs and ZIF-301 nanocrystals.

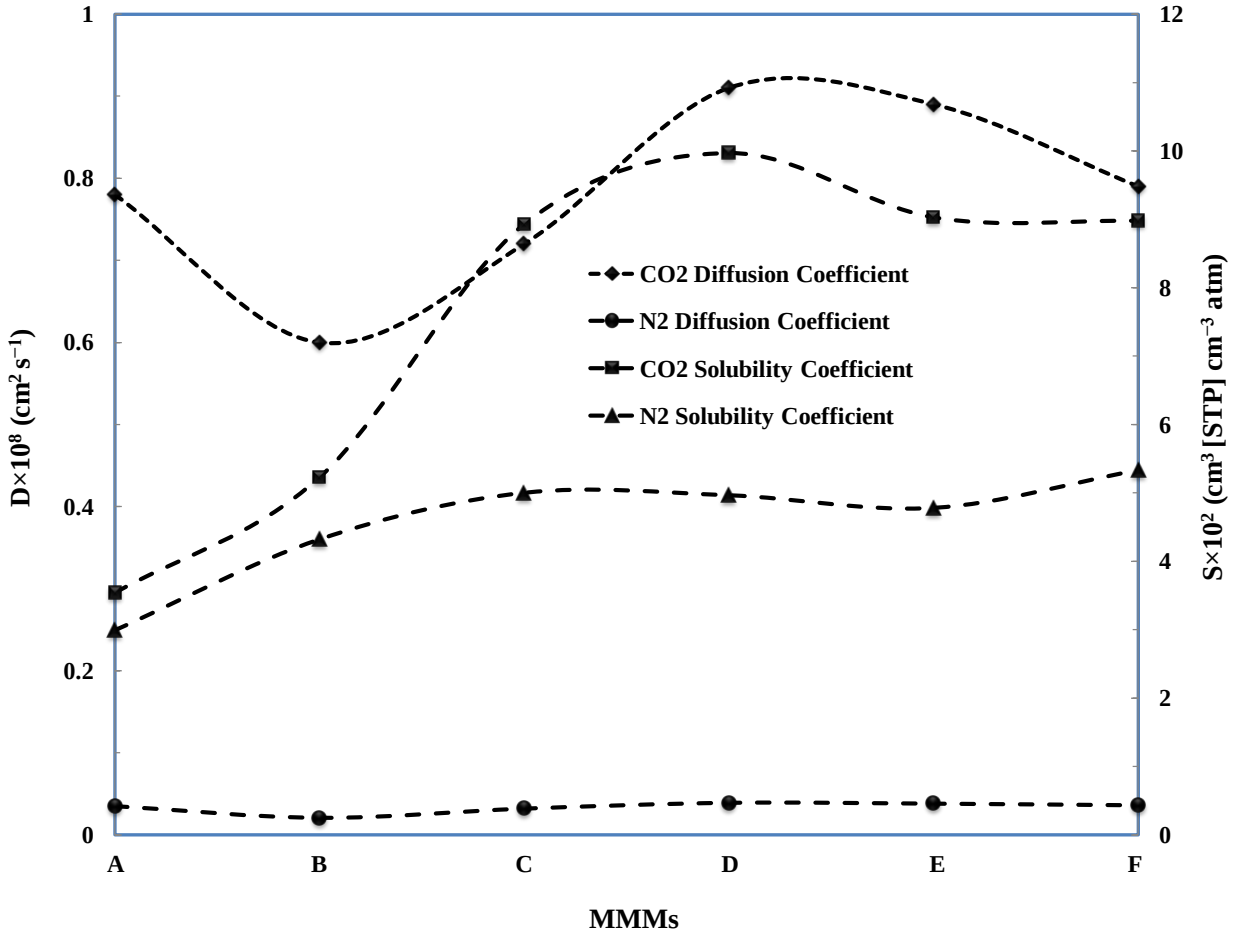

Fig. 5.6 Pure gas diffusion (D) and solubility (S) coefficients for bare PSF [A], PSF/CNTs(10)/ZIF-301(6) [B], PSF/CNTs(8)/ZIF-301(12) [C], PSF/CNTs(6)/ZIF-301(18) [D], PSF/CNTs(4)/ZIF-301(24) [E], and PSF/CNTs(2)/ZIF-301(30) [F] MMMs containing different loadings of CNTs and ZIF-301 nanocrystals.

Due to their relatively large pore diameter and smooth inner surfaces, the exclusive incorporation of CNTs into the polymer matrix extensively improved CO_2 permeability but at the expense of deteriorated CO_2/N_2 permselectivity [39]. The sole inclusion of ZIF-301 nanocrystals into polymer-based hybrid membranes reasonably increased both CO_2 permeability and CO_2/N_2 permselectivity due to the chemical structure of ZIF-301. Both

the CO_2 permeability and CO_2/N_2 ideal selectivity of the hybrid membranes were appreciably enhanced by the harmonious effect of adding CNTs and ZIF-301 nanofillers as shown in Fig. 5. The optimum filler loading was found to be 6 wt % CNTs and 18 wt % ZIF-301 nanocrystals. At the optimal filler loading the CO_2 permeability of the MMM was determined to be 33 Barrer with CO_2/N_2 selectivity of 72. The most preferable loading favored homogeneous distribution of the nanofillers so as to exploit the pathways of CNTs pores to amplify CO_2 permeability and the CO_2/N_2 selective affinity of amine-functionalized ZIF-301 nanocrystals to render high selectivity.

The gas permeation through a membrane occurs via solubility followed by diffusivity of the permeating gas molecules; this phenomenon can be well elucidated by estimating the coefficient of solubility (S) and coefficient of diffusivity (D) of CO_2 and N_2 gas molecules in mixed-matrix membranes. The essential data pertaining to gas solubility and diffusivity for the prepared membranes are illustrated in Figs. 5.5 and 5.6. The diffusivity coefficients of both CO_2 and N_2 were slightly changed with different nanofiller loadings reaching a maximum value at the optimal nanofiller loading. The diffusivities were improved due to the preferential orientation and close packing of cylindrical smooth-walled CNTs within the polymer matrix. The variation in CO_2 solubility coefficient was much pronounced as compared to that of N_2; the solubility coefficient of CO_2, in contrast to N_2, was significantly improved at the optimum loading. The solubility coefficient, in general, depends on both chemical composition and structural arrangement of the membrane. The basic nature of both CNTs hydroxyl groups and ZIF-301 amine groups generated a collegial impact to preferably adsorb the acidic CO_2 molecules as compared to non-polar N_2 molecules. This effect resulted in higher CO_2 solubility and limited that

of N_2, consequently improving the CO_2/N_2 solubility-based selectivity. The improved permselectivity of CO_2 over N_2 can also be ascribed to the enlarged number of interaction sites and basic functional groups due to the addition of CNTs and ZIF-301 nanocrystals into PSF matrix.

The time-lag method (eq. 6) was used to determine the values of diffusion coefficients. CO_2 and N_2 adsorption isotherms obtained at 25 ^oC under varying pressure helped to calculate Langmuir parameters to determine the correction parameters (bracketed term in eq. 3). The D values thus determined were used to calculate solubility coefficients of the membranes under the same conditions of temperature and pressure using eq. 4. The values of gas diffusivity coefficient selectivity (D_{CO2}/D_{N2}) slightly varied with different nanofiller loadings, while the gas solubility coefficient selectivity (S_{CO2}/S_{N2}) significantly changed for all the hybrid membranes attaining a peak value for the optimized MMM containing 6 wt % CNTs and 18 wt % ZIF-301 as shown in Fig. 5.5.

Almost defect-free CNTs permitted both CO_2 and N_2 gas molecules to diffuse quickly through its internally smooth-walled channels. Since the proper distribution of CNTs in PSF matrix acted as efficient pathways to proficiently transport gas molecules, the overall gas permeability was highly improved. Also the preferential solubility of CO_2, over N_2, into the ZIF-301 nanocrystals significantly improved its permeation through the hybrid membranes. The narrowing down of pore size of MMMs due to incorporation of ZIF-301 nanocrystals limited the N_2 adsorption as compared to CO_2. In a nutshell the CO_2/N_2 permselectivities of composite membranes are improved due to selective CO_2 solubility and restricted N_2 diffusion. Both the nanofillers mutually interacted so as to offer controlled passages for improved CO_2 permeability and CO_2/N_2 selectivity through the

composite membranes. The overall analysis based on improved performance of PSF/CNTs/ZIF-301 MMMs strongly support the development of a true mixed matrix membrane.

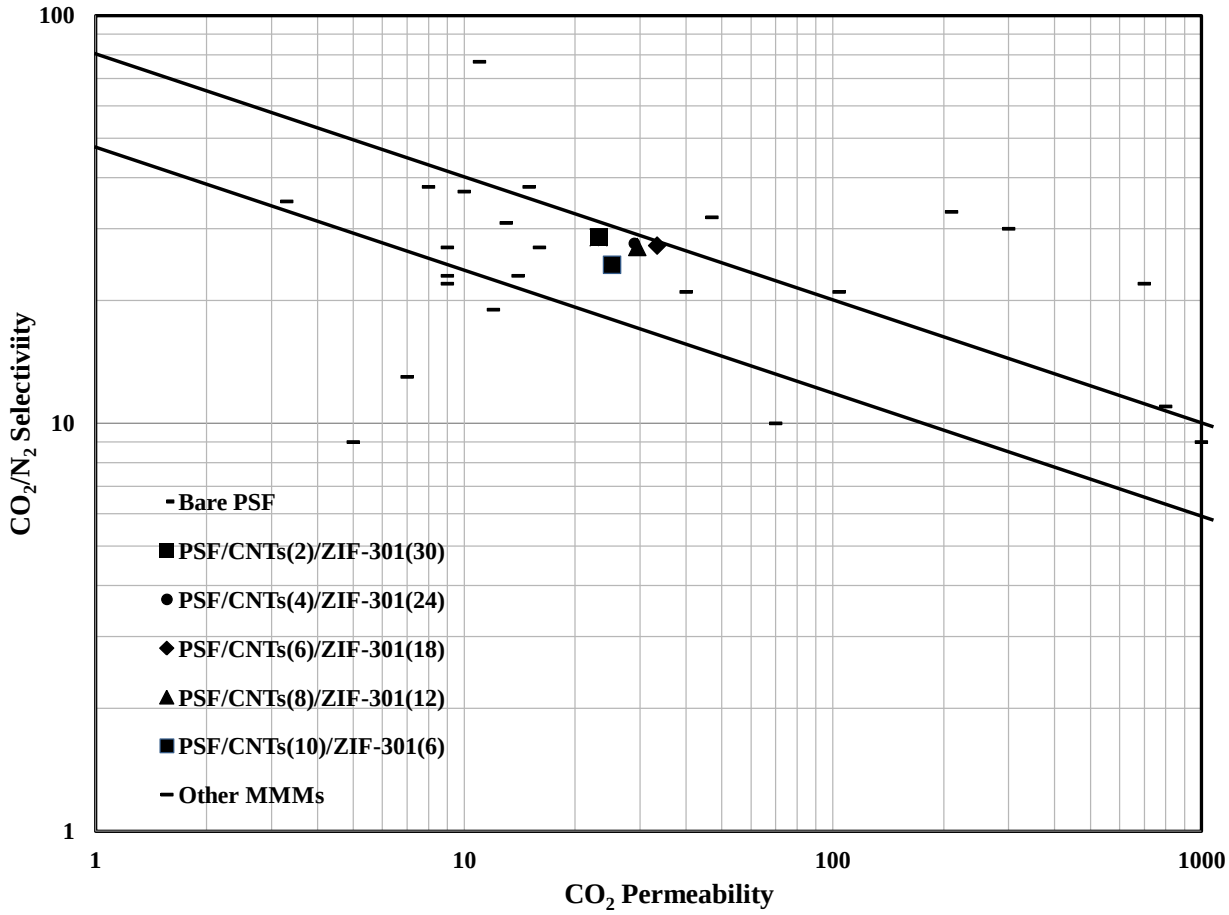

Fig. 5.7 Comparison of CO_2/N_2 separation performance of PSF/CNTs/ZIF-301 MMMs with other ZIF or MOF containing MMMs obtained from literature data. The Robeson 1991 and 2008 upper bounds for polymer separation performance are also shown.

A comparison of the CO_2/N_2 gas pair separation performance of nanofilled MMMs, along with Robeson 1991 and 2008 upper bounds [14], is made on a permeability-selectivity chart as illustrate in Fig. 5.7. The diagram indicates that the incorporation of CNTs and ZIF-301 nanofillers into PSF matrix has enhanced the permselectivity of the MMMs as compared to bare polysulfone membrane. The permselectivity values of all the composite membranes reported here are located between 1991- and 2008-upper bound lines, an important achievement of this work.

Since a membrane having high CO_2 permeability coupled with improved CO_2/N_2 ideal selectivity characteristics fulfills industrial requirements, it corroborates that CNTs and ZIF-301 nanofillers are competent materials to fabricate MMMs for post combustion carbon capture.

5.4 Conclusions

Hydrothermally stable high performance mixed-matrix membranes were fabricated by incorporating multiwalled CNTs and ZIF-301 nanofillers to selectively capture CO_2 from post combustion flue gases. Characterization of the MMMs carried out by XRD, TGA, SEM and gas sorption experiments indicated that they are thermally stable, microporous, partially crystalline materials exhibiting nanofillers homogeneous dispersion and good interfacial matrix-filler adhesion without adding any compatibilizing agent. The hybrid membranes prepared in this work demonstrated more than 5 times increment in CO_2 permeability as compared to that of bare PSF membrane while the CO_2/N_2 ideal selectivity was enhanced by more than 3 times. Furthermore the MMMs perform well under wet conditions as compared to dry ones. The separation performance of the

composite membranes produced in this work were above the Robeson 1991 upper bound and the CO_2/N_2 ideal selectivity is considered to be high enough to meet industrial applications.

Acknowledgement

The authors are thankful to KACST-TIC on Carbon Capture and Sequestration (CCS), King Fahd University of Petroleum and Minerals, Dhahran, Kingdom of Saudi Arabia for providing support for this work.

References

[1] D. M. D'Alessandro, B. Smit, J. R. Long, Carbon Dioxide Capture: Prospects for New Materials, Angew. Chem. Int. Ed. 49 (2010) 6058-6082.

[2] M. Z. Jacobson, Review of Solutions to Global Warming, Air Pollution, and Energy Security, Energy Environ. Sci. 2 (2009) 148-173.

[3] N. MacDowell, N. Florin, A. Buchard, J. Hallett, A. Galindo, G. Jackson, C. S. Adjiman, C. K. Williams, N. Shah, P. Fennell, An Overview of CO_2 Capture Technologies, Energy Environ. Sci. 3 (2010) 1645-1669.

[4] H. Herzog, D. Golomb, Carbon capture and storage from fossil fuel use, Encyc. Energy 1 (2004) 277-287.

[5] A. Hussain, M.B. Hägg, A feasibility study of CO_2 capture from flue gas by a facilitated transport membrane, J. Membr. Sci. 359 (2010) 140-148.

[6] J. Zhao, Z. Wang, J.X. Wang, S.C. Wang, Influence of heat-treatment on CO_2 separation performance of novel fixed carrier composite membranes prepared by interfacial polymerization, J. Membr. Sci. 283 (2006) 346-356.

[7] P. Pandey, R.S. Chauhan, Membranes for gas separation, Prog. Polym. Sci. 26 (2001) 853-893.

[8] R. Mahajan, W.J. Koros, Factors controlling successful formation of mixed-matrix gas separation materials, Ind. Eng. Chem. Res. 39 (2000) 2692–2696.

[9] E.P. Fawas, G.C. Kapantaidakis, J.W. Nolan, A.C. Mitropoulos, N.K. Kanellopoulos, Preparation, characterization and gas permeation properties of carbon hollow fiber membranes based on Matrimid® 5218 precursor, J. Mater. Process. Technol. 186 (2007) 102–110.

[10] R.W. Baker, Future directions of membrane gas separation technology, J. Ind. Eng. Chem. Res. 41 (2002) 1393–1411.

[11] D.L. Gin, R.D. Noble, Designing the next generation of chemical separation membranes, Science 332 (2011) 674-676.

[12] Y. Xiao, T.-S. Chung, Grafting thermally labile molecules on cross-linkable polyimide to design membrane materials for natural gas purification and CO_2 capture. Energy Environ. Sci. 4 (2011) 201-208.

[13] C. Staudt-Bickel, W.J. Koros, Improvement of CO_2/CH_4 separation characteristics of polyimides by chemical crosslinking. J. Membr. Sci. 155 (1999) 145-154.

[14] T.C. Merkel, B.D. Freeman, R.J. Spontak, Z. He, I. Pinnau, P. Meakin, A. Hill, J. Ultrapermeable, reverse-selective nanocomposite membranes, Science 296 (2002) 519-522.

[15] J. Ahn, W.-J. Chung, I. Pinnau, M.D. Guiver, Polysulfone/silica nanoparticle mixed-matrix membranes for gas separation, J. Membr. Sci. 314 (2008) 123-133.

[16] B.D. Reid, A. Ruiz-Trevino, I.H. Musselman, K.J. Balkus, J.P. Ferraris, Gas permeability properties of polysulfone membranes containing the mesoporous molecular sieve MCM-41, Chem. Mater. 13 (2001) 2366-2373.

[17] S. Kim, E. Marand, J. Ida, V.V. Guliants, Polysulfone and mesoporous molecular sieve MCM-48 mixed matrix membranes for gas separation, Chem. Mater. 18 (2006) 1149-1155.

[18] S. Kim, E. Marand, High permeability nano-composite membranes based on mesoporous MCM-41 nanoparticles in a polysulfone matrix, Microp. Mesop. Mater. 114 (2008) 129-136.

[19] D.Q. Vu, W.J. Koros, S.J. Miller, Mixed matrix membranes using carbon molecular sieves. II. Modeling permeation behavior, J. Membr. Sci. 211 (2003) 335-348.

[20] H.L. Cong, J.M. Zhang, M. Radosz, Y.Q. Shen, Carbon nanotube composite membranes of brominated poly(2,6-diphenyl-1,4-phenylene oxide) for gas separation, J. Membr. Sci. 294 (2007) 178–185.

[21] S. Kim, L. Chen, J.K. Johnson, E. Marand, Polysulfone and functionalized carbon nanotube mixed matrix membranes for gas separation: Theory and experiment, J. Membr. Sci. 294 (2007) 147–158.

[22] P. Gorgojo, S. Uriel, C. Tellez, J. Coronas, Development of mixed matrix membranes based on zeolite Nu-6(2) for gas separation, J. Microporous Mesoporous Mater. 115 (2008) 85–92.

[23] Y. Liu, D. Peng, G. He, S. Wang, Y. Li, H. Wu, Z. Jiang, Enhanced CO_2 permeability of membranes by incorporating polyzwitterion@CNT composite particles into polyimide matrix, ACS Appl. Mater. Interfaces 6 (2014) 13051-13060.

[24] B. Harold, T. Jeazet, C. Staudt, C. Janiak, Metal–organic frameworks in mixed-matrix membranes for gas separation, Dalton Trans. 41 (2012) 14003–14027.

[25] T. Li, Y. Pan, K.V. Peinemann, Z. Lai, Carbon dioxide selective mixed matrix composite membrane containing ZIF-7 nano-fillers, J. Membr. Sci. 425–426 (2013) 235–242.

[26] Chen Zhang, Kuang Zhang, Liren Xu, Ying Labreche, Brian Kraftschik, W.J. Koros, Highly scalable ZIF-based mixed-matrix hollow fiber membranes for advanced hydrocarbon separations, AIChE J. 60 (2014) 2625–2635.

[27] Mohammad Askari, T.S. Chung, Natural gas purification and olefin/paraffin separation using thermal cross-link ableco-polyimide/ZIF-8 mixed matrix membranes, J. Membr. Sci. 444 (2013) 173–183.

[28] T.T.N. Nhung, H. Furukawa, F. Gandara, H.T. Nguyen, K.E. Cordova, O.M. Yaghi, Selective capture of carbon dioxide under humid conditions by hydrophobic chabazite-type zeolitic imidazolate frameworks, Angew. Chem. 126 (2014) 10821–10824.

[29] H. Chen, D.S. Sholl, Predictions of selectivity and flux for CH_4/H_2 separations using single walled carbon nanotubes as membranes, J. Membr. Sci. 269 (2006) 152–160.

[30] D.S. Sholl, J.K. Johnson, Making high-flux membranes with carbon nanotubes, Science 312 (2006) 1003–1004.

[31] A.I. Skoulidas, D.S. Sholl, J.K. Johnson, Adsorption and diffusion of carbon dioxide and nitrogen through single-walled carbon nanotube membranes, J. Chem. Phys. 124 (2006) 054708.

[32] S. Kim, J.R. Jinschek, H. Chen, D.S. Sholl, E. Marand, Scalable fabrication of carbon nanotube/polymer nanocomposite membranes for high flux gas transport, Nano Lett. 7 (2007) 2806–2811.

[33] T.W. Chamberlain, J.C. Meyer, J. Biskupek, J. Leschner, A. Santana, N.A. Besley, E. Bichoutskaia, U. Kaiser, A.N. Khlobystov, Reactions of the inner surface of carbon nanotubes and nanoprotrusion processes imaged at the atomic scale, Nat. Chem. 3 (2011) 732–737.

[34] A.F. Ismail, P.S. Goh, S.M. Sanip, M. Aziz, Transport and separation properties of carbon nanotube-mixed matrix membrane, Sep. Purif. Technol. 70 (2009) 12–26.

[35] L. Ge, L. Wang, V. Rudolph, Z. Zhu, Hierarchically structured metal-organic framework/vertically-aligned carbon nanotubes hybrids for CO_2 capture, RSC Adv. 3 (2013) 25360–25366.

[36] B. Zornoza, B. Seoane, J. M. Zamaro, C. Téllez and J. Coronas, Combination of MOFs and zeolites for mixed-matrix membranes, Chem-PhysChem, 12 (2011) 2781–2785.

[37] M. Valero, B. Zornoza, C. Téllez, J. Coronas, Mixed matrix membranes for gas separation by combination of silica MCM-41 and MOF NH2-MIL-53 (Al) in glassy polymers, Microporous Mesoporous Mater. 192 (2013) 23–28.

[38] A. Galve, D. Sieffert, C. Staudt, M. Ferrando, C. Güell, C. Téllez, J. Coronas, Combination of ordered mesoporous silica MCM-41 and layered titanosilicate JDF-L1

fillers for 6FDA-based copolyimide mixed matrix membranes, J. Membr. Sci. 431 (2013) 163-170.

[39] X. Li, L. Ma, H. Zhang, S. Wang, Z. Jiang, R. Guo, H. Wu, X.Z. Cao, J. Yang, B. Wang, Synergistic effect of combining carbon nanotubes and grapheme oxide in mixed matrix membranes for efficient CO_2 separation, J. Memb. Sc. 479 (2015) 1-10

[40] X.W. Yu, Z. Wang, Z.H. Wei, S.J. Yuan, J. Zhao, J.X. Wang, S.C. Wang, Novel tertiary amino containing thin film composite membranes prepared by interfacial polymerization for CO_2 capture, J. Membr. Sci. 362 (2010) 265-278.

[41] D.R. Paul, D.R. Kemp, The diffusion time lag in polymer membranes containing adsorptive fillers, J. Polym Sc: Polym. Symp. 41 (1973) 79–93.

[42] V. Gupta, T. Saleh, Synthesis of Carbon Nanotube-Metal Oxides Composites; Adsorption and Photo-Degradation, Carbon 59 (2013)308–314.

[43] Y.C. Xiao, T.S. Chung, H.M. Guan, M.D. Guiver, Synthesis, cross-linking and carbonization of co-polyimides containing internal acetylene units for gas separation, J. Membr. Sci. 302 (2007) 254-264.

[44] A.C.C. Chang, S.S.C. Chuang, M. Gray, Y. Soong, In-situ infrared study of CO_2 adsorption on SBA-15 grafted with γ-(aminopropyl) triethoxysilane, Energy Fuels 17 (2003) 468-473.

CHAPTER 6

ENHANCED CO_2 SEPARATION FROM HUMIDIFIED POST COMBUSTION GASES: SYNERGISTIC EFFECT OF INTEGRATING CNTS AND ZIFS INTO POLYSULFONE TO FABRICATE HIGH PERFORMANCE MMMS

Abstract

Multiwalled CNTs and zeolitic imidazole frameworks (ZIF-302) were collegially incorporated into glassy polysulfone (PSF) to prepare mixed-matrix membranes (MMMs) to separate CO_2 from post combustion flue gas stream. Varying loadings of both nanofillers were incorporated into PSF using solution-casting technique to optimize CO_2 separation performance of MMMs under dry and wet conditions. The flexible MMMs rendered homogeneous dispersion of fillers, improved polymer-filler adhesion, and thermally stable structure. Gas sorption analyses along with dry and wet gas permeation experiments demonstrated improved CO_2 permeability and CO_2/N_2 ideal selectivity of MMMs owing to collegial effect of nanofillers. The composite membrane containing 8 wt % CNTs and 12 wt % ZIF-302 nanofillers showed an optimum separation performance by providing a CO_2 permeability of 18 Barrers with CO_2/N_2 selectivity of

35. The permeation features of MMMs were slightly improved under humid conditions as compared to dry ones.

6.1 Introduction

CO_2 emissions from burning of fossil fuels induce environmental warming concerns throughout the globe [1-3]. Economically viable processes to reduce CO_2 releases include its sequestration or capture from a mixture of CO_2-containing gases [4-5]. On account of its flexible design, ease of scale up, high efficiency, low energy requirement, simple function, low capital and operating costs and environmental friendliness, polymer-based mixed-matrix membrane gas separation technology- among other conventional processes- has gained momentous attention [6-13].

Majority of glassy polymers have been studied to fabricate MMMs by adding inorganic fillers like nonporous silica [14-15], structured mesoporous silica [16-18], carbon molecular sieves [19], carbon nanotubes [20-21], zeolites [22], and microporous metal organic frameworks (MOFs) [23] in order to design efficient composite membranes showing better permselectivity characteristics as compared to unfilled polymer membranes. Advantages of adding microporous nanomaterials (such as ZIFs/MOFs and/or CNTs/graphenes etc.) into polymer matrix to form MMMs comprise the ability to combine the simplicity of casting and processability, enhanced mechanical and chemical performance of polymers conjoined with improved gas separation efficiency of nanocrystals possessing adjustable pore dimensions, modifiable surface functionality, and high surface areas [24].

Nanocrystals of microporous zeolitic imidazolate frameworks are interesting materials to fabricate efficient MMMs for gas separation on account of their high surface areas, tunable nano-sized pores, modifiable surface functionality, good wetting characteristics, improved thermal and chemical stability [25–27]. Hydrothermally stable ZIF-302 crystals [28] selectively capture CO_2 gas from $CO_2/N_2/H_2O$ wet gaseous mixture and their inclusion into polymer matrices is expected to improve separation performance of MMMs under wet conditions.

Owing to their internal smooth walls, nano-sized configuration, large pore diameter, high aspect ratio, excellent mechanical and thermal properties [29–31], gas permeation through CNTs is exceptionally higher as compared to other microporous materials. The selectivity of as-synthesized CNTs for various gas molecules is comparatively low and tricky to recover by chemical modification/functionalization due to their inert nature [32–34]. Although CNTs-filled MMMs are significantly efficient as compared to MOF/ZIF-based MMMs, good adhesion and uniform dispersion of nanofillers in polymer matrices is the central challenge. A more refined strategy to engineer MMMs with enhanced permselectivity is the collegial incorporation of naonfillers possessing diversified morphology, nature, and dimensions into a polymer matrix [35].

Different types of zeolites (e.g. S1C), MOFs (e.g. HKUST-1), MILs (e.g. NH_2-MIL-53(Al)) and ZIFs (e.g. ZIF-8) were added into PSF to prepare MMMs to study the permeation of CO_2, N_2, CH_4, O_2, and H_2 gases [36]. The CO_2/N_2 permselectivity did not ameliorate for S1C-ZIF-8/PSF MMMs. The CO_2 permeation characteristics of HKUST-1/ZIF-8/PSF, S1C/PSF, HKUST-1/PSF, and ZIF-8/PSF MMMs were found to be 8.4, 9.4, 9.5 and 12.3 Barrers respectively with corresponding CO_2/N_2 permselectivities of 38,

23, 24, and 19. The collegial impact of adding mesoporous silica MCM-41 and amine-functionalized MIL-53(Al) nanofillers into polymer-based MMMs improved their gas separation efficiency [37]. Galve and group [38] fabricated hybrid membranes by introducing mesoporous silica MCM-41 spheres and layered microporous titanosilicate JDF-L1 sheets into glassy polyimide matrix; the uniform distribution of MCM-41 spheres in the polymer matrix were facilitated by JDF-L1 sheets. Li et al. [39] investigated the combined inclusion of graphene oxide and CNTs into PSF to determine optimal loadings of the nanofillers.

The exclusive incorporation of CNTs and ZIFs into PSF matrix helped to improve gas separation efficiency of CO_2. The current work focuses on combined inclusion of CNTs and ZIF-302 nanocrystals into glassy PSF matrix for the first time to fabricate PSF/CNTs/ZIF-302 MMMs to efficiently separate CO_2 from CO_2/N_2 mixture. The main objective of this study is to determine the optimum loadings of both the nanofillers to attain high CO_2 permselectivity and to systematically investigate the solubility-diffusivity separation mechanism under dry and wet conditions.

6.2 Experimental

6.2.1 Materials

Commercially available polysulfone having average molecular weight ~ 35000 by LS and density 1.25 g cm^{-3}, was purchased from Sigma Aldrich. Multi-walled CNTs having average length 1.2 μm and diameter 8 nm were obtained from Nanjing XFNANO Materials Tech. Co., Ltd. Zinc nitrate hexahydrate and 2-methylimidazole were obtained from Merck Chemical Company. 5(6)-methylbenzimidazole, methanol, and N,N-

dimethylformamide (DMF) were purchased from Aldrich Chemical Company. Polymer and all the chemicals were used as received without further treatment. Highly pure CO_2, N_2 and He gases were used for gas sorption and permeation experiments.

6.2.2 Synthesis of ZIF-302 nanocrystals

ZIF-302 nanocrystals were synthesized by dissolving 0.28 mmol (83.3 mg) of the metal salt $Zn(NO_3)_2 \cdot 6H_2O$, 0.24 mmol (19.8 mg) of the primary organic linker 2-methylimidazole, and 0.28 mmol (42.8 mg) of the secondary organic linker 5(6)-methylbenzimidazole in a mixture of 7 mL DMF and 1 mL distilled water by sonication in a 20-mL vial for 10 minutes. The resulting solution was moderately stirred on a hot plate at 50 °C for 70 hours to obtain colorless nanocrystals of ZIF-302 in suspended form. The suspended nanocrystals were separated from the mother liquor via centrifuge and washed with 7 mL of fresh DMF. This process was repeated five times to make them ready to prepare MMMs of varying composition.

6.2.3 Preparation of PSF/CNTs/ZIF-302 MMMs

PSF, CNTs and ZIF-302 nanocrystals were degassed at 100 ^oC under vacuum for 20 h to remove adsorbed gases and/or moisture in order to prepare different membranes. Bare PSF membrane was prepared by dissolving 1g PSF in 10 mL DMF followed by stirring at room temperature for 24 hours to get a viscous solution. The MMMs containing different loadings of CNTs and ZIF-302 nanocrystals were prepared as follows. 1 g PSF was added in 10 mL DMF and stirred at room temperature for 20 h. Then a weighed quantity of CNTs was dispersed in 4 mL DMF by sonicating for 1 h to get well dispersed

homogeneous suspension. In addition, a specified amount of ZIF-302 nanocrystals was redispersed in DMF by stirring for 10 minutes. The three solutions were mixed together and subjected to vigorous stirring for another 12 h to obtain a homogeneous solution. All the membranes were knife casted on clean glass plates at a specified gate height using a flat sheet membrane casting system (FSMCS). After allowing the solvent to slowly evaporate from the membranes under ambient conditions overnight, the membranes were detached from the glass plates and placed in a vacuum oven to dry the MMMs at 80, 100 and 180 ^{o}C for 12, 20 and 60 hours respectively to ensure complete removal of solvent traces before subjecting them to gas permeation experiments.

The prepared MMMs were designated as PSF/CNTs(X)/ZIF-302(Y), where X (ranging from 2-10), and Y (ranging from 6-30) represent loadings of CNTs and ZIF-302 by wt % respectively. As an illustration the MMM denoted by PSF/CNTs(8)/ZIF-302(12) contains 8 and 12 wt % loadings of CNTs and ZIF-302 nanocrystals respectively. The thicknesses of the membranes were determined in the range of 50-80 μm as measured by a digital micrometer.

6.2.4 Materials Characterization Methods

The characterization techniques applied to the casted membranes comprise of x-ray diffraction, scanning electron microscopy, thermogravimetric and gas sorption analyses. The fractional volume of nanofillers added to caste MMMs can be defined as:

$$\Phi_D = \frac{m_D/\rho_D}{m_D/\rho_D + m_C/\rho_C} \times 100 \qquad (1)$$

where m and ρ represent mass and density of PSF (continuous phase denoted by subscript C) and CNTs and/or ZIF-302 nanofillers (dispersed phase denoted by subscript D) respectively. Usually the void volume at the polymer-filler interface is negligible as supported by SEM micrographs and gas sorption analyses. The apparent volume fraction of nanofillers can readily be taken as the exact volume fraction of CNTs and/or ZIF-302 nanocrystals mutually incorporated into the composite membranes.

Powder XRD patterns of the membranes were registered using a Bruker D8 X-ray Diffractometer using Cu K_α radiation (λ = 1.5406 Å) operated at 45 mA and 40 kV with a step size increment of 0.02^o in 2θ at a scanning rate of 0.02^o s^{-1}. The membrane sample was loaded in a sample holder placed on silicon substrate. The hybrid membranes were characterized by XRD to check whether the crystalline structure of the nanofillers sustains after their addition to the polymeric matrix.

In order to examine their morphology and quality of filler-polymer interface, the membranes were scanned to obtain relevant micrographs using a Hitachi S-4300SE/N SEM instrument. Testing specimens were cryofractured in liquid nitrogen and their outer surfaces were coated with a thin gold film to avoid charging of electrons. The SEM machine was operated at an accelerating voltage of 20 kV.

Thermal stability and other pertinent properties of the membranes were evaluated by thermogravimetric analysis using a TGA/SDTA 851 (Mettler Toledo) system in air by heating from ambient temperature to 700 ^oC at a heating rate of 10 ^oC min^{-1}. Glass transition temperature (T_g) of the membranes were determined by differential scanning calorimetry (DSC) using Netzsch DSC 200F3 Calorimeter in the temperature range of

40−200 °C at a heating rate of 5°C/min, under a nitrogen atmosphere with a flow rate of 50 mL/min.

CO_2 and N_2 adsorption isotherms obtained at 77 and 298 K using a Quantachrome Autosorb iQ gas sorption analyzer were used to assess various microporous characteristics (e.g., CO_2 and N_2 gas uptakes, specific BET and Langmuir surface areas, total microporous volume) of the membranes. The membrane samples were chopped into tiny pieces and degassed at 100 ^oC under vacuum ($<10^{-6}$ bar) for 6 hours. Physisorption data of CO_2 and N_2 gases were measured at 298 K under a gas pressure ranging from 10^{-6} to 1 bar.

6.2.5 Gas Permeation Measurements

CO_2 and N_2 gas transport properties (i.e., permeability, ideal selectivity, and separation performance) of the membranes were determined using single gas permeation cell following the variable-pressure/constant-volume method at a temperature of 298 K [40]. After measuring its average thickness the membrane was fixed in the permeation cell. While keeping the feed side valve closed the lines of the cell were evacuated. The valve between the permeate side line and the vacuum pump was then closed followed by opening the feed side valve to maintain a low feed pressure (e.g., 2 bars) for a specific time (i.e., 2 h) to record the permeation measurements. At least three replicas were prepared and tested corresponding to each membrane in order to assess error and identify imperfect membranes.

Gas permeability (P_i, *Barrer*) of the membrane was determined using eq. (2):

$$P_i = \frac{22414}{A} \times \frac{V}{RT} \times \frac{l}{\Delta P_i} \frac{dP_i}{dt} \qquad (2)$$

where *l, A, V, R, T,* ΔP and $\Delta P_i/dt$ are respectively membrane thickness (*cm*), membrane active area (cm^2), downstream volume (cm^3), universal gas constant (6236.56 cm^3 *cmHg/mol/K*), absolute temperature (*K*), pressure difference across the membrane (*psi*), and permeation rate (*psi/s*) of component i.

Time-lag method, suggested by Paul and Kemp [41], was used to determine diffusion coefficient (D) by using *diffusivity vs. time-lag* (D-θ) relationship for the membranes:

$$D = \frac{l^2}{6\theta}\left[1 + \frac{6K}{y^3}\left\{\frac{y^2}{2} + y - (1+y)\ln(1+y)\right\}\left(\frac{V_d}{V_p}\right)\right] \qquad (3)$$

where V_d and V_p are respectively the volume fractions of filler and polymer phases; K and y are adsorption parameters determined from Langmuir adsorption isotherm.

The solubility coefficient (S) can be calculated from Eq. (4):

$$S = \frac{P}{D} \qquad (4)$$

The ideal selectivity of gas i over j (α_{ij}) can be determined using Eq. (5):

$$\alpha_{ij} = \frac{P_i}{P_j} = \left(\frac{D_i}{D_j}\right)\left(\frac{S_i}{S_j}\right) \qquad (5)$$

Here (D_i/Dj) and (S_i/S_j) represent diffusion- and solubility-based selectivity terms respectively.

6.3 Results and discussion

6.3.1 Powder X-ray Diffraction

Powder x-ray diffraction is a useful method to study the effect of nanofillers on the configuration of polymer chains in composite membranes and to corroborate the existence of crystalline structure of materials in amorphous polymer matrices. XRD measurements in the range of 2-50^o were registered to ensure the existence of crystallinity of CNTs and ZIF-302 in mixed matrix membranes as depicted in Fig. 6.1. The specific peak intensities appearing at 2θ positions of 10.7^o, 13.0^o and 22.8^o in XRD patterns of MMMs correspond to ZIF-302 nanocrystals [28], while those arising at 25.8^o and 44.1^o confirmed the dispersion of CNTs within PSF matrix [42]. The fine coincidence of XRD patterns of hybrid membranes with those of CNTs and ZIF-302 nanocrystals imply they maintain the crystallinity even after integrating to polymer matrix. The peak intensifications at the specified 2θ positions are in accordance with the loadings of respective nanofillers in composite membranes. All the membranes showed a characteristic broad peak pertaining to PSF centered at an angle of 2θ = 17.2^o. In addition the slight shift of broad peak position (2θ) of bare PSF from 17.2° (d-spacing = 5.21 Å) to 17.3° (d-spacing = 5.17 Å) can be attributed to the strong polymer-filler interactions thus reducing the polymer inter-chain distance. The inter-chain size reduction behavior promotes the improvement of CO_2/N_2 permselectivity owing to size exclusion phenomenon.

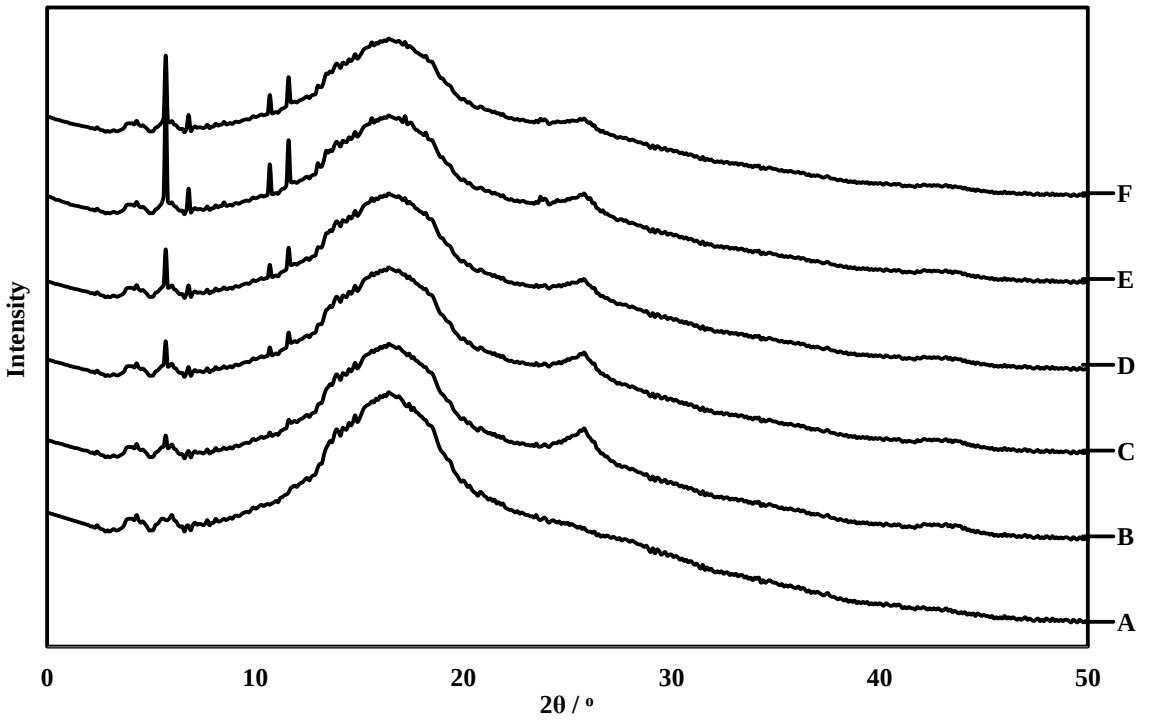

Fig. 6.1 Powder x-ray patterns of bare PSF [A], PSF/CNTs(10)/ZIF-302(6) [B], PSF/CNTs(8)/ZIF-302(12) [C], PSF/CNTs(6)/ZIF-302(18) [D], PSF/CNTs(4)/ZIF-302(24) [E], and PSF/CNTs(2)/ZIF-302(30) [F] MMMs containing different loadings of CNTs and ZIF-302 nanocrystals.

6.3.2 Morphology of PSF/CNTs/ZIF-302 MMMs

The morphology and structural characteristics of the hybrid membranes primarily depend on the essence of both the polymer matrix and the inserted nanofiller(s). Cross sectional micrographs of MMMs were examined by SEM to inspect the morphology of prepared MMMs, adhesion between filler-polymer interface and dispersion of CNTs and ZIF-302 nanoparticles within the polymer matrix as illustrated in Fig. 6.2. All MMMs loaded with different amounts of nanofillers exhibited continuous phases, almost free of interfacial voids.

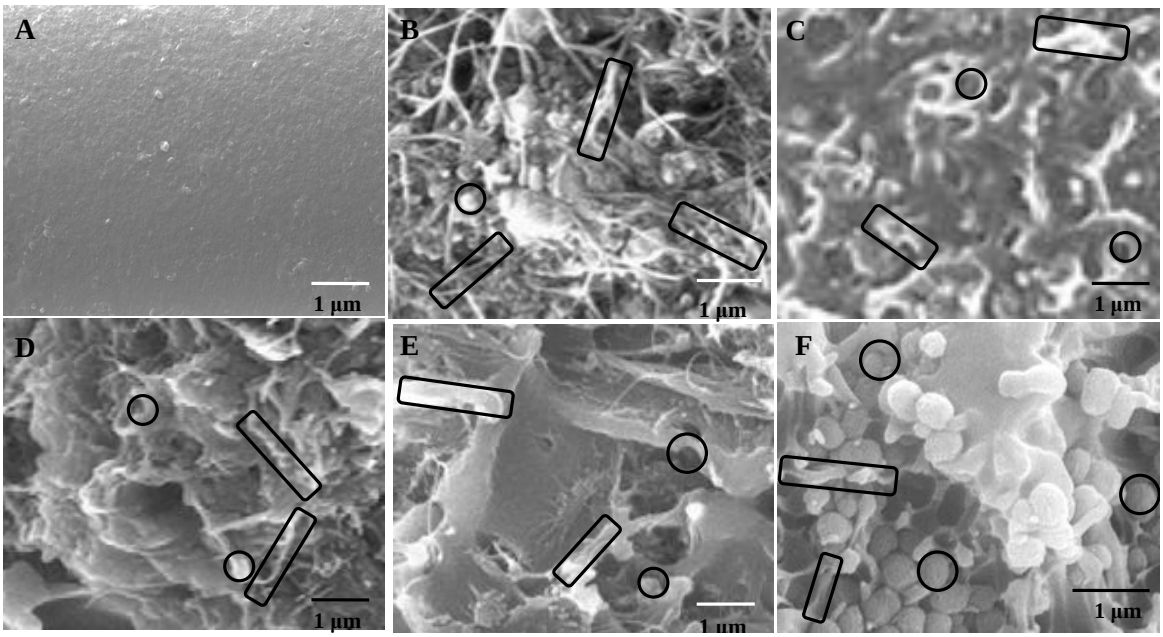

Fig. 6.2 Scanning electron micrographs of bare PSF [A], PSF/CNTs(10)/ZIF-302(6) [B], PSF/CNTs(8)/ZIF-302(12) [C], PSF/CNTs(6)/ZIF-302(18) [D], PSF/CNTs(4)/ZIF-302(24) [E], and PSF/CNTs(2)/ZIF-302(30) [F] MMMs containing different loadings of CNTs (enclosed by rectangles) and ZIF-302 nanocrystals (surrounded by circles).

In case of composite membranes containing high loadings of CNTs and low ZIF-302 contents, the CNTs agglomerated owing to their large surface energy while ZIF-302 nanocrystals showed homogeneous dispersion and good polymer-filler adhesion on account of their tiny particle size (Figs. 6.2 [B]). The MMMs filled with high ZIF-302 and low CNTs loadings demonstrated uniform CNTs distribution but improper dispersion and poor adhesion of ZIF-302 nanoparticles with PSF matrix (Figs. 6.2 [D]-[F]). The mixed-matrix membrane containing optimal loading of nanofillers (8 wt % CNTs and 12 wt % ZIF-302) showed uniform dispersion and good filler-polymer interfacial adhesion as the cross sectional view of MMM exhibits defect-free interconnected network

morphology (Fig. 6.2 [C]). The controlled morphology of ZIF-302 nanocrystals dispersed in the optimized MMM provided significant steric effect to reduce CNTs aggregation; conversely the strong polymer-filler interaction led to homogeneous dispersion of ZIF-302 nanocrystals. The synergistic effect of ZIF-302 nanocrystals and CNTs helped to orient some of the CNTs parallel to gas permeation passages through the MMMs thickness.

6.3.3 Thermal Gravimetric Analysis

To assess the mutual effect of CNTs and ZIF-302 nanofillers on phase transitions, thermal stability, chemical and physical behavior of MMMs, TGA-DTG analyses of bare PSF and hybrid membranes were performed in the range of 100-700 ^{o}C. The TGA curves of the prepared membranes showed consistent decomposition profiles demonstrating a two-stage weight loss owing to desolvation (at around 100-200 ^{o}C) and pyrolysis (460-670 ^{o}C) processes as indicated in Fig. 6.3 [A]. The desolvation step refers to the release of volatile solvent molecules such as DMF, water, CCl_4 etc. imprisoned within the pores of MMMs while the decomposition of organic ligands of the imidazole frameworks and degradation of CNTs and PSF constituting entities occur during pyrolysis step. The residual ash left behind at the end of thermal test validated the nominal mass contents of nanofillers incorporated in corresponding MMMs.

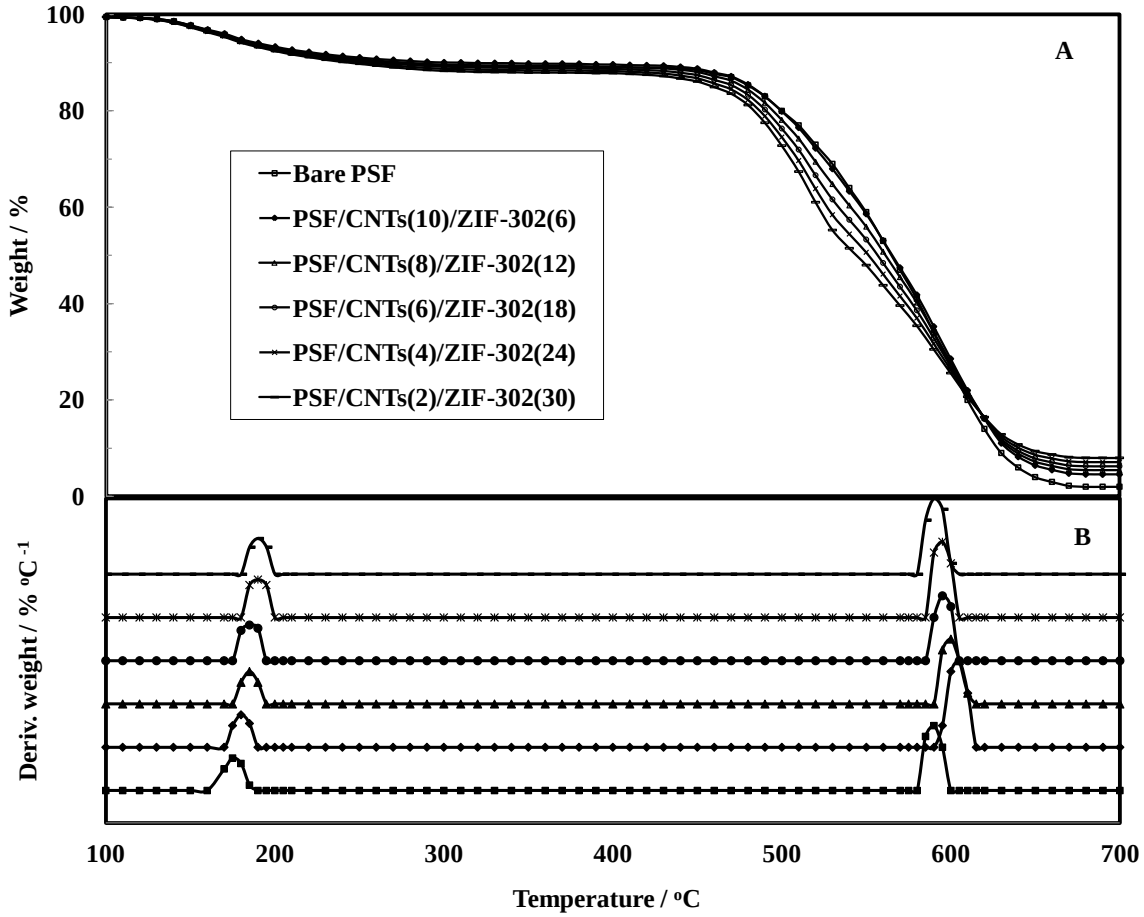

Fig. 6.3 TGA-DTG curves: TGA [A] and DTG [B] bare PSF and MMMs containing different loadings of CNTs and ZIF-302 nanocrystals.

The thermal stability of a material can be evaluated, via TGA analysis, in terms of $T_{d5\%}$ *and* $T_{d10\%}$ values- the temperatures at which testing specimen loses its 5 and 10 percent weight respectively [43]. Being increasing function of nanofiller contents, values of $T_{d5\%}$ and $T_{d10\%}$ occur in the range of 172-179 °C and 246-310 °C respectively. Some of the notable thermal properties of hybrid membranes are outlined in Table 6.1. The derivative thermogravimetric (DTG) curves illustrated in Fig. 6.3 [B] provide essential information on pyrolysis rates in terms of 1st and 2nd DTG peaks. The degree of rigidity of the polymer chains in MMMs can be determined in terms of glass transition temperature

(T_g), 1st and 2nd DTG peak values. The upgrading of these parameters, especially T_g, with increased nanofiller loadings (Table 6.1) signify improved rigidity of MMMs due to the constrained motion of polymer chains resulting from mutual interactions among polymer chains and nanofiller entities.

Table 6.1 Characteristic temperatures of membrane materials acquired from TGA-DTG data

Sample Designation	**T_g (^oC)**	**$T_{d5\%}$ (^oC)**	**$T_{d10\%}$ (^oC)**	**1st DTG peak (^oC)**	**2nd DTG peak (^oC)**	**Residual mass (%)**
Bare PSF	177	177	264	177	591	2
PSF/CNTs(10)/ZIF-302(6)	185	179	310	182	603	4.4
PSF/CNTs(8)/ZIF-302(12)	183	176	281	185	599	4.9
PSF/CNTs(6)/ZIF-302(18)	182	174	263	186	597	5.7
PSF/CNTs(4)/ZIF-302(24)	181	172	254	188	594	6.4
PSF/CNTs(2)/ZIF-302(30)	182	173	246	190	592	7.1

In contrast to bare PSF membrane, occurrence of thermal disintegration of hybrid membranes at higher temperatures can be attributed to improved polymer-filler interactions and good thermal stability of CNTs and ZIF-302 nanocrystals. Thermal stability of hybrid membrane containing 10 wt % CNTs and 6 wt % ZIF-302, along with others, was found to be the highest due to harmonious effect of nanofillers. Thermal stability of mixed membranes determined in terms of 2nd DTG peaks, improved with increasing nanofiller loadings as supported by weight loss curves. Since the maximum temperature observed in different gas separation and combustion processes occurs in the

range of 30 to 350 °C, these MMMs can safely be used in gas separation applications [44].

6.3.4 Gas Sorption Analysis

N_2 adsorption isotherms, normally performed at 77 K under relative pressure of ~ 0-1 bar, were applied to measure surface area and microporosity of the membranes. CO_2 and N_2 adsorption isotherms were obtained to determine their respective loading capacities under low pressure at 298 K as shown in Fig. 6.4.

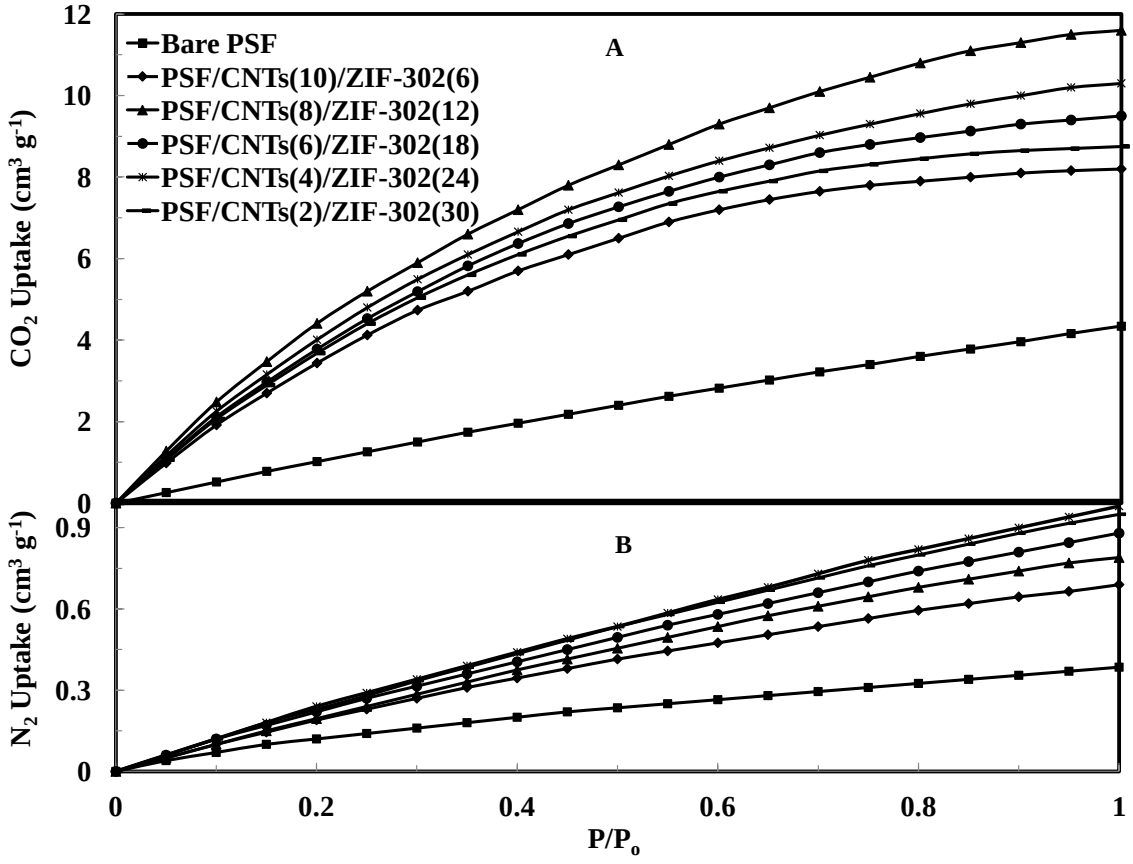

Fig. 6.4 CO_2 [A] and N_2 [B] adsorption isotherms for bare PSF and PSF/CNTs/ZIF-302 MMMs containing varying loadings of CNTs and ZIF-302 nanocrystals at 298 ^oC.

Key physical macroscopic properties (density, fractional volume of nanofillers) and major microporous characteristics such as Brunauer-Emmett-Teller (S_{BET}) and Langmuir (S_{Lang}) surface areas, total micropore volume, CO_2 and N_2 uptakes, and CO_2/N_2 adsorption selectivity of the specimen were improved with the incorporation of nanofillers as summarized in Table 6.2. These outcomes precisely corroborated the existence of uniform distribution, improved adhesion and interfaces between PSF matrix and nanofillers resulting in fine quality MMMs.

Table 6.2 Physical and microporous properties of bare PSF and PSF/CNTs/ZIF-302 MMMs

Sample Designation	**Density ($g\ cm^{-3}$)**	**Φ_d (%)**	**S_{BET} (m^2g^{-1})**	**S_{Lang} (m^2g^{-1})**	**$V_{micro\text{-}total}$ (cm^3g^{-1})**	**CO_2 uptake ($cm^3\ g^{-1}$)**	**N_2 uptake ($cm^3\ g^{-1}$)**	**α_{CO_2/N_2}**
Bare PSF	1.25	0.00	12	18	0.02	4.3	0.38	11
PSF/CNTs(10)/ZIF-302(6)	1.33	12.7	95	110	0.18	8.2	0.69	12
PSF/CNTs(8)/ZIF-302(12)	1.31	17.8	100	120	0.19	10.1	0.79	13
PSF/CNTs(6)/ZIF-302(18)	1.29	22.8	105	125	0.21	11.9	0.88	14
PSF/CNTs(4)/ZIF-302(24)	1.27	27.7	105	120	0.20	10.3	0.98	11
PSF/CNTs(2)/ZIF-302(30)	1.25	32.5	100	115	0.17	8.7	0.95	9

As compared to bare PSF, CO_2 uptake for all the MMMs considerably improved with increasing pressure on account of specific chemical affinity of both the nanofillers for quadro-polar CO_2 molecules. The hybrid membrane filled with 8 wt % CNTs and 12 wt % ZIF-302 nanocrystals yielded the highest CO_2 loading ca. 12 cm^3/g (≈ 0.6 mmol/g) at

298 K which can be further improved by lowering the temperature. The N_2 gas was almost linearly adsorbed with pressure up to 1 bar for all the membranes indicating very poor chemical affinity for nanofillers. In addition all the membranes showed preferably high adsorption affinity for CO_2 as compared to N_2, especially at low CO_2 partial pressure. The CO_2/N_2 sorption selectivities of the MMMs significantly increased with nanofillers (especially ZIF-302) loadings. These findings suggest the fabricated MMMs as potential candidate to separate CO_2 from CO_2/N_2 mixture from post combustion flue gases.

6.3.5 Gas Permeation Properties

Single gas CO_2 and N_2 permeation experiments were performed to evaluate the permeability and ideal selectivity of the prepared membranes under dry and wet conditions at 25 °C subjected to a varying upstream pressure. On account of favorable CO_2-nanofillers mutual affinity, CO_2 permeability and CO_2/N_2 selectivity of the hybrid membranes were significantly improved by adding CNTs and ZIF-302 nanocrystals as depicted in Fig. 5. The permeation experiments performed under wet conditions lead to slight improvement of CO_2 transport properties along with its separation from N_2.

Due to their relatively large pore diameter and smooth inner surfaces, the exclusive incorporation of CNTs into the polymer matrix extensively improved CO_2 permeability but at the expense of deteriorated CO_2/N_2 permselectivity [39]. The sole inclusion of ZIF-302 nanocrystals into polymer-based hybrid membranes reasonably increased both CO_2 permeability and CO_2/N_2 permselectivity due to specific chemical structure of ZIF-302. Both the CO_2 permeability and CO_2/N_2 ideal selectivity of the hybrid membranes were

appreciably enhanced by the harmonious effect of adding CNTs and ZIF-302 nanofillers as shown in Fig. 6.5. The optimum filler loading was found to be 8 wt % CNTs and 12 wt % ZIF-302 nanocrystals. At the optimal filler loading the CO_2 permeability of the MMM was determined to be 18 Barrer with CO_2/N_2 selectivity of 35. The most preferable loading favored homogeneous distribution of the nanofillers so as to exploit the pathways of CNTs pores to amplify CO_2 permeability and the CO_2/N_2 selective affinity of amine-functionalized ZIF-302 nanocrystals to render high selectivity.

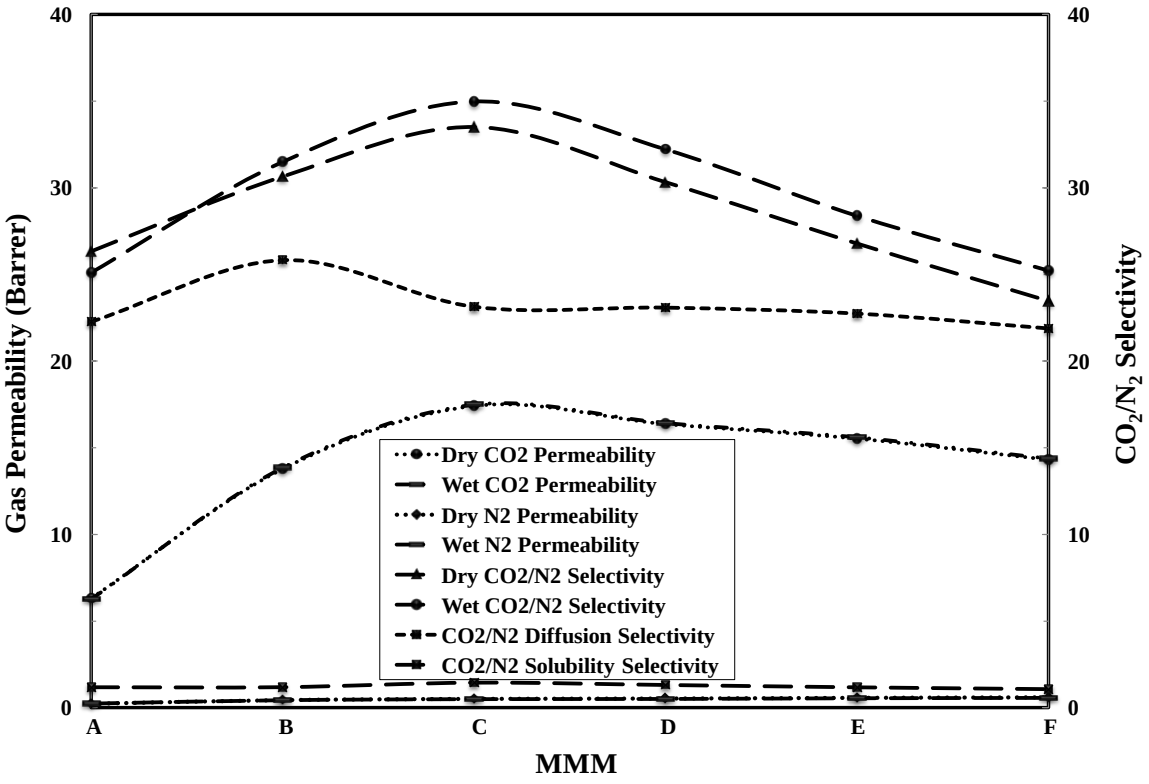

Fig. 6.5 Dry and wet gas CO_2 and N_2 permeabilities and CO_2/N_2 selectivity of bare PSF [A], PSF/CNTs(10)/ZIF-302(6) [B], PSF/CNTs(8)/ZIF-302(12) [C], PSF/CNTs(6)/ZIF-302(18) [D], PSF/CNTs(4)/ZIF-302(24) [E], and PSF/CNTs(2)/ZIF-302(30) [F] MMMs containing different loadings of CNTs and ZIF-302 nanocrystals.

The gas permeation through a membrane occurs via solubility followed by diffusivity of the permeating gas molecules; this phenomenon can be well elucidated by estimating the coefficient of solubility (S) and coefficient of diffusivity (D) of CO_2 and N_2 gas molecules in mixed-matrix membranes. The essential data pertaining to gas solubility and diffusivity for the prepared membranes are illustrated in Figs. 6.5 and 6.6. The diffusivity coefficients of both CO_2 and N_2 were slightly changed with different nanofiller loadings reaching a maximum value at the optimal nanofiller loading. The diffusivities were improved due to the preferential orientation and close packing of cylindrical smooth-walled CNTs within the polymer matrix. The variation in CO_2 solubility coefficient was much pronounced as compared to that of N_2; the solubility coefficient of CO_2, in contrast to N_2, was significantly improved at the optimum loading. The solubility coefficient, in general, depends on both chemical composition and structural arrangement of the membrane. The basic nature of both CNTs hydroxyl groups and ZIF-302 amine groups generated a collegial impact to preferably adsorb the acidic CO_2 molecules as compared to non-polar N_2 molecules. This effect resulted in higher CO_2 solubility and limited that of N_2, consequently improving the CO_2/N_2 solubility-based selectivity. The improved permselectivity of CO_2 over N_2 can also be ascribed to the enlarged number of interaction sites and basic functional groups due to the addition of CNTs and ZIF-302 nanocrystals into PSF matrix.

The time-lag method (eq. 6) was used to determine the values of diffusion coefficients. CO_2 and N_2 adsorption isotherms obtained at 25 ^{o}C under varying pressure helped to calculate Langmuir parameters to determine the correction parameters (bracketed term in eq. 3). The D values thus determined were used to calculate solubility coefficients of the

membranes under the same conditions of temperature and pressure using eq. 4. The values of gas diffusivity coefficient selectivity (D_{CO2}/D_{N2}) slightly varied with different nanofiller loadings, while the gas solubility coefficient selectivity (S_{CO2}/S_{N2}) significantly changed for all the hybrid membranes attaining a peak value for the optimized MMM containing 8 wt % CNTs and 12 wt % ZIF-302 as shown in Fig. 6.5.

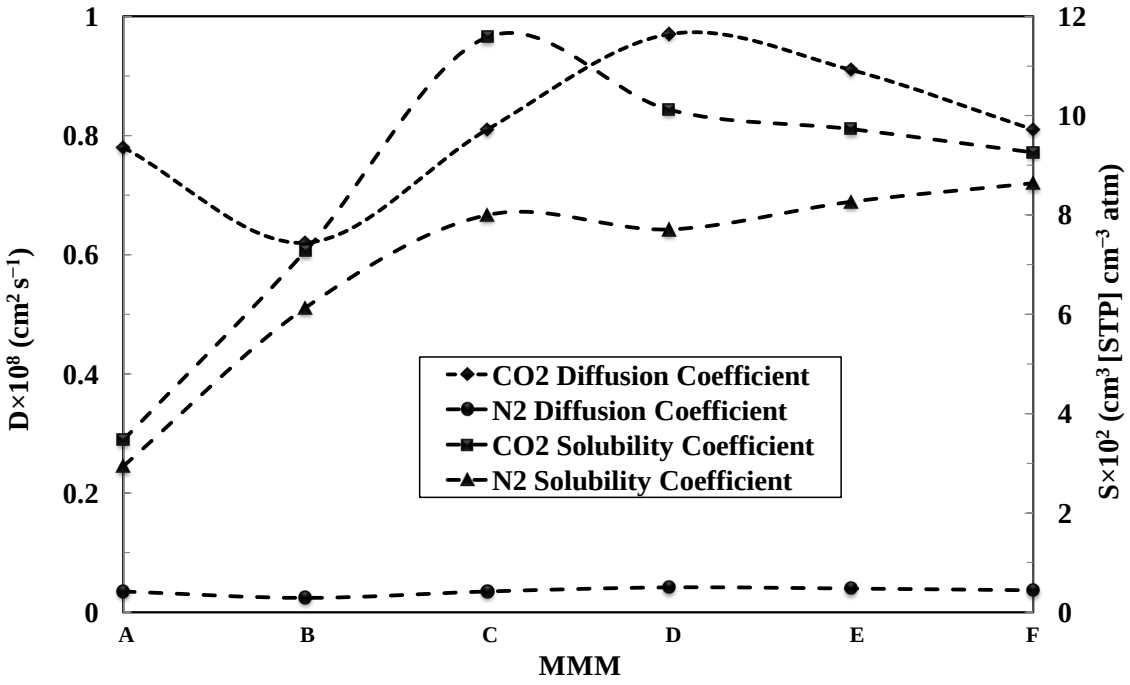

Fig. 6.6 Pure gas diffusion (D) and solubility (S) coefficients for bare PSF [A], PSF/CNTs(10)/ZIF-302(6) [B], PSF/CNTs(8)/ZIF-302(12) [C], PSF/CNTs(6)/ZIF-302(18) [D], PSF/CNTs(4)/ZIF-302(24) [E], and PSF/CNTs(2)/ZIF-302(30) [F] MMMs containing different loadings of CNTs and ZIF-302 nanocrystals.

Almost defect-free CNTs permitted both CO_2 and N_2 gas molecules to diffuse quickly through its internally smooth-walled channels. Since the proper distribution of CNTs in PSF matrix acted as efficient pathways to proficiently transport gas molecules, the overall gas permeability was highly improved. Also the preferential solubility of CO_2, over N_2, into the ZIF-302 nanocrystals significantly improved its permeation through the hybrid membranes. The narrowing down of pore size of MMMs due to incorporation of ZIF-302 nanocrystals limited the N_2 adsorption as compared to CO_2. In a nutshell the CO_2/N_2 permselectivities of composite membranes are improved due to selective CO_2 solubility and restricted N_2 diffusion. Both the nanofillers mutually interacted so as to offer controlled passages for improved CO_2 permeability and CO_2/N_2 selectivity through the composite membranes. The overall analysis based on improved performance of PSF/CNTs/ZIF-302 MMMs strongly support the development of a true mixed matrix membrane.

A comparison of the CO_2/N_2 gas pair separation performance of nanofilled MMMs, along with Robeson 1991 and 2008 upper bounds [14], is made on a permeability-selectivity chart as illustrate in Fig. 6.7. The diagram indicates that the incorporation of CNTs and ZIF-302 nanofillers into PSF matrix has enhanced the permselectivity of the MMMs as compared to bare polysulfone membrane. The permselectivity values of all the composite membranes reported here are located between 1991- and 2008-upper bound lines, an important achievement of this work.

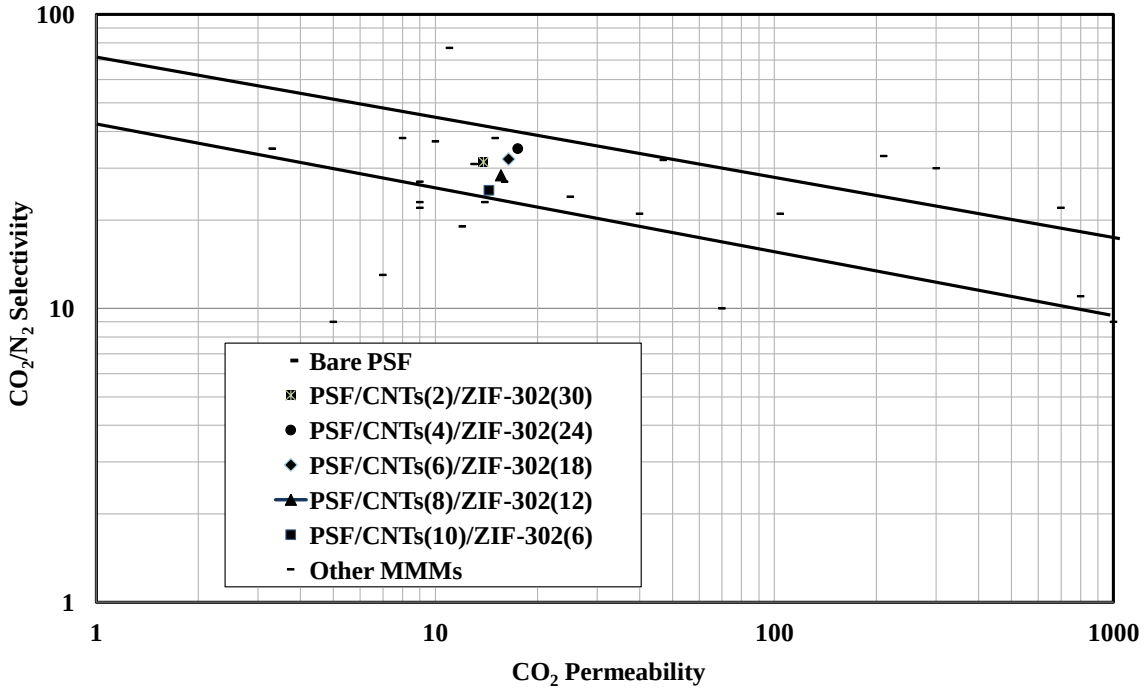

Fig. 6.7 Comparison of CO_2/N_2 separation performance of PSF/CNTs/ZIF-302 MMMs with other ZIF or MOF containing MMMs obtained from literature data. The Robeson 1991 and 2008 upper bounds for polymer separation performance are also shown.

Since a membrane having high CO_2 permeability coupled with improved CO_2/N_2 ideal selectivity characteristics fulfills industrial requirements, it corroborates that CNTs and ZIF-302 nanofillers are competent materials to fabricate MMMs for post combustion carbon capture.

6.4 Conclusions

Hydrothermally stable high performance mixed-matrix membranes were fabricated by incorporating multiwalled CNTs and ZIF-302 nanofillers to selectively capture CO_2 from post combustion flue gases. Characterization of the MMMs carried out by XRD, TGA,

SEM and gas sorption experiments indicated that they are thermally stable, microporous, partially crystalline materials exhibiting nanofillers homogeneous dispersion and good interfacial matrix-filler adhesion without adding any compatibilizing agent. The hybrid membranes prepared in this work demonstrated about 3 times increment in CO_2 permeability as compared to that of bare PSF membrane while the CO_2/N_2 ideal selectivity was enhanced by a factor of 1.7. Furthermore the MMMs perform well under wet conditions as compared to dry ones. The separation performance of the composite membranes produced in this work were above the Robeson 1991 upper bound and the CO_2/N_2 ideal selectivity is considered to be high enough to meet industrial applications.

Acknowledgement

The authors are thankful to KACST-TIC on Carbon Capture and Sequestration (CCS), King Fahd University of Petroleum and Minerals, Dhahran, Kingdom of Saudi Arabia for providing support for this work.

References

[1] D. M. D'Alessandro, B. Smit, J. R. Long, Carbon Dioxide Capture: Prospects for New Materials, Angew. Chem. Int. Ed. 49 (2010) 6058-6082.

[2] M. Z. Jacobson, Review of Solutions to Global Warming, Air Pollution, and Energy Security, Energy Environ. Sci. 2 (2009) 148-173.

[3] N. MacDowell, N. Florin, A. Buchard, J. Hallett, A. Galindo, G. Jackson, C. S. Adjiman, C. K. Williams, N. Shah, P. Fennell, An Overview of CO_2 Capture Technologies, Energy Environ. Sci. 3 (2010) 1645-1669.

[4] H. Herzog, D. Golomb, Carbon capture and storage from fossil fuel use, Encyc. Energy 1 (2004) 277-287.

[5] A. Hussain, M.B. Hägg, A feasibility study of CO_2 capture from flue gas by a facilitated transport membrane, J. Membr. Sci. 359 (2010) 140-148.

[6] J. Zhao, Z. Wang, J.X. Wang, S.C. Wang, Influence of heat-treatment on CO_2 separation performance of novel fixed carrier composite membranes prepared by interfacial polymerization, J. Membr. Sci. 283 (2006) 346-356.

[7] P. Pandey, R.S. Chauhan, Membranes for gas separation, Prog. Polym. Sci. 26 (2001) 853-893.

[8] R. Mahajan, W.J. Koros, Factors controlling successful formation of mixed-matrix gas separation materials, Ind. Eng. Chem. Res. 39 (2000) 2692–2696.

[9] E.P. Fawas, G.C. Kapantaidakis, J.W. Nolan, A.C. Mitropoulos, N.K. Kanellopoulos, Preparation, characterization and gas permeation properties of carbon hollow fiber membranes based on Matrimid® 5218 precursor, J. Mater. Process. Technol. 186 (2007) 102–110.

[10] R.W. Baker, Future directions of membrane gas separation technology, J. Ind. Eng. Chem. Res. 41 (2002) 1393–1411.

[11] D.L. Gin, R.D. Noble, Designing the next generation of chemical separation membranes, Science 332 (2011) 674-676.

[12] Y. Xiao, T.-S. Chung, Grafting thermally labile molecules on cross-linkable polyimide to design membrane materials for natural gas purification and CO_2 capture. Energy Environ. Sci. 4 (2011) 201-208.

[13] C. Staudt-Bickel, W.J. Koros, Improvement of CO_2/CH_4 separation characteristics of polyimides by chemical crosslinking. J. Membr. Sci. 155 (1999) 145-154.

[14] T.C. Merkel, B.D. Freeman, R.J. Spontak, Z. He, I. Pinnau, P. Meakin, A. Hill, J. Ultrapermeable, reverse-selective nanocomposite membranes, Science 296 (2002) 519-522.

[15] J. Ahn, W.-J. Chung, I. Pinnau, M.D. Guiver, Polysulfone/silica nanoparticle mixed-matrix membranes for gas separation, J. Membr. Sci. 314 (2008) 123-133.

[16] B.D. Reid, A. Ruiz-Trevino, I.H. Musselman, K.J. Balkus, J.P. Ferraris, Gas permeability properties of polysulfone membranes containing the mesoporous molecular sieve MCM-41, Chem. Mater. 13 (2001) 2366-2373.

[17] S. Kim, E. Marand, J. Ida, V.V. Guliants, Polysulfone and mesoporous molecular sieve MCM-48 mixed matrix membranes for gas separation, Chem. Mater. 18 (2006) 1149-1155.

[18] S. Kim, E. Marand, High permeability nano-composite membranes based on mesoporous MCM-41 nanoparticles in a polysulfone matrix, Microp. Mesop. Mater. 114 (2008) 129-136.

[19] D.Q. Vu, W.J. Koros, S.J. Miller, Mixed matrix membranes using carbon molecular sieves. II. Modeling permeation behavior, J. Membr. Sci. 211 (2003) 335-348.

[20] H.L. Cong, J.M. Zhang, M. Radosz, Y.Q. Shen, Carbon nanotube composite membranes of brominated poly(2,6-diphenyl-1,4-phenylene oxide) for gas separation, J. Membr. Sci. 294 (2007) 178–185.

[21] S. Kim, L. Chen, J.K. Johnson, E. Marand, Polysulfone and functionalized carbon nanotube mixed matrix membranes for gas separation: Theory and experiment, J. Membr. Sci. 294 (2007) 147–158.

[22] P. Gorgojo, S. Uriel, C. Tellez, J. Coronas, Development of mixed matrix membranes based on zeolite Nu-6(2) for gas separation, J. Microporous Mesoporous Mater. 115 (2008) 85–92.

[23] Y. Liu, D. Peng, G. He, S. Wang, Y. Li, H. Wu, Z. Jiang, Enhanced CO_2 permeability of membranes by incorporating polyzwitterion@CNT composite particles into polyimide matrix, ACS Appl. Mater. Interfaces 6 (2014) 13051-13060.

[24] B. Harold, T. Jeazet, C. Staudt, C. Janiak, Metal–organic frameworks in mixed-matrix membranes for gas separation, Dalton Trans. 41 (2012) 14003–14027.

[25] T. Li, Y. Pan, K.V. Peinemann, Z. Lai, Carbon dioxide selective mixed matrix composite membrane containing ZIF-7 nano-fillers, J. Membr. Sci. 425–426 (2013) 235–242.

[26] Chen Zhang, Kuang Zhang, Liren Xu, Ying Labreche, Brian Kraftschik, W.J. Koros, Highly scalable ZIF-based mixed-matrix hollow fiber membranes for advanced hydrocarbon separations, AIChE J. 60 (2014) 2625–2635.

[27] Mohammad Askari, T.S. Chung, Natural gas purification and olefin/paraffin separation using thermal cross-link ableco-polyimide/ZIF-8 mixed matrix membranes, J. Membr. Sci. 444 (2013) 173–183.

[28] T.T.N. Nhung, H. Furukawa, F. Gandara, H.T. Nguyen, K.E. Cordova, O.M. Yaghi, Selective capture of carbon dioxide under humid conditions by hydrophobic chabazite-type zeolitic imidazolate frameworks, Angew. Chem. 126 (2014) 10821–10824.

[29] H. Chen, D.S. Sholl, Predictions of selectivity and flux for CH_4/H_2 separations using single walled carbon nanotubes as membranes, J. Membr. Sci. 269 (2006) 152–160.

[30] D.S. Sholl, J.K. Johnson, Making high-flux membranes with carbon nanotubes, Science 312 (2006) 1003–1004.

[31] A.I. Skoulidas, D.S. Sholl, J.K. Johnson, Adsorption and diffusion of carbon dioxide and nitrogen through single-walled carbon nanotube membranes, J. Chem. Phys. 124 (2006) 054708.

[32] S. Kim, J.R. Jinschek, H. Chen, D.S. Sholl, E. Marand, Scalable fabrication of carbon nanotube/polymer nanocomposite membranes for high flux gas transport, Nano Lett. 7 (2007) 2806–2811.

[33] T.W. Chamberlain, J.C. Meyer, J. Biskupek, J. Leschner, A. Santana, N.A. Besley, E. Bichoutskaia, U. Kaiser, A.N. Khlobystov, Reactions of the inner surface of carbon nanotubes and nanoprotrusion processes imaged at the atomic scale, Nat. Chem. 3 (2011) 732–737.

[34] A.F. Ismail, P.S. Goh, S.M. Sanip, M. Aziz, Transport and separation properties of carbon nanotube-mixed matrix membrane, Sep. Purif. Technol. 70 (2009) 12–26.

[35] L. Ge, L. Wang, V. Rudolph, Z. Zhu, Hierarchically structured metal-organic framework/vertically-aligned carbon nanotubes hybrids for CO_2 capture, RSC Adv. 3 (2013) 25360–25366.

[36] B. Zornoza, B. Seoane, J. M. Zamaro, C. Téllez and J. Coronas, Combination of MOFs and zeolites for mixed-matrix membranes, Chem-PhysChem, 12 (2011) 2781–2785.

[37] M. Valero, B. Zornoza, C. Téllez, J. Coronas, Mixed matrix membranes for gas separation by combination of silica MCM-41 and MOF NH2-MIL-53 (Al) in glassy polymers, Microporous Mesoporous Mater. 192 (2013) 23–28.

[38] A. Galve, D. Sieffert, C. Staudt, M. Ferrando, C. Güell, C. Téllez, J. Coronas, Combination of ordered mesoporous silica MCM-41 and layered titanosilicate JDF-L1 fillers for 6FDA-based copolyimide mixed matrix membranes, J. Membr. Sci. 431 (2013) 163-170.

[39] X. Li, L. Ma, H. Zhang, S. Wang, Z. Jiang, R. Guo, H. Wu, X.Z. Cao, J. Yang, B. Wang, Synergistic effect of combining carbon nanotubes and grapheme oxide in mixed matrix membranes for efficient CO_2 separation, J. Memb. Sc. 479 (2015) 1-10

[40] X.W. Yu, Z. Wang, Z.H. Wei, S.J. Yuan, J. Zhao, J.X. Wang, S.C. Wang, Novel tertiary amino containing thin film composite membranes prepared by interfacial polymerization for CO_2 capture, J. Membr. Sci. 362 (2010) 265-278.

[41] D.R. Paul, D.R. Kemp, The diffusion time lag in polymer membranes containing adsorptive fillers, J. Polym Sc: Polym. Symp. 41 (1973) 79–93.

[42] V. Gupta, T. Saleh, Synthesis of Carbon Nanotube-Metal Oxides Composites; Adsorption and Photo-Degradation, Carbon 59 (2013)308–314.

[43] Y.C. Xiao, T.S. Chung, H.M. Guan, M.D. Guiver, Synthesis, cross-linking and carbonization of co-polyimides containing internal acetylene units for gas separation, J. Membr. Sci. 302 (2007) 254-264.

[44] A.C.C. Chang, S.S.C. Chuang, M. Gray, Y. Soong, In-situ infrared study of CO_2 adsorption on SBA-15 grafted with γ-(aminopropyl) triethoxysilane, Energy Fuels 17 (2003) 468-473.

CHAPTER 7

CONCLUSIONS AND RECOMMENDATIONS

7.1 Conclusions

Hydrothermally stable nanocrystals of zeolitic imidazolate frameworks ZIF-300, ZIF-301 and ZIF-3002 with narrow particle size distribution were incorporated exclusively as well as along with multiwalled carbon nanotubes into polysulfone matrix to fabricate hydrothermally stable high performance mixed-matrix membranes for selective CO_2 separation from post combustion flue gas. Characterization of the MMMs done by XRD, TGA, SEM and gas sorption experiments indicated that they are thermally stable, mesoporous, crystalline materials possessing homogeneous filler dispersion and good interfacial filler-matrix adhesion without adding any compatibilizing agent.

The MMMs developed in this work demonstrated reasonable improvement in CO_2 permeability and CO_2/N_2 ideal selectivity as compared to that of pure PSF membrane. Owing to their relatively wide tube diameter as compared to those of gas molecules, the CNTs drastically enhanced CO_2 permeability while ZIF nanoparicles served to enhance CO_2/N_2 ideal selectivity due to their high affinity for CO_2 over N_2.

Two- and three-phase permeability models were employed to predict CO_2 permeability through the prepared MMMs. The two-phase Maxwell and Singh models well predicted the permeability at low filler loadings, while the three-phase modified Felske and

Bruggeman models more accurately described the MMMs behavior at higher filler concentrations. The error in three-phase models is lower than two-phase models thus dictating non-ideal morphology of the MMMs.

The separation performance of the MMMs produced in this work were above the Robeson 1991 upper bound and were coincided with the Robeson 2008 upper bound. The CO_2/N_2 ideal selectivity is considered to be high enough to meet industrial applications. Furthermore the MMMs performed well under wet conditions as compared to dry ones.

7.2 Recommendations

The separation performance of organic polymer based mixed matrix membranes doped with metal organic frameworks or zeolitic imidazolate frameworks can be improved by introducing another selective material like graphene oxide nanosheets or nanoplates to enhance CO_2/N_2 permselectively. Different combinations of polymers in different proportions can be employed with different porous materials to investigate the efficiency of resulting MMMs. Various combinations of MOFs and/or ZIFs having different particle sizes can also be incorporated into different polymers to optimize their separation performance.

NOMENCLATURE

Symbols

A	effective membrane area (cm^2)
D	diffusion coefficient (cm^2/s)
K	adsorption parameter determined from Langmuir adsorption isotherm
L	membrane thickness (cm)
m	mass or weight of the specimen
P	gas permeability (Barrer; 1 Barrer = 10^{-10} cm^3 (STP) cm/(cm s cmHg))
R	universal gas constant (6236.56 cm^3 cmHg/mol/K)
S	solubility coefficient (cm^3 (STP)/cm^3 cmHg)
T	absolute temperature (K)
V	cell downstream volume (cm^3)
y	parameter to be determined from Langmuir adsorption isotherm
Δp	pressure difference across the membrane (psi)
$\Delta P/dt$	gas permeation rate (psi/s) in terms of time rate of pressure

Greek letters

α	membrane gas selectivity
β	matrix rigidification or chain immobilization factor
γ	ratio of interphase thickness to particle radius

δ ratio of outer radius of rigidified interfacial matrix chain layer to radius of core particle

θ x-rays diffraction angle (^{o})

λ permeability ratio

ρ density (g/cm^{3})

ψ function of packing volume fraction of filler particles

Φ fractional volume of fillers (%)

Subscripts

C continuous phase

D dispersed phase

d5% 5 percent specimen weight loss

d10% 10 percent specimen weight loss

eff effective

g glass transition

i interphase

i gas 'i'

j gas 'j'

m polymer matrix

r relative

Superscripts

o degree

VITAE

Name	: Muhammad Sarfraz
Nationality	: Pakistani
Date of Birth	: November 15, 1982
Email	: g201203900@kfupm.edu.sa
Address	: Room # 117, Building 804, KFUPM Students Housing, Dhahran 31261, Kingdom of Saudi Arabia
Academic Background	: M.Sc. Polymer Engineering